SISSA
Scuola Internazionale Superiore di Studi Avanzati

Neuroscience Area – PhD course in Neurobiology

Modulation of pheromone responses in vomeronasal sensory neurons

Candidate: Nicole Sarno

Advisor:
Prof. Anna Menini
Co-advisors:
Prof. Simone Pifferi
PhD. Andres Hernandez-Clavijo

Academic Year 2020-21

Scuola Internazionale di Studi Avanzati

Trieste



Modulation of pheromone responses in vomeronasal sensory neurons

Thesis submitted for the degree of "Doctor Philosophiae"

Academic Year 2020/2021

CANDIDATE
Nicole Sarno

SUPERVISOR
Prof. Anna Menini

CO-SUPERVISORS
Prof. Simone Pifferi
PhD. Andres Hernandez-Clavijo

TABLE OF CONTENTS

List of abbreviations ***i***

Abstract ***iii***

1 Introduction ***- 1 -***

1.1 Chemosensation and Pheromones - 2 -

1.2 Pheromone-mediated behaviors - 4 -

1.3 The Vomeronasal organ - 5 -

1.3.1 The discovery of the Vomeronasal Organ (VNO) - 5 -

1.3.2 Vomeronasal sensory neurons (VSNs) - 7 -

1.4 VSN's Ligands - 8 -

1.4.1 Mouse urine - 9 -

1.4.1.1 Volatile small molecules - 9 -

1.4.1.2 Major Urinary Proteins (MUPs) - 9 -

1.4.1.3 Class I major histocompatibility complex peptides (MHC peptides) - 10 -

1.4.1.4 Sulfated Steroids - 10 -

1.4.2 Exocrine gland-Secreting Peptides (ESPs) - 11 -

1.4.3 Formyl-peptides (FPs) - 11 -

1.4.4 Bile Acids - 11 -

1.5 Sensory transduction in VSNs - 12 -

1.5.1 General mechanisms of sensory transduction - 12 -

1.5.2 Vomeronasal Receptors - 13 -

1.5.2.1 V1Rs - 14 -

1.5.2.2 V2Rs - 14 -

1.5.2.3 FPRs ..... - 15 -

1.5.2.4 H2-Mv ..... - 15 -

1.5.3 Phospholipase C (PLC) and diacylglycerol (DAG) ..... - 15 -

1.5.4 Transient receptor potential channel, subfamily C, type 2 (TRPC2) ..... - 17 -

1.5.5 Calcium-activated chloride channels (CaCCs) ..... - 18 -

1.6 Electrical properties of VSNs ..... - 20 -

1.7 Adaptation in VNO: the state of art ..... - 22 -

1.8 Central pathway ..... - 24 -

1.9 TMEM16A and TMEM16B ..... - 26 -

2 Aims ..... - 29 -

3 Results ..... - 30 -

3.1 TMEM16A and TMEM16B modulate pheromone-evoked action potential firing in mouse vomeronasal sensory neurons ..... - 30 -

3.2 Voltage-gated sodium channels slow inactivation contributes to pheromone short-term adaptation in vomeronasal sensory neurons ..... -46-

4 Conclusions ..... -76-

5 References .....

LIST OF ABBREVIATIONS:

(c)GMP: (cyclic) guanosine monophosphate

ANO1: anoctamin 1 (see TMEM16A)

ANO2: anoctamin 2 (see TMEM16B)

AOB: accessory olfactory bulb

AOS: accessory olfactory system

BK: large conductance calcium-activated potassium channels

CaCC(s): calcium-activated chloride channel(s)

cAMP: cyclic adenosine monophosphate

CNG: cyclic nucleotide – gated ion channel

DAG: diacylglycerol

ESP(s): exocrine gland-secreting peptide(s),

FP(s): formyl-peptides

FPR(s): formyl-peptide receptor(s)

GIRK channel: G protein-activated inward rectifier potassium channel

GPCR(s): G protein-coupled receptor(s)

GTP: guanosine triphosphate

Gαi2: guanosine triphosphate (GTP)-binding protein αi2

Gαo: guanosine triphosphate (GTP)-binding protein αo

HCN2-4: hyperpolarization-activated cyclic nucleotide-gated channel 2-4

IP3: inositol (1,4,5)-trisphosphate

MHC: major histocompatibility complex

MOE: main olfactory epithelium

MOS: main olfactory system

MUP(s): major urinary proteins

OB: olfactory bulb

OMP: olfactory marker protein

OR(s): olfactory receptor(s)

OSN(s): olfactory sensory neurons

PIP2: phosphatidylinositol (4,5)-bisphosphate

PLC: phospholipase C

sGC: soluble guanylyl cyclase

SK: small conductance calcium-activated potassium channels

TM(s): transmembrane domain(s)

TMEM16 family: transmembrane protein family 16, comprise calcium-activated chloride channels and lipid scramblases

TMEM16A: calcium-activated chloride channel belonging to the TMEM16 family

TMEM16B: calcium-activated chloride channel belonging to the TMEM16 family

TRPC2: transient receptor potential cation channel, subfamily C, member 2,

TTX: tetrodotoxin

V1R/V2R(s): vomeronasal receptor(s) type 1/type 2

VNO: vomeronasal organ

VSN(s): vomeronasal sensory neuron(s)

ABSTRACT

Chemosensation allows individuals to perceive chemical stimuli from the surrounding environment leading the survival of all the species. The vomeronasal organ (VNO) is a peripheral sensory organ present in many mammals that is involved in the detection of pheromones. Pheromones are substances released by animals which trigger behavior and physiological changes of other individuals of the same species. The binding of pheromones is transduced into electrical signals by specialized neurons that transfer to the central nervous system the information carried by social cues. Ligand binding to vomeronasal receptors on microvilli of the dendritic knobs of vomeronasal sensory neurons (VSNs) triggers a biochemical cascade that activates a PLC-dependent second messenger transduction that ultimately results in the TRPC2 channel gating allowing the inward flow of sodium and calcium. The increase in cytosolic calcium concentration plays several roles in signal transduction, involving the activation of other ion channels. Previous studies showed that calcium activated chloride currents are activated by cytosolic calcium increase in mouse VSNs, and that both TMEM16A and TMEM16B, two proteins forming calcium-activated chloride channels, are co-expressed in microvilli of VSNs, but their physiological role is still uncertain.

With the help of two mouse models, TMEM16A cKO and TMEM16B KO mice, we provide evidence of the role of both channels in spontaneous firing and evoked activity in VSNs. Extracellular recordings in loose-patch configuration showed that firing pattern of spontaneous activity was affected in VSNs from TMEM16A cKO mice, showing less activity with respect to WT neurons, while VSNs from TMEM16B KO mice showed spontaneous firing comparable to WT. During urine-evoked activity both channels are involved in modulation of firing. Inter spike interval (ISI) distribution of evoked activity showed that VSNs from TMEM16A cKO and TMEM16B KO fire with shorter intervals than WT neurons. We conclude that calcium-activated chloride current modulates the firing of VSNs varying the effect with an activity-dependent mode.

Adaptation is an additional mechanism of response modulation common in sensory systems. To evaluate the molecular players involved in sensory adaptation in VNO during early pheromone processing, we used whole-cell recordings in the current-clamp mode to measure the action potential firing of VSNs stimulated by diluted urine. We performed a paired pulse protocol with different inter-pulse intervals (IPIs), ranging from 5 to 60 seconds. We found that VSNs reduced their firing rate depending on the duration of preceding stimulation and on IPIs. Surprisingly, similar results were obtained also upon stimulation with direct injection of current, which does not activate neither the receptors nor the signaling cascade, suggesting that the adaptation would be, at least partially,

independent from the initial sensory transduction cascade. We reveal that sodium currents in VSNs undergo to a slow recovery from inactivation that last several seconds mirroring the time scale of paired pulse experiments.

Our results provide a foundation for future work investigating the precise molecular mechanisms of modulation of pheromones signaling at peripheral level during early stages of firing in VSNs.

1 INTRODUCTION

The ability to perceive signals from the environment drives the existence of all the species across the animal kingdom, in every habitat and in wide-ranging biological contexts. This work will focus on a specific family of signals related to social communication adding information to the knowledge of how chemical cues are translated into electrical signals by the peripheral sensory neurons in the accessory olfactory system. In the following introduction the focus will be the processing of pheromones: molecules that carry social information and turn into electrical signals which are sent to the central nuclei that control behavioral responses. Particular attention will be given to the modulation of the evoked activity in vomeronasal sensory neurons: the role of TMEM16A and TMEM16B channels and the firing adaptation.

1.1 CHEMOSENSATION AND PHEROMONES

Chemosensation is the capability to perceive chemicals in the environment. Olfactory and gustatory systems are responsible for the physiological response that results in regulating behaviors strictly connected with the survival of individuals and species. The discrimination between potential food or toxicants, the choice of desirable partners or the fight-or-flight behavior, pup cares are only few examples of crucial events modulated by chemical cues in preserving life. Smell and taste have evolved to recognize a broad and complex molecules range including an immense chemical variety and with a sensitivity far higher that any electronic detector. Volatile compounds are generally detected by the olfactory system while nutrition compounds and ion content of food are identified by the gustatory system. Both senses, smell and taste, are equipped with peripheral receptors. Olfaction starts with the binding of an odorant molecule with an olfactory receptor, a G-protein coupled receptor protein on the membrane of olfactory sensory neurons (Buck and Axel, 1991). Taste, according to taste modalities, operate through G-protein coupled receptors for bitter, sweet and umami, while salt and sour interact directly with ion channels and exchangers on the membrane of taste receptor cells (Mombaerts, 2004; Roper and Chaudhari, 2017; Taruno et al., 2021).

A particular class of olfactory cues that provides chemical messages between individuals are generically named *semiochemicals*. In vertebrates, different sensory systems in the nasal cavity evolved to detect semiochemicals: the main olfactory system, the vomeronasal organ, the septal organ of Masera and the Grueneberg ganglion (Fig. 1) (Mohrhardt et al., 2018; Tirindelli et al., 2009). Semiochemicals can be classified in two families: allelochemicals, acting between members of different species; and pheromones, acting between members of the same species. The term pheromone was used for the first time in 1959 to identify "*specific biologically active substances which are secreted to outside by an individual and received by a second individual of the same species, in which they release a specific reaction, for example, a definitive behaviour or a developmental process*" (Karlson and Lusher, 1959).

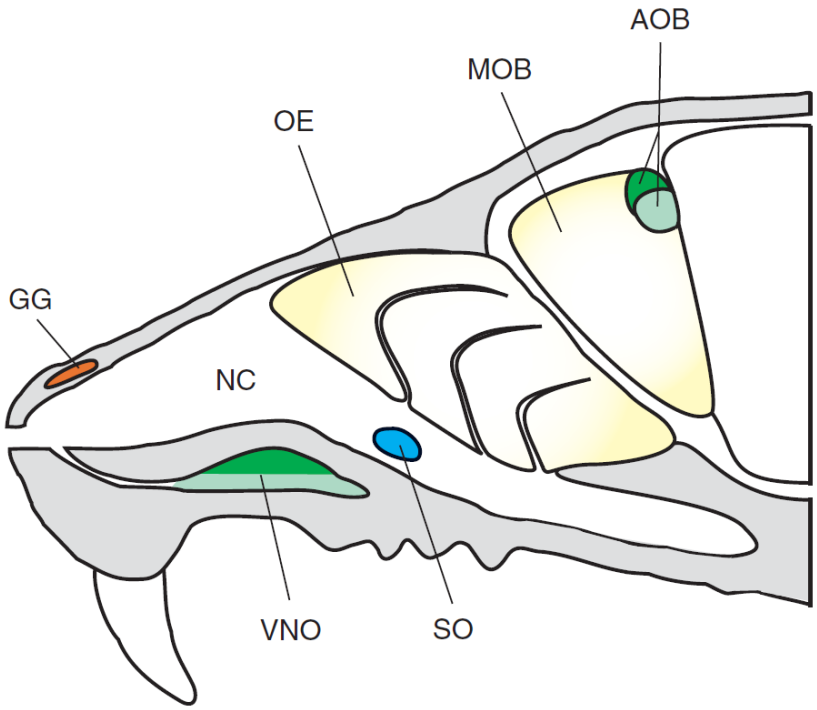


Figure 1. Sensory systems in mouse nasal cavity. *The olfactory epithelium (OE), the vomeronasal organ (VNO), the Grueneberg ganglion (GG), and the septal organ of Masera (SO). Sensory neurons of the OE, SO, and GG project to the main olfactory bulb (MOB), while vomeronasal sensory neurons project to the accessory olfactory bulb (AOB) (Modified from Ferrero and Liberles, 2010).*

Historically, the first substance classified as pheromone was the *Bombykol*, a poly-unsaturated primary alcohol that works as sex attractant in silk moth *Bombyx mori* (Karlson and Lusher, 1959). Insects are the animal model in which pheromone signaling has been extensively investigated and a complete genetically dissection from enzymes producing pheromones to chemosensory receptors and neural circuits has been well established (Wyatt, 2017). Pheromones do not belong to a specific chemical class and any kind of molecule can evolve into a pheromone, if it gives selective advantage (Wyatt, 2014). There are probably two main ways for chemical cues to evolve into pheromone signals: by increasing in the receiver the sensitivity to molecules that are reliable cues to a behavior or by evolutionary selection of the sender that produces the molecules to which the receiver is already sensitive (Mucignat-Caretta, 2014a). The effects triggered by pheromones can be classified in releaser and primer. Releaser effects are immediate and innate behavioral reactions, instead primer effects are long-term responses that results in developmental changes and endocrine controls of physiological functions (Bossert and Wilson, 1963).

1.2 PHEROMONE-MEDIATED BEHAVIORS

Pheromones are detected by olfactory systems and processed to ultimately drive behavior. The accessory olfactory system (AOS) plays a central role in guiding behavioral and physiological responses to social and reproductive interactions in many mammalian species. Rodents, and mice in particular, have become the model system of choice to study vertebrate chemical communication; the tools available for manipulating neuronal activity have made the mouse a particularly attractive model for research (Chamero et al., 2012). Many behaviors mediated by pheromones have been identified by surgical removal of the peripheral organ of AOS, the vomeronasal organ (VNO, see chapter 1.3), or by genetic deletion of specific transduction molecules, thus expanding our understanding of this system (Wyatt, 2014). Ablation of VNO in male mice results in impairments in territorial marking and male-male aggression (Clancy et al., 1984; Maruniak et al., 1986). Female mice are still able to discriminate the gender of conspecifics after VNO removal, but they lose the ability to discriminate non-volatile odors and to make lordosis during male mount (Keller et al., 2006). Moreover, VNO-mediated pheromone inputs act in wild-type females to repress male behaviors and activate female behaviors, indeed VNO-lacking female mice show a reduction in female-specific behavior, including maternal aggression and lactating behavior, and instead display male sexual and courtship behaviors such as mounting, anogenital olfactory investigation, and emission of ultrasonic vocalizations towards males and females (Kimchi et al., 2007).

Furthermore, many endocrine functions depend on pheromones. Lee-Boot effect is the suppression of the estrus cycle that occurs in adult female mice when isolated from males (Van Der Lee and Boot, 1955) and the exposure to male urine, an enriched source of pheromones, is sufficient to restore estrus cycle in non-cycling females (known as Whitten effect, Whitten, 1959). Female mice recently inseminated can interrupt the pregnancy after exposure to new non-mated male urine and can return in estrus, an effect known as Bruce effect (Bruce, 1959). The Bruce effect depends on functional vomeronasal system (Bellringer et al., 1980). Volatile organic molecules present in male mouse urine are able to accelerate puberty in female mice (Novotny et al., 1999). Collectively these data provide evidence of the involvement of pheromones detection mainly in sexual and reproductive behaviors.

1.3 THE VOMERONASAL ORGAN

1.3.1 The discovery of the Vomeronasal Organ (VNO)

In 1703 the anatomist Ruysh reported for the first time an illustration of the VNO in a drawing of nasal septum of a child (Ruysh, 1703). Nonetheless, the discovery of the VNO is ascribed to Ludvig Levis Jacobson who in 1813 reported the VNO structure in many mammals including rodents (Trotier and Døving, 1998). Jacobson detailed description contains the major macroscopic features of the VNO: "[…] *It is located in the foremost part of the nasal cavity, in close contact with the nasal cartilage (septum),* […] *What in particular has hidden this organ from the eyes of the observers is a cartilaginous capsule that surrounds the parts comprising the organ, namely a secretory apparatus, a receptacle and an exit duct* […] *All these parts are usually enclosed in this capsule* […] *The capsule consists of a flat sheet of cartilage, which is curled and therefore hollow in the middle* […]" (Trotier and Døving, 1998).

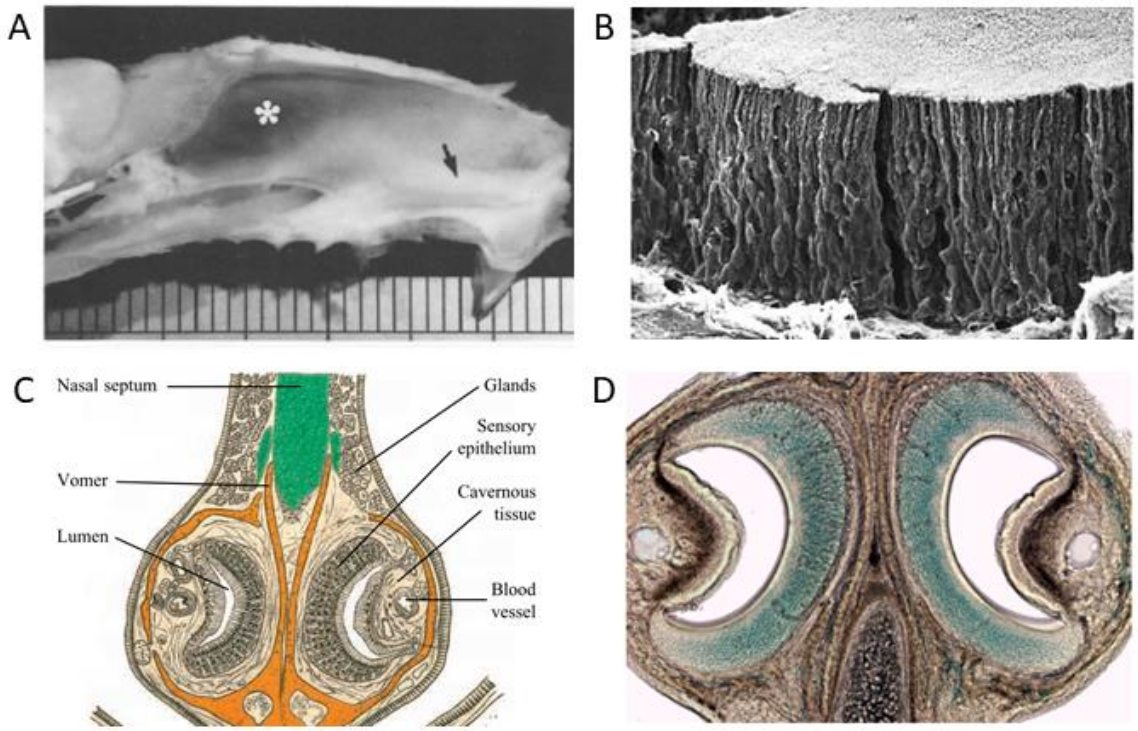


Figure 2. The VNO is a tubular structure enclosed in a cartilaginous capsule placed in the anterior part of the nasal cavity. *(**A**) Lateral view of the rat nasal septum. The asterisk indicates the localization of the olfactory epithelium and the arrow the VNO. Scale in mm (from Mendoza, 1993).* ***(B)*** *Scanning electron micrograph of the sensory epithelium of rat vomeronasal organ shows the columnar organization of the tissue (from Trotier et al., 1998).* ***(C)*** *Schematic representation of localization and histological architecture of a frontal section of mouse VNO (from Doving and Trotier, 1998).* ***(D)*** *Coronal section histology of mouse VNO with vomeronasal sensory epithelium in blue (from Ibarra-Soria et al., 2013).*

The VNO is a bilateral tubular structure (about 5 mm long in the mouse; Mendoza, 1993) placed at the anterior part of the nasal cavity at the base of the nasal septum, it is enclosed in a anteriorly open cartilaginous capsule where the encapsulated VNO comes into contact with the nasal cavity. In rodents, the elongated organ has a central crescent-shaped lumen full of fluids in direct contact with the nasal cavity fluids (Fig. 2) (Døving and Trotier, 1998; Mendoza, 1993; Tirindelli et al., 2009; Trotier and Døving, 1998).

In most VNO-possessing vertebrates two types of epithelial components are identifiable: sensory epithelium and non-sensory epithelium. In rodents, the non-sensory epithelium is well-developed, it is mainly composed of a cavernous body containing venous sinuses, smooth muscles, and unmyelinated nerve fibers. Blood vessels are innervated by the autonomic nervous system that promotes vasodilation and vasoconstriction producing a pump-like action through which stimuli access the lumen: the vasoconstriction of the central plexus allows the restriction of the cavernous body with a consequent increasing volume of the lumen, promoting a suction. This "pumping" mechanism is responsible for sucking into the lumen of the organ the mucus carrying the stimuli (Døving and Trotier, 1998; Mendoza, 1993; Takami, 2002; Tirindelli et al., 2009; Trotier and Døving, 1998; Zancanaro, 2014). The rodent sensory epithelium is a pseudostratified columnar epithelium of approximately 170-120 µm in height and is primarily composed by vomeronasal sensory neurons (VSNs), basal cells and supporting cells. At least three regions can be distinguished in the neuroepithelium: *i*) an apical border close to the lumen, including the supporting cells and the dendrites of the VSNs; *ii*) a central region with nuclei of supporting cells; and *iii*) a basal layer, including apical and basal VSNs (Fig. 3). Supporting cells are found in the more superficial layer of the sensory epithelium and protrude into the lumen of the VNO with numerous long not branched microvilli, while VSNs form two overlapping populations along the basal layer up to the luminal surface that they cover with microvilli (Tirindelli et al., 2009). A further characteristic of the VNO sensory epithelium is the presence of intraepithelial blood vessels (Døving and Trotier, 1998; Keverne, 1999; Mendoza, 1993; Mucignat-Caretta, 2014a; Tirindelli et al., 2009). The VSN's nuclear region covers almost two-thirds of the epithelium. In the following section I will make a detailed description of VSNs.

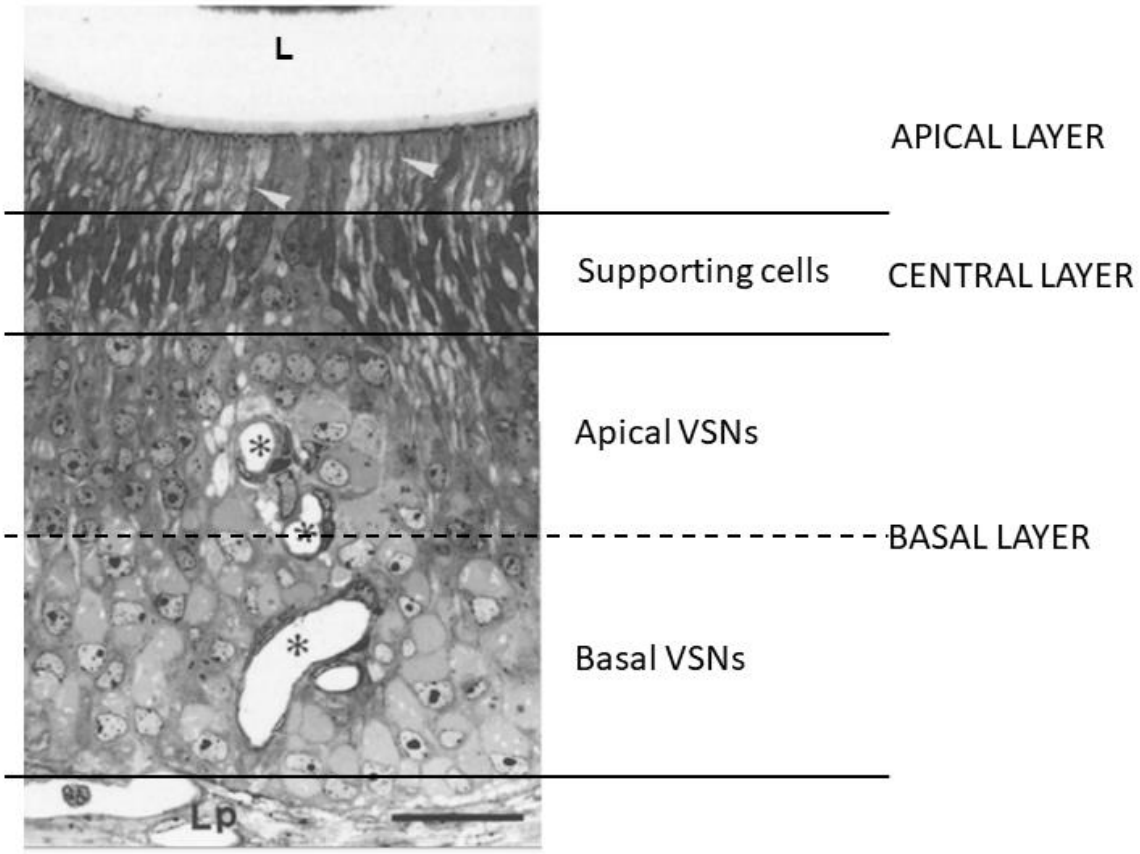


Figure 3. Cytoarchitecture of the mouse vomeronasal neuroepithelium. *Three regions can be distinguished in the neuroepithelium: an apical layer including the supranuclear portions of the supporting cells and the dendrites of the VSNs (narrows), a central layer of supporting cell, and a basal layer containing apical and basal neurons structurally and functionally distinct, however the boundary between the zones is diffuse. VSNs nuclei cover almost two thirds of the epithelial height. * =capillaries, Lp = lamina propria, L=lumen. Bar 30 µm (From Mendoza, 1993).*

1.3.2 Vomeronasal sensory neurons (VSNs)

The vomeronasal sensory epithelium is mainly composed of VSNs, which are bipolar neurons with a round-shaped soma (Fig. 4). From the apical part of the soma a long dendrite projects towards the lumen, the dendrite enlarges at the end in a knob from which many microvilli depart and protrude into the VNO lumen covering all the luminal surface. Microvilli in the lumen take contact with vomeronasal ligands embedded in the VNO's mucus. The signal transduction takes place at the level of the microvilli membrane. From the basal side of the soma an axon projects to the brain. Several axons from VSNs form fascicles and are organized in fiber bundles forming vomeronasal nerves. Vomeronasal nerves enter the cranial cavity and project to the accessory olfactory bulb (AOB , see section 1.8) (Mendoza, 1993; Takami, 2002; Tirindelli et al., 2009; Trotier and Døving, 1998). Based on the anatomical position and mostly on the expression of specific signaling proteins, VSNs are

divided into two populations: basal neurons positioned near the basal lamina and apical neurons placed near the luminal surface. The spatially segregated subsets of VSNs are also functionally different, indeed they use different vomeronasal receptors (see later Chapter 1.5.2) and G proteins. Apical neurons express $G_{\alpha i2}$ isoform in combination with the VR type-1 receptors (V1R), while basal neurons express the $G_{\alpha o}$ isoform in combination mainly with the VR type-2 receptors (V2R) (Fig. 4). Moreover, the two subsets of neurons project to different zones of the AOB (Dulac and Axel, 1995; Francia et al., 2014; Rodriguez, 2016; Ryba and Tirindelli, 1997).

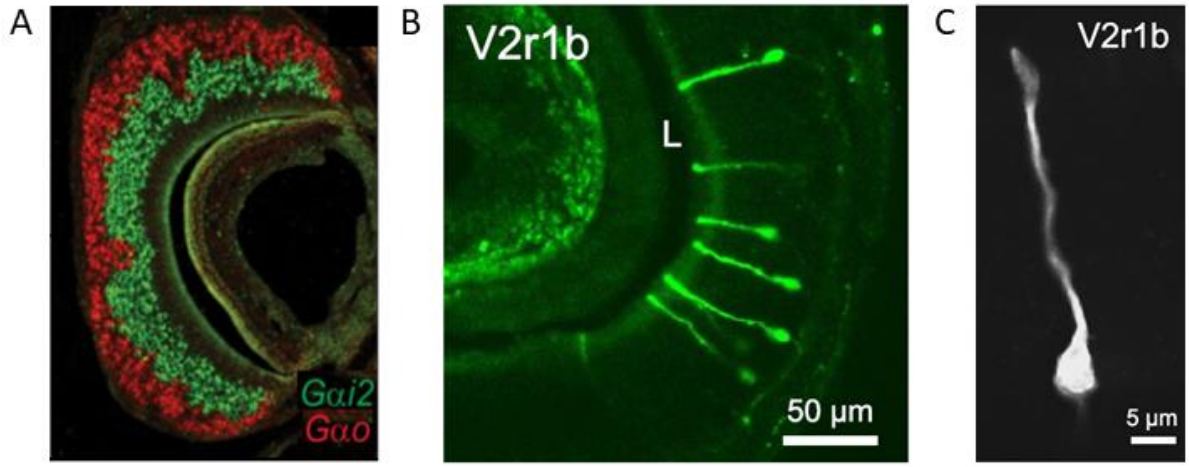


Figure 4. VSNs are bipolar neurons and are spatially segregated, based on receptor repertoire, in apical neurons expressing Gαi2-V1Rs and basal neurons expressing Gαo-V2Rs. (A) *The spatial segregation of VSNs expressing Gαi2 (apical VSNs, green) and Gαo (basal VSNs, red) visualized by two colors in situ hybridization in a coronal section of mouse VNO. Apical neurons co-express V1R receptors with Gαi2 protein while basal neurons co-express V2R receptors with Gαo protein (Modified from Leinders-Zufall et al., 2014).* ***(B)*** *The spatial localization of V2r1b-tau-GFP VSNs of genetically labelled cells from acute coronal VNO tissue slices 250 µm thick.* ***(C)*** *Magnification of a V2r1b-tau-GFP neuron from the slice in B showing the bipolar shape of VSNs with round soma and the knob at the end of the dendrite (fluorescent microscope, greyscale) (Modified from Ukhanov et al., 2007).*

1.4 VSN'S LIGANDS

Animals use a variety of different mechanisms for releasing pheromones into the environment. In many cases, the pheromonal release takes advantage of existing ways for excretion, such as urine and faeces, which may be placed in the environment as territorial marks; in other cases, chemical signals are released in secretions such as vaginal secretions, saliva, tears and other products of exocrine glands (Brennan, 2009). Six main categories of chemosensory ligands that stimulate VNO have been identified: exocrine gland-secreting peptides (ESPs), major histocompatibility complex

(MHC) peptide ligands, formyl-peptides (FPs), sulfated steroids, volatile small molecules and major urinary proteins (MUPs) (Zufall and Munger, 2016).

1.4.1 Mouse urine

Urine is a water-based solution and contains an assortment of inorganic salts and organic compounds, including proteins, hormones, and a good range of metabolites. Mouse urine consists of a complex mixture of chemosignals including a variety of small volatile molecules that are bound to MUPs. In addition, mouse urine also conveys information about individuality due to MHC peptides present in there, as described later. Urine is the most enriched source of pheromones, for this reason is commonly used in experiments to physiologically stimulate VSNs. When examined by high-performance liquid chromatography, urine can be fractionated in high molecular weight urinary fraction containing MUPs and MHC peptides, and low molecular weight fraction containing sulfated steroids and volatile ligands (Peele et al., 2003).

1.4.1.1 Volatile small molecules

Canonical methods of urine fractionation risk the loss of volatile compounds. Combining solid-phase microextraction and gas chromatography-mass spectrometry it was possible to identify small volatile molecules (Arnáiz et al., 2014; Ouyang et al., 2011). Male and female mouse urine differ in amount and type of volatile compounds present. Benzaldehyde is the main compound detected in all the stages of the female estrous cycle whereas it is less present in male urine samples (Arnáiz et al., 2014). In male urine samples, percentages of phenyl ethanone are higher than those detected in females. Terpenes are in general higher in males than in females. Some compounds have been detected exclusively in urine from one gender (Arnáiz et al., 2014). For example, 2-Heptanone, trans-5-Hepten-2-one, trans-4-Hepten-2-one, n-Pentyl-acetate are exclusively observed in female urine and are puberty-delaying pheromones for female mice. Other compounds, found in male urine, have the opposite effect of accelerating puberty in females: β-farnese, 2-sec-butyl-4,5-dihydrothiazol, 6-Hydroxy-6-methyl-3-heptanon (Novotny et al., 1999). Moreover, 2-sec-butyl-4,5-dihydrothiazol acts also as female attractant and induces the estrous synchronization (Jemiolo et al., 1986; Whitten, 1959).

1.4.1.2 Major Urinary Proteins (MUPs)

Volatile compounds in urine are unstable and need carriers to be released into the air from urine marks. These carriers not only extend their lifetime but also regulate the release of the scent substances based on their rate of dissociation. The MUPs family proteins bind small molecules in a

central hydrophobic pocket to concentrate and stabilize many volatile scent substances, thereby controlling both pheromone transport in circulation and pheromone release into the air (Beynon and Hurst, 2003; Tirindelli et al., 2009; Zhou and Rui, 2010). MUPs are synthetized and secreted by the liver and are excreted into the urine in the kidney.

Additionally, MUPs themselves may serve as chemical signals, indeed an atypical male-specific MUP20, named darcin, works as female attractant and elicit intermale aggression (Chamero et al., 2007; Demir et al., 2020; Kaur et al., 2014; Roberts et al., 2010). Moreover, MUP's family is extremely polymorphic and it has been reported that MUPs act as a type of individuality 'bar code' for the identity of the owner of the scent mark (Beynon et al., 2002).

1.4.1.3 Class I major histocompatibility complex peptides (MHC peptides)

The MHC antigens are cell-surface glycoproteins that provide a unique molecular signature for each individual essential for immune system response; MHC class I peptides are excellent candidates to be social recognition signals that convey information about genetic individuality. MHC peptides in normal rats and mice are constitutively excreted in the urine (Overath et al., 2014; Röck et al., 2007; Singer et al., 1997; Singh et al., 1987; Yamaguchi et al., 1981) and it has been reported that they also work as sensory stimuli for VSNs, that can discriminate single amino-acid variation peptides (Leinders-Zufall et al., 2004; Sturm et al., 2013). A possible role for the MHC peptides detection is to imprint the memory of the mating partner for mouse females: those peptides allow recently mated female mice to distinguish the urinary chemosignals of the mating male from those of an unfamiliar male (Leinders-Zufall et al., 2004; Zufall and Munger, 2016).

1.4.1.4 Sulfated Steroids

Many studies reported the responses of VSNs upon the exposure to natural or synthetic sulfated steroids, using different experimental approaches: calcium imaging, microelectrodes array, single cell recordings (Celsi et al., 2012; Cherian et al., 2014; Haga-Yamanaka et al., 2014; Nodari et al., 2008). Sulfated steroids include a big family of compounds that transmit an individual's physiological state, from pregnancy to stress conditions (Geyer et al., 2017; Nodari et al., 2008). For instance, sulfated estrogens are abundant in female urine during estrus and stimulate courtship behavior in male mice by binding the V1rj receptor in male VNO (Haga-Yamanaka et al., 2014). Moreover, a sulfated steroid isolated in male mice, Corticosterone 21-sulfate (cort21S), increases in urine during stress conditions indicating that its concentration in urine reflects the physiological status of the animal; furthermore, it was demonstrated that sulfatase treatment of urine-extracts caused their loss of activity, suggesting that sulfated compounds are the most active ligands for VSNs (Nodari et

al., 2008). From all the studies in which VSNs have been stimulated with sulfated steroids, it is clear that only the subpopulation of neurons that express V1R is activated by them (Haga-Yamanaka et al., 2014; Isogai et al., 2011; Nodari et al., 2008).

1.4.2 Exocrine gland-Secreting Peptides (ESPs)

Kimoto and colleagues (2005) investigated the VNO activation after exposure of BALB/c female mice to bedding soiled by adult male conspecific evaluating c-Fos signal as index of VSNs activation. They found a specific compound made exclusively in male mice able to trigger mating behavior in females. Shaved fur from male mice induced c-Fos expression in female VSNs only by direct contact suggesting the presence of non-volatile sex-specific compounds that originate in glands of adult male mice. They examined different exocrine glands concluding that the products of male extra orbital lacrimal glands can induce c-Fos expression in female VSNs. The compound found was a 7 kDa peptide able to activate a specific vomeronasal receptor (V2Rp5, Haga et al., 2010); they called the new peptide ESP1 and determined the gene encoding for it (Kimoto et al., 2005). *Esp1* gene turned out to be a member of a large multigene family with at least 38 members. From the 38 *Esp* genes, 15 are expressed in extra orbital lacrimal gland, the Harderian gland, and/or the submaxillary gland. Therefore, several ESPs are expected to be secreted in tear fluid or saliva. Moreover, ESPs expression appear to be hormonally regulated and sexually dimorphic (Kimoto et al., 2007; Touhara, 2007). Many studies demonstrated the role of ESPs in eliciting and regulating sexual behavior by activation of VSNs (Haga et al., 2010; Hattori et al., 2017)

1.4.3 Formyl-peptides (FPs)

Formylated peptides are produced by bacteria during infections and are actively secreted by invading pathogens or passively released from dead and dying host cells. (Dorward et al., 2015). The expression of receptors for FPs has been reported in mice (Rivière et al., 2009); it is not clear the role of FPs signaling but they may indicate the health status of an individual. The avoidance of sick conspecifics can be induced by FPs in rodents: the release of illness-related aversive odor cues from the sick individual serves to inhibit social investigation by healthy conspecifics (Arakawa et al., 2011; Boillat et al., 2015; Zufall and Munger, 2016).

1.4.4 Bile Acids

A new class of VSNs ligands have been identified by isolation of water-soluble chemosignals from female BALB/cJ faeces (Doyle et al., 2016). The active polar ligand that can activate mitral

cells in AOB are specific bile acids produced by liver: ω-muricholic acid, β-muricholic acid, cholic acid and deoxycholic acid. There are sex-specific differences in the concentrations and/or identities of faecal chemosignals because mitral cells discriminate the mouse gender of the faeces used as stimuli (Doyle et al., 2016). Recent data combining RNA-seq with live imaging showed that bile acids bind to a subpopulation of apical VSNs (Wong et al., 2020).

1.5 SENSORY TRANSDUCTION IN VSNS

1.5.1 General mechanisms of sensory transduction

Sensory transduction is the mechanism by which external chemical cues are transformed into electrical signals that can be processed by the central nervous system. This processes in VSNs start with the binding of a pheromone molecule with a G-protein coupled receptor (see 1.5.2 for further details), in turn the G-proteins Gαi2 or Gαo activate a phospholipase C (PLC) that, hydrolyzing PIP_2, produce two different second messengers: diacylglycerol (DAG) and inositol 1,4,5-trisphosphate (IP_3) (see 1.5.3). DAG seems to directly interact with the transient receptor potential channel type 2 (TRPC2) expressed in VSNs allowing the influx of sodium and calcium ions that depolarize the neurons (section 1.5.4). The increase in calcium concentration due to entry of calcium and/or the calcium released from the intracellular stores opens calcium-activated chloride channels promoting a further depolarization of the VSNs (Fig. 5) (section 1.5.5) (Døving and Trotier, 1998; Francia et al., 2014; Tirindelli et al., 2009). Furthermore, calcium ions are involved in many secondary events described in section 1.6; calcium activates a calcium-Calmodulin feedback which is involved in adaptation (Spehr et al., 2009) (section 1.7) and VSNs express potassium channels activated by calcium (Kim et al., 2012; Ukhanov et al., 2007; Zhang et al., 2008). The following sections are dedicated to single steps of the transduction signaling.

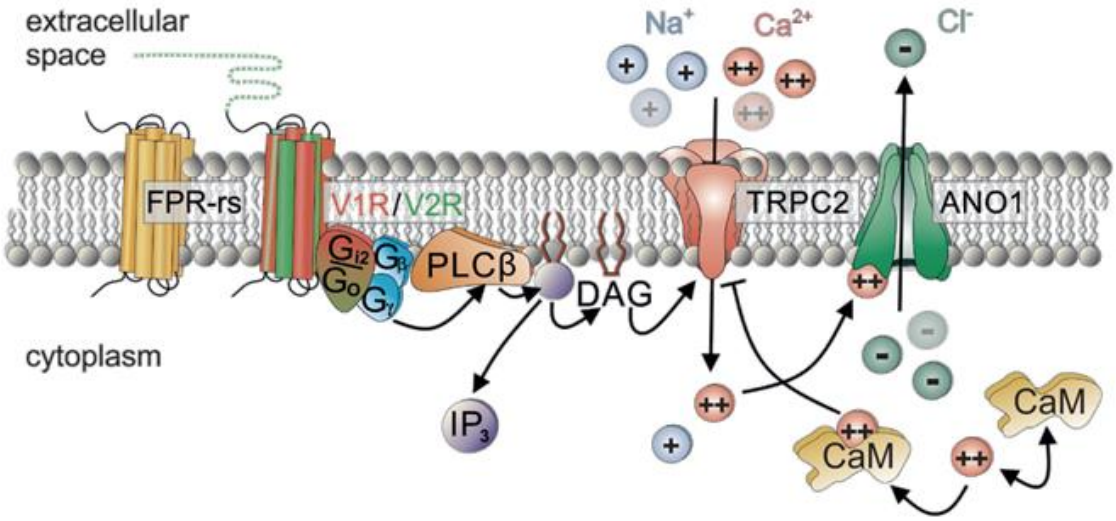


Figure 5. Signal transduction mechanisms in vomeronasal microvilli. *Model of signal transduction pathways of rodent VSNs. Downstream vomeronasal receptor (FPR, V1R or V2R) activation, a specific G protein (Gαi2 or Gαo) activates phospholipase C (PLC). Cleavage of phosphatidylinositol-4,5-bisphosphate (PIP2) into soluble inositol-1,4,5-trisphosphate (IP3) and membrane-bound diacylglycerol (DAG), results in gating of primary transduction channels TRPC2 by direct interaction with DAG. The Ca2+ entered through TRPC2 has different targets including calcium-activated chloride channels, likely TMEM16A (also named ANO1) (Modified from Mohrhardt et al., 2018).*

1.5.2 Vomeronasal Receptors

The neuroepithelium in the VNO is organized in two main layers of VSNs expressing two families of VRs: type-1 (V1R) and type-2 (V2R). Both receptors belong to the seven-transmembrane G protein-coupled receptor (GPCR) family (Dulac and Axel, 1995; Weis and Kobilka, 2018). V1Rs co-express with Gαi2 proteins in the apical layer of the vomeronasal organ, whereas the V2Rs are coupled with Gαo protein and are expressed in the basal layer of the vomeronasal epithelium (Dulac and Axel, 1995; Matsunami and Buck, 1997; Ryba and Tirindelli, 1997; Silva and Antunes, 2017). The spatial segregation is maintained also in the projections, indeed apical neurons send axons to the anterior part of the AOB instead, basal neurons project to the posterior part of the AOB (Belluscio et al., 1999; Rodriguez et al., 1999)

There are two additional classes of receptors expressed in both apical and basal regions: the formyl-peptide receptors (FPRs) (Dulac and Torello, 2003; Liberles et al., 2009) and a family of non-classical molecules of the MHC, H2-Mv, expressed selectively in basal neurons (Ishii et al., 2003; Loconto et al., 2003; Silvotti et al., 2007).

1.5.2.1 V1Rs

V1Rs are seven transmembrane domain receptors identified in 1995 (Dulac and Axel, 1995). V1Rs are part of rhodopsin-like family GPCRs. The proteins are about 300 amino acids long, with short extracellular and intracellular N- and C-termini, respectively (Rodriguez, 2016). Mouse V1R genes, *Vmn1rs*, have a very simple structure of one or two non-coding exon(s) followed by a single coding exon. In the mouse genome, 392 *Vmn1r* genes are present and 239 seem to be functional (Rodriguez, 2016; Rodriguez et al., 2002; Young et al., 2010). According to their sequence similarities, V1Rs are divided in 12 subfamilies in the mouse, named from V1Ra to V1Rl. Between 1 – 4% of the VSNs show a non-overlapping expression of several V1Rs indicating that VSNs follow the one cell one receptor rule, where just one receptor is expressed in a given VSN, similar to odorant receptors (ORs) expression in olfactory sensory neuron in the main olfactory epithelium (Dulac and Axel, 1998; Nagai et al., 2016). At the functional level, V1Rs seem to be mainly associated with the detection of small volatile molecules involved in gender discrimination and sexual behaviors, indeed the deletion of a cluster of V1R genes in mice can cause dramatic behavioral alterations, including reduced male libido and inappropriate maternal aggressive behavior (Boschat et al., 2002; Liberles, 2014; Del Punta et al., 2002; Silva and Antunes, 2017).

1.5.2.2 V2Rs

In mice, the V2R family comprises 61 intact genes, called *Vmn2rs*, out of a total of 209 genes including pseudogenes; the coding sequence is split into multiple exons (usually 6 exons) but only a single large exon encodes for the seven transmembrane part of the receptor (Rodriguez, 2016; Touhara, 2007). V2Rs possess a long extracellular N-terminus that is common to calcium-sensing and metabotropic glutamate receptors. The long N-terminus interacts with the MHC class Ib and V2Rs expressing neurons participate in sensing MHC peptides (Mombaerts, 2004; Silva and Antunes, 2017; Touhara, 2007). The expression of V2Rs/Gαo-coupled protein is restricted to the basal neuroepithelium (Dulac and Axel, 1998; Matsunami and Buck, 1997; Ryba and Tirindelli, 1997; Tirindelli et al., 1998). In the mouse, V2R gene products are classified into four families named from A to D that are functionally different: single nucleotide polymorphisms contribute to define the families and result in cluster of V2Rs tuned to detect specific cues (e.g. predatory or non-predatory cues) (Wynn et al., 2012). Individual basal neurons express a multimolecular complex constituted by three receptors: V2Rs from family-C are expressed by the entire population of basal neurons (Martini et al., 2001) and are co-expressed with family-A or -B or -D and with MHC Ib (Silvotti et al., 2007). Therefore, V2Rs do not strictly follow the rule of mutually exclusive expression as V1Rs and ORs

(Dulac and Axel, 1998; Nagai et al., 2016; Rodriguez, 2016). In general, at the functional level, V2Rs are involved in the detection of water-soluble proteinaceous ligands and control of pheromone-induced male-male aggression (Chamero et al., 2012; Silva and Antunes, 2017; Yang et al., 2005); potential ligands for V2Rs include peptide pheromones such as MUPs, MHC peptides, and ESPs (Haga et al., 2010; Kimoto et al., 2007; Leinders-Zufall et al., 2004).

1.5.2.3 FPRs

In 2009, five of the seven members of the FPRs' family were reported to be expressed in rodent VSNs (Liberles et al., 2009; Rivière et al., 2009). Usually, FPRs are immune cells' receptors and recognize peptides produced by bacteria and compounds related to pathogenic states. While two transcripts are strictly present in mice immune cells, *Fpr-rs2* and *Fpr-rs5*, the others, *Fpr-rs1*, *Fpr-rs3*, *Fpr-rs4*, *Fpr-rs6* and *Fpr-rs7*, have been found exclusively in vomeronasal tissue extracts and the expression seems to be limited to rodent species (Rodriguez, 2016). Fpr-rs1 is mainly present in basal VSNs, whereas Fpr-rs3-4-6-7 are co-expressed with Gαi2 proteins in the apical layer. The functional expression of these types of receptors means that the VNO can sense compounds related to pathogens, exhibiting also stereoselectivity (Bufe et al., 2012; Rivière et al., 2009).

1.5.2.4 H2-Mv

In 2003, the expression of genes of the MHC family that belong to a nonclassical class I gene (or class Ib gene) were reported in VSNs, originally designated Mb1 (Ishii et al., 2003; Singer et al., 1988). The expression of the Mb1 genes has been found spatially restricted to a small population of cells placed in the basal layer of the vomeronasal epithelium. At least 50% of basal neurons express the multigene family of nonclassical class I MHC, H2-Mv, co-expressed with the family-C of V2Rs. H2-Mv are present selectively in the basal part of the basal layer of the VNO (Ishii et al., 2003; Ishii & Mombaerts, 2008; Loconto et al., 2003; Silvotti et al., 2007). The lack of H2-Mv in mice greatly decreased VSNs' sensitivity to MHC peptides and mice display pronounced deficits in aggressive and sexual behaviors. However, H2-Mv genes are not necessary for the generation of these physiological responses, but are required for ultrasensitive chemodetection by a subset of VSNs (Leinders-Zufall et al., 2014).

1.5.3 Phospholipase C (PLC) and diacylglycerol (DAG)

The enzymatic role of PLC is to hydrolyze phosphatidylinositol-4,5-bisphosphate (PIP_2) into inositol-1,4,5-trisphosphate (IP_3) and diacylglycerol (DAG); many studies reported the role of IP_3 and DAG produced by PLC as principal second messengers in VSNs of different species (Inamura et

al., 1997a; Kroner et al., 1996b; Taniguchi et al., 2000). In mice, the use of the PLC inhibitor U73122 causes the block of the activity in VSNs (Holy et al., 2000; Spehr et al., 2002). The PLCβ family is the most expressed in VSNs based on RNA-seq data. Moreover, different isoforms of PLCβ play distinct roles in pheromone signal transduction. For instance, MUP-responsive neurons express PLCβ2 isoform, while PLCβ4 is dominant in non-MUP stimuli detection (Dey et al., 2015). Fascinatingly, PLCβ2 expression is regulated by the estrous cycle, this finding provides a new insight into the regulation of sensory perception by endocrine state (Dey et al., 2015; Stowers and Liberles, 2016).

The roles of PLC, IP_3 and DAG are numerous; it has been reported that DAG as well as its metabolites (e.g. arachidonic acid) can directly target membrane proteins acting as second messengers (M. Spehr et al., 2002; Zhang et al., 2010). DAG can directly activate DAG-gated channels, indeed different DAG analogues activate an inward current in membrane patch of knob/microvilli from dissociated VSNs; the current evoked by DAG analogues is similar to the currents evoked by pheromones and is strongly reduced, but not abolished, in *Trpc2*$^{-/-}$ mice (Lucas et al., 2003). It has been shown also that the activation of photoswitchable DAG (PhoDAG-3) can reversibly promote cation currents in VSNs. Moreover, by combining photostimulation with calcium imaging it has been observed that PhoDAG-3 activation promotes a calcium transient that is absent in VSN from *Trpc2*$^{-/-}$ mice (Leinders-Zufall et al., 2018). These data suggest the direct interaction between DAG and TRPC2 channels and sustain the role of DAG in its gating.

IP_3 is usually associated with a large calcium release from internal stores (Bezprozvanny et al., 1991; Parker and Yao, 1991). In rat VSNs, dialysis of IP_3 induces inward currents and many authors have proposed the direct involvement of IP_3 in gating ionic channels (Inamura et al., 1997b; Takami, 2002); indeed the inhibition of IP_3 receptors by ruthenium red blocks the urine-evoked activity in rat VSNs suggesting an IP_3-dependent pathway in pheromone signaling (Inamura et al., 1997a). However, it has been shown that depletion of intracellular calcium stores does not affect urine responses in rat VSNs, suggesting that the urine-induced increase in intracellular calcium is not primarily dependent on intracellular calcium stores; furthermore, the block of IP_3-mediated calcium release by Xestospongin C does not change the urine-evoked calcium signal increase (Spehr et al., 2002). IP_3 receptors are expressed in VSNs: while the type 2 receptors have a sexually-dimorphic expression, the type 3 receptors colocalize with TRPC2 forming a protein-protein interaction complex and are expressed throughout the sensory epithelium including the receptor zone and the apical processes (Brann et al., 2002). However, a more recent study reported that IP_3 receptors type 3 in VSNs are not required for activation of VSN sensory currents suggesting that IP3R type 3 is

dispensable for VSNs' responses (Chamero et al., 2017). The role of IP_3 in signal transduction is not yet clear, more evidence supports the hypothesis that IP_3 could be involved in secondary signaling process, but it is not involved in the primary pathway of urine perception.

1.5.4 Transient receptor potential channel, subfamily C, type 2 (TRPC2)

Cyclic-nucleotide gated ion channels are involved in olfactory transduction in olfactory sensory neurons of the main olfactory epithelium (Pifferi et al., 2006) but not in VSNs. Only the β subunits of these channels were identified in rat VSNs and do not form a functional channel when expressed alone in heterologous cell types (Berghard et al., 1996; Broillet and Firestein, 1997). Cyclic nucleotides dialyzed in VSNs in whole cell configuration failed to develop any current, supporting the idea that VSNs transduction differ from olfactory transduction (Liman and Corey, 1996). In 1999, Liman and colleagues found a specific expression of the transient receptor potential channel type 2 (TRPC2) in the rat VNO. The intense staining only in a highly limited region at the dendritic tip of VSNs containing the sensory microvilli, the proposed site of sensory transduction, suggests its role in signaling processes (Liman et al., 1999). Two groups independently show alteration in behavioral responses and in VSNs activity in TRPC2-deficient mice (Leypold et al., 2002; Stowers et al., 2002). Extracellular action potential recordings show that VSNs from $TRPC2^{-/-}$ mice are electrically active but unable to respond to dilute urine, in the same way, pheromone-induced VNO field potential responses were either absent or strongly diminished, depending on the stimulus concentration. Both studies conclude that TRPC2 is a component of the VSN signal transduction machinery. *Trpc2*$^{-/-}$ mice have defects in sexual and in aggressive behaviors, showing anomalous male-male mating and absence of intermale aggression (Leypold et al., 2002; Stowers et al., 2002; Zufall, 2005). Notably, basal neurons are more affected by the absence of TRPC2 than apical neurons; *Trpc2*$^{-/-}$ mice show a selective loss of basal layer, more than 50% of basal VSNs, while the apical layer appears intact (Kim et al., 2012; Ron Yu, 2015; Stowers et al., 2002), and show a reduction of posterior AOB size (Hasen and Gammie, 2009). From the selective loss of basal neurons two inferences arise: the TRPC2 is necessary for the correct development of the VNO and basal neurons from *Trpc2*$^{-/-}$ mice die since inactive; and TRPC2 is not the only ion channel involved in the VSNs transduction, but new components are still unknown because of the reduction of VSNs responses instead of the total loss of them (Leypold et al., 2002), thus apical neurons still alive should have a complementary way of activation. It is important to notice that in mouse it has been reported that a subclass of olfactory sensory neurons express TRPC2 and therefore the interpretation of the behavioral phenotypes of *Trpc2*$^{-/-}$ mice is questionable (Omura and Mombaerts, 2014).

1.5.5 Calcium-activated chloride channels (CaCCs)

During the last decade, many publications showed the presence of an additional current involved in primary vomeronasal signaling. This current is mainly carried by chloride ions and shows a dependence on intracellular calcium (Dibattista et al., 2012; Kim et al., 2011; Yang and Delay, 2010). The spatial and temporal controlled release of calcium using photolysis of caged-calcium around the VSNs' knobs directly activates a large chloride current in the apical portion of dissociated VSNs; the ionic nature of the current has been determined by the ionic replacement of chloride in extracellular solutions with other anions methanesulfonate or isothiocyanate resulting in the shift of the reversal potential of the calcium induced current (Dibattista et al., 2012). The chloride current in dissociated VSNs is abolished using blockers of CaCCs as NFA, CaCCinh-A01, A9C and DIDS in whole-cell recorded VSNs (Amjad et al., 2015; Dibattista et al., 2012). RT-PCR experiments and immunohistological data suggested the molecular identity of the calcium-activated chloride current: TMEM16A and TMEM16B are both expressed in microvilli of apical and basal VSNs (Fig. 6), site of the transduction machinery (Billig et al., 2011; Dauner et al., 2012; Dibattista et al., 2012; Münch et al., 2018).
The strong evidence of the identity of CaCCs in VSNs comes from the recordings on dissociated neurons from cKO *Tmem16a* mice showing that TMEM16A is necessary to mediate the calcium activated chloride current in VSNs (Amjad et al., 2015). Indeed, calcium-activated chloride currents were abolished in VSNs from cKO *Tmem16a* mice (Amjad et al., 2015).

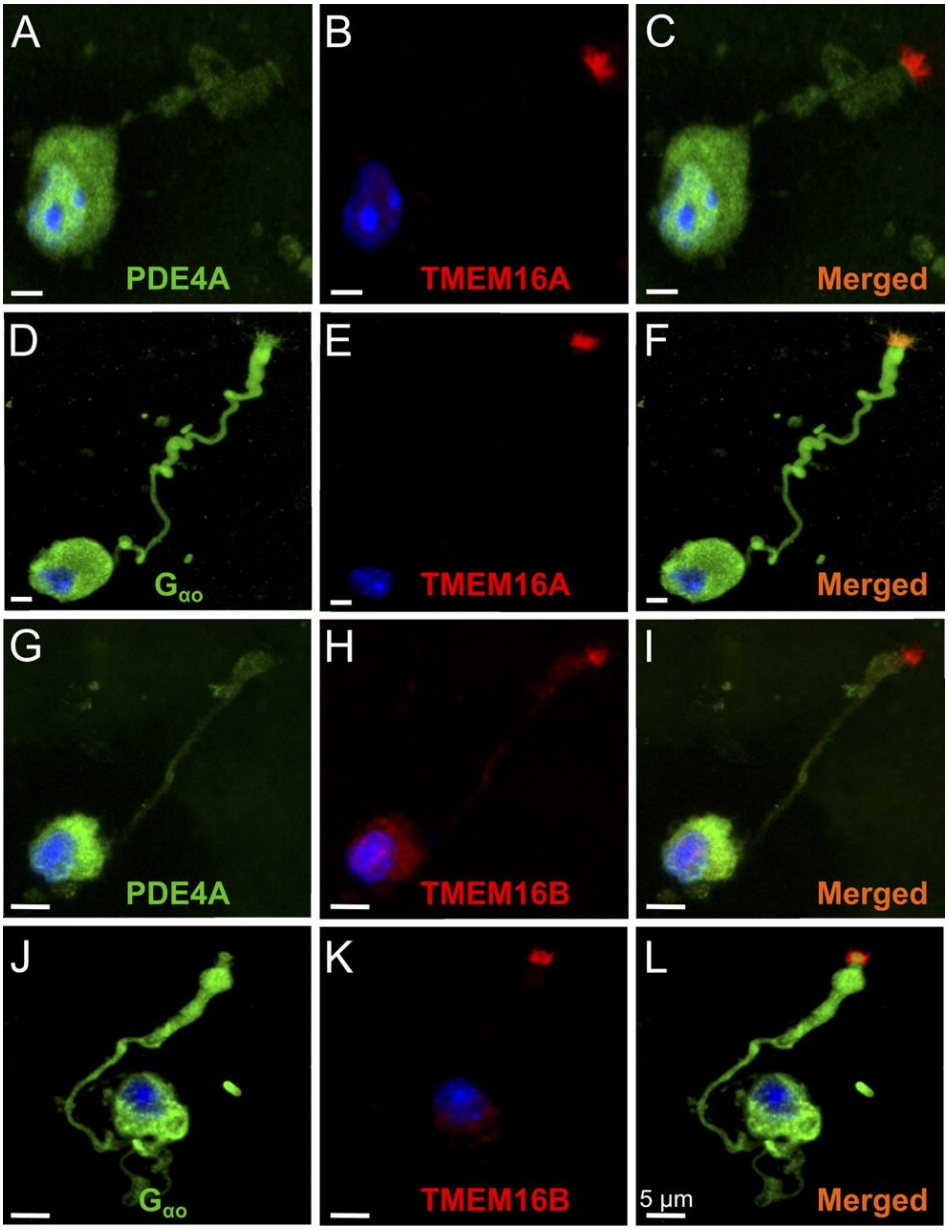


Figure 6. TMEM16A and TMEM16B are expressed in the microvilli of both apical and basal vomeronasal sensory neurons. *TMEM16A is expressed in the microvilli of both dissociated apical neurons labeled with anti-PDE4A* ***(A–C)****, and dissociated basal neurons, labeled with anti-Gαo antibody* ***(D–F)****; PDE4A and Gαo are two specific markers for apical and basal layers. TMEM16B is also located in the microvilli of both apical* ***(G–I)*** *and basal* ***(J–L)*** *neurons. Bars, 5 µm (From Dibattista et al., 2012).*

It has been demonstrated in dissociated VSNs, using whole-cell and perforated patch clamp recordings, that the chloride current acts as a downstream element able to amplify the initial cation current, indeed chloride is the main component of the urine-evoked current leading up to 80% of it (Yang and Delay, 2010). Calcium must be present outside (Yang and Delay, 2010) and/or inside (Kim et al., 2011) the VSNs' microvilli to allow the activation of chloride current: calcium ions can flow through TRPC2 channels, likewise, the calcium

released by intracellular stores can promote chloride currents. Moreover, the urine-evoked current in *Trpc2*$^{-/-}$ mice is completely blocked by inhibition of IP_3-triggered intracellular calcium release (Kim et al., 2011).
However, the physiological role of TMEM16A and TMEM16B-mediated currents is still unknown. Kim and co-workers (2011) demonstrated that both spontaneous and urine-evoked firing activities are eliminated by blockers of calcium-activated chloride channels (Kim et al., 2011).
Moreover, Münch and colleagues (2018) performed experiments in VSNs from the double KO mice model where *Tmem16a* and *Tmem16b* were deleted; they show that the lack of CaCCs results in drastically diminished urine-evoked spiking of VSNs and a reduction in the percentage of VSNs showing spontaneous firing, but the contribution of both channels in modulating the firing was not completely elucidated by their experiments. Conversely calcium-activated chloride currents were still present in mice lacking TMEM16B supposing a minor role of it in bulking calcium-activated chloride currents (Münch et al., 2018). Nevertheless, in *Tmem16a/Tmem16b* double KO mice they do not report any corresponding deficits in male-male territorial aggression in contrast with the results reported in *Trpc2* KO mice or after VNO ablation (Leypold et al., 2002; Maruniak et al., 1986; Münch et al., 2018; Stowers et al., 2002). Since TMEM16B is expressed also in olfactory neurons, the behavioral experiments on *Tmem16b* KO could be biased by olfactory deficits. Moreover, in olfactory neurons the TMEM16B deletion affects the firing pattern of spontaneous and stimulus-evoked activity (Pietra et al., 2016) confirming that calcium-activated chloride currents are involved in modulating the firing of the cells more than leading an all-or-none effects.
Thus, the controversy on the role of TMEM16A and TMEM16B in modulating the VNO signaling is nowadays open. A central point that should be crucial is the value of the chloride equilibrium potential, indeed the contribute of chloride in depolarizing or hyperpolarizing VSNs depends on the direction of the flux of chloride ions. Thus, the physiological role of calcium-activated chloride currents is a direct function of the chloride equilibrium potential. The chloride intracellular concentration was estimated to be around 40-80 mM, depending on the experimental approaches; although differing in methodology and quantitative results, it has been reported that chloride currents amplify overall response in VSNs. Therefore, based on the chloride concentration in the mucus from MOE between 55 and 84 mM (Billig et al., 2011; Kleene, 2008; Reuter et al., 1998) and assuming the same chloride concentration in VNO fluids, elevated chloride level in VSNs provides the electrochemical driving force necessary to boost sensory responses by a depolarizing chloride efflux (Kim et al., 2015; Untiet et al., 2016).

1.6 ELECTRICAL PROPERTIES OF VSNS

In VSNs, it has been reported several ion conductances involved in secondary events, downstream the transduction processes, carry by different ion channels: Nav channels, L-type and T-type calcium channels, BK, SK and GIRK channels for potassium, HCN2-4 channels (Dibattista et al., 2008; Fieni et al., 2003; Kim et al., 2012; Liman and Corey, 1996; Zhang et al., 2008). Urine

stimulation of a VSN generates a receptor current which depolarize the membrane till it reaches the firing threshold and sodium channels opening initiates the spike generation.

Near resting condition in VSNs (-70 mV) the sodium current is completely available showing an activation $V_{m1/2}$ at -44.7 mV at holding potential of -70 mV and an inactivation $V_{h1/2}$ at -56.2 mV (Dean et al., 2004; Fieni et al., 2003; Liman and Corey, 1996; Shimazaki et al., 2006). Sodium currents in VSNs are held by two components that differ in sensitivity to TTX; the TTX-insensitive steady-state inactivation is shifted by 30 mV in the hyperpolarizing direction compared with the TTX-sensitive component (Liman and Corey, 1996). Basal VSNs expressing V2R1b receptor show bigger sodium currents with respect to apical neurons expressing V1R2b receptor (Fieni et al., 2003; Ukhanov et al., 2007). This difference in sodium current amplitude could be extended to apical and basal VSNs, and could be explained by the segregation of different isoforms of Nav channels observed in immunohistological experiments in which Nav1.2 expression is restricted to basal VSNs somata, dendrites, and dendritic knobs, while Nav1.6 staining is detectible in VSNs of both apical and basal VNO layers (Bolz et al., 2017).

Mouse VSNs express at least two current components related to the activity of voltage-activated calcium channels: a low-voltage–activated T-type current and an L-type current (Fieni et al., 2003; Liman and Corey, 1996; Ukhanov et al., 2007). Both L- and T-type Cav channels could underlie low-threshold calcium spikes and contribute to action-potential–dependent calcium entry in VSNs; they promote a much more prominent calcium current in basal cells than in apical cells (Fieni et al., 2003; Ukhanov et al., 2007).

Calcium entry in VSNs is linked also with the activation of calcium-activated potassium channels BK responsible for the repolarization of neurons, therefore block of L-type Cav channels by nimodipine caused action potential broadening and a loss of afterhyperpolarization, together with an increase in the inter-spike interval (Ukhanov et al., 2007). BK channels play an inhibitory role in signal transduction, their blockage has as consequence the increase of the transduction current amplitude and the firing rate in VSNs stimulated with urine (Zhang et al., 2008). Other ion channels are involved in the secondary event of the VNO signaling, two additional potassium channels are highly expressed in VSNs, the small conductance calcium-activated potassium channel (SK) and the G protein–activated inwardly rectifying potassium channel (GIRK) (Fig.7). Those channels participate in the urine-evoked activity in depolarizing direction given the high potassium concentration (50 mM) in the mucus filling the VNO (Kim et al., 2012).

In VSNs is identifiable an I_h current modulated by cAMP and likely mediated by HCN4 and/or HCN2 channels; the I_h might contribute to setting the membrane resting potential and increase the

sensitivity to elicit action potentials in response to small current injections (Dibattista et al., 2008; Liman and Corey, 1996; Trotier et al., 1993, 1998).

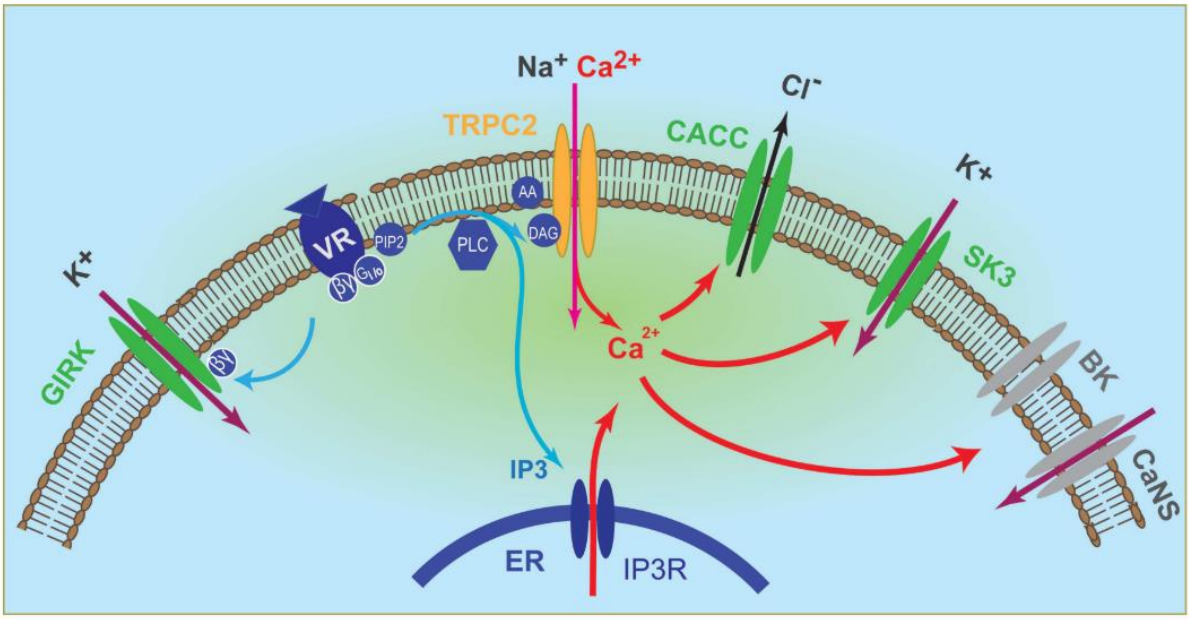


Figure 7. Secondary events downstream the transduction cascade. *Primary events in blue. The influx of calcium through TRPC2 channels boosts the secondary events. Increase in intracellular calcium levels activates calcium-activated chloride conductance (CACC) and the small conductance calcium-activated potassium channel SK3. Activation of G protein also releases βγ subunits, which activate the G-protein activated inward rectifier channel (GIRK). Both GIRK and SK3 mediate influx of potassium to depolarize the VSN because of a high extracellular potassium concentration in the vomeronasal luminal mucus. Increase in cytosolic calcium level can also activates the large conductance calcium-activated potassium channel BK and an unidentified calcium-activated non-selective (CaNS) cationic channel in the dendrite or in the cell body (From Yu, 2015).*

1.7 Adaptation in VNO: the state of art

Among the secondary events, peripheral adaptation is the most decisive in all sensory systems. Peripheral sensory adaptation is an initial mechanism for experience-driven feedback in the nervous system. The relevant advantage coming from sensory adaptation is the extension of the dynamic range of signals detection associated with a shift in the stimulus–response curve to higher concentrations/intensities (Kurahashi and Menini, 1997; Torre et al., 1995). Odor adaptation refers to the ability of the olfactory system to adjust its sensitivity at different stimulus intensities, an operation that is likely to be essential for preventing saturation of the cellular transduction machinery and allowing the retention of high sensitivity during continuous or repetitive odor stimulation (Zufall and Leinders-Zufall, 2000). Sensory adaptation can be defined as neuronal plasticity and in olfactory neurons three different forms of odor adaptation are identifiable: short-term adaptation,

desensitization, long-lasting adaptation (Zufall and Leinders-Zufall, 2000). The lower response observed in salamander and newt olfactory neurons after a conditional odor stimulation that recover within ten seconds is called short-term adaptation (Kurahashi and Shibuya, 1990; Zufall and Leinders-Zufall, 1998). The comparison of the properties of adaptation induced by consecutive brief odor pulses with adaptation induced by photolysis of caged cAMP (the second messenger involved in odor transduction) results in no differences; in solitary olfactory neurons from newt, adaptation occurs entirely downstream from adenylyl cyclase and the cyclic-nucleotide gated (CNG) channel is the only target of modulation (Kurahashi and Menini, 1997). The repetitive photorelease of 8-Br-cAMP, a cAMP analogue resistant to hydrolyzation, confirm the occurrence of fast adaptation mechanisms that works independently from the hydrolysis of cAMP in mouse olfactory neurons (Boccaccio et al., 2006). Indeed the calcium-calmodulin feedback that operate on CNG channels is the mechanism underlying the olfactory sensory adaptation (Balasubramanian et al., 1996; Bradley et al., 2001, 2004; Kurahashi and Menini, 1997; Liu et al., 1994; Munger et al., 2001). Instead, the term desensitization is referred to a combination of mechanisms involving G-protein coupled receptors rapid loss of responsiveness in the continuing or recurring presence of an agonist or stimulus (Kato and Touhara, 2009). These mechanisms include uncoupling of receptor from heterotrimeric G proteins in response to receptor phosphorylation (Dawson et al., 1993) and the internalization of cell surface receptors to the cytosol (Antunes et al., 2014). Recent data propose a stochastic kinetic model based on electrophysiological data that confirm the vesicle cycling of G-protein coupled receptors regulated through G-protein coupled receptors kinase 3 (GRK3)-dependent receptors internalization and consecutive recycling (re-sensitization) (Antunes et al., 2014). The last example of plasticity in olfaction is the long-lasting adaptation, a persistent form of adaptation. Long-lasting adaptation occurs after high stimulus strength, and it is associated with a generation of a persistent background current that recovers in 6.5 min period without odor stimulation. The mechanism underlying this long-term plasticity involved carbon monoxide/cyclic GMP second messengers: it is promoted by endogenous release of carbon monoxide leading to stimulation of soluble guanylyl cyclase (sGC) and subsequent cGMP formation, indeed was completely abolished by agents that are known to inhibit the function of the carbon monoxide-producing enzyme heme oxygenase type 2 (HO-2) (Zufall and Leinders-Zufall, 1997). cGMP may be involved in several important long-term cellular responses to odor stimulation (Kroner et al., 1996a) and sGC can be stimulated also by nitric oxide (Pietrobon et al., 2011).

Because of the time-dependence of the onset of odor adaptation, the temporally dynamic properties of the process must also play critical roles in determining the temporal response assets of

the olfactory system (Moore, 1994). By the other hand, the temporal properties of AOB neurons' responses have been determined in behaving conscious animals and reveals that the detection of pheromonal cues by the AOB is far slower compared with processing times in the MOB; this suggests that the accessory olfactory system is not designed to sense fleeting changes in the chemical environment (Luo et al., 2003). In AOB the optimal stimulus identification is achieved in 10-15 seconds after the onset and decoding using fine temporal ranges is not favored (Yoles-Frenkel et al., 2018). VSNs have been thought to lack any form of sensory adaptation as observed in multielectrode recordings from intact vomeronasal epithelium (Holy et al., 2000). More recent studies demonstrate different form of adaptation in VSNs using several approaches. Using a combination of in situ calcium imaging and electrophysiology extracellular recordings, Wong and colleagues found evidence for short- and long-term adaptation on repeated stimulation at defined intervals (Wong et al., 2018). Via the immunological detection of the S6 ribosomal protein phosphorylation it has been reported the existence of a filtering mechanism to adapt the VNO to a persistent stimulation with pheromonal cues (Silvotti et al., 2018). Moreover, there is a modulation at level of sensory transduction machinery that promote adaptation by a calcium-calmodulin feedback, indeed the presence of calcium-calmodulin is sufficient to block DAG-analogues evoked currents in dissociated VSNs and the calcium-calmodulin inhibitors can revert adaptation in field potential recordings by electro-vomeronasogram and in whole cell recordings. (Spehr et al., 2009). It remains to be determined how spike frequency adaptation affects the encoding of different classes of chemical cues in the VNO.

1.8 CENTRAL PATHWAY

The VSN axonal projections towards the AOB maintain the spatial segregation of V1R- and V2R-expressing VSN cell bodies in the VNO. Indeed V1R-expressing VSNs from the apical layer of the VNO project axons to the anterior portion of the AOB and make synapses with rostral mitral cells, while VSNs from basal layer that express V2Rs innervate the posterior region of the AOB and make synapses with caudal mitral cells. VSNs that share the same receptor identity converge onto mitral cells in 6-10 glomeruli. This organization into mixed glomeruli is suited to integrate sensory information (Belluscio et al., 1999; Mucignat-Caretta, 2014b; Rodriguez et al., 1999; Zufall and Munger, 2016). The lack of connection to a known cortical region may indicate that VNO-mediated olfaction provides a direct route into limbic system to rapidly initiate specialized behaviors. From the glomerular layer, the second order mitral and tufted cells directly projects to amygdala nuclei

including medial amygdala, bed nucleus of the stria terminalis, nucleus of the lateral olfactory tract and anterior amygdala (Mohrhardt et al., 2018). In general, the amygdala works as vigilance system for information and establishes their positiveness for individuals' fitness and survival. The amygdala can directly engage the hypothalamus that is the central nuclei for the homeostasis preservation and releasing hormones (Fig.8).

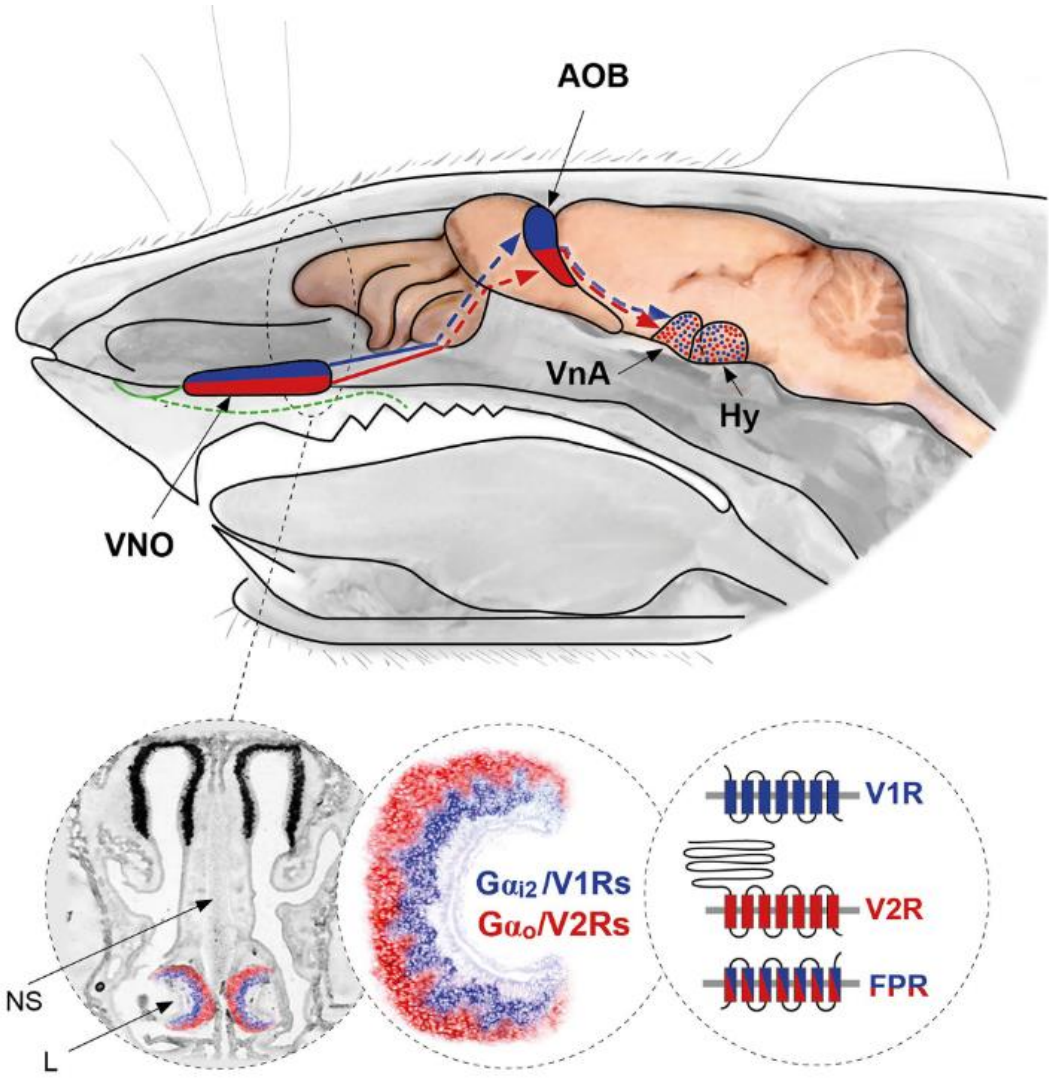


Figure 8. The VSNs project to AOB. *Midsagittal view of a mouse head showing the the vomeronasal organ (VNO) and its projections to the accessory olfactory bulb (AOB). The cross section of the head shows the position of the VNO (red/blue) relatively to the nasal cavity, nasal septum (NS), VNO lumen (L). The magnified cross sections of the VNO is represented by two colors according to the dichotomic G-protein (Gαi2 and Gαo) and vomeronasal receptor expression (V1Rs and V2Rs). Gαi2 expressing neurons project to the anterior accessory olfactory bulb (AOB) while Gαo expressing neurons, to the posterior AOB. Second order AOB neurons project to the bed nucleus of the stria terminalis (not shown) and to the vomeronasal amygdala (VnA), which includes the medial amygdaloid nuclei, the posteromedial cortical amygdaloid nucleus, the bed nucleus of the accessory olfactory tract, and the ventral and dorsal components of the anterior amygdala. Third order*

neuronal fibers are sent to several hypothalamic areas (Hy) including the ventromedial hypothalamus and medial preoptic areas (Modified from Tirindelli, 2021).

1.9 TMEM16A AND TMEM16B

TMEM16 proteins belong to a widespread protein family of "transmembrane proteins with unknown function 16," abbreviated as TMEM16. The TMEM16 family of genes has been proposed to encode calcium-activated chloride channels (CaCC) proteins. This family includes nine members labelled with letters from A to K, excluding I (Milenkovic et al., 2010). In 2008, three independent laboratories identified TMEM16A, also known as anoctamin-1, as a CaCC and suggested a role for TMEM16A in glandular (mammary, salivary) secretion. One team, by bioinformatic approach, identified TMEM16A and its CaCC function by expression cloning in HEK-293 cells and small interfering RNA knockdown in mouse salivary glands (Yang et al., 2008). The same year, the increase of CaCC activity in airway epithelial cells has been associated with TMEM16A gating by microarray analysis that demonstrates that TMEM16A showed an ion channel activation, inhibition, and anion selectivity profile consistent with airway CaCCs (Caputo et al., 2008). In the end, expression cloning approach identified TMEM16A as CaCCs (Schroeder et al., 2008). Collectively, TMEM16A demonstrates many of the characteristics required of a candidate gene for CaCC proteins. Because of anionic conductance of TMEM16A, and a putative structure with eight transmembrane domains, anoctamin was proposed as alternative name for TMEM16 protein family. However, not all members from TMEM16 family are anionic channels and cryo-electron microscopy revealed a structure with ten transmembrane domains (Paulino et al., 2017a, 2017b). Thus, the name anoctamin is not the most appropriate to refer to TMEM16 protein family.

Not all TMEM16 proteins mediate CaCCs, some members of the family are also involved in a variety of functions that include ion transport, phospholipid scrambling, and regulation of other membrane proteins (Dibattista et al., 2017; Falzone et al., 2018; Hartzell et al., 2009; Rock et al., 2009). Only TMEM16A and TMEM16B, encode for CaCCs, a type of ion channel that plays important functions such as transepithelial ion transport, smooth muscle contraction, olfaction, phototransduction, nociception, and control of neuronal excitability (Pedemonte and Galietta, 2014).

TMEM16A and TMEM16B are closely related members of TMEM16 family sharing about 62% of amino acids (Milenkovic et al., 2010). Despite similar biophysical properties, TMEM16A and TMEM16B differ in calcium sensitivity and activation/deactivation kinetics; TMEM16A channels have a half effective calcium concentration of about 0.4 – 0.6 μM at positive membrane potentials (Ferrera et al., 2009), while TMEM16B channels are less sensitive, with 1 – 3 μM of half effective calcium concentration at positive membrane potentials (Pifferi et al., 2009). Moreover, TMEM16B shows a 10-fold much faster activation/deactivation kinetic than TMEM16A (Caputo et al., 2008; Pifferi et al., 2009). TMEM16A and TMEM16B are directly gated by sub-micromolar/micromolar concentrations of intracellular calcium, and the apparent calcium-sensitivity depends on membrane voltage: the current-voltage relationship is linear at high

calcium intracellular concentration, while shows outward rectification at low intracellular calcium concentration (Fig. 9).

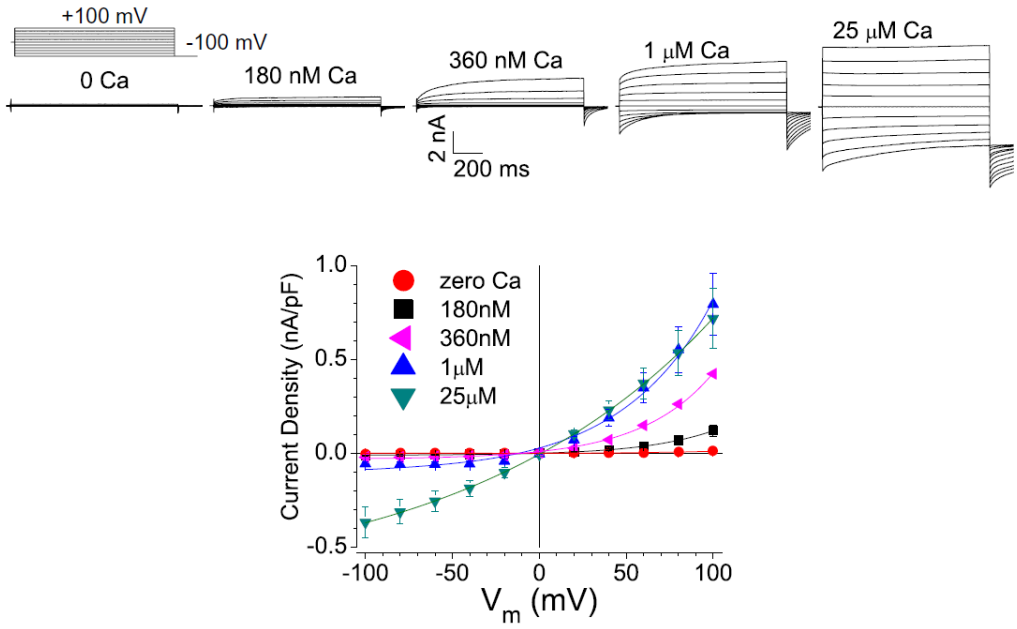


Figure 9. TMEM16A mediated currents modulated by intracellular Ca^{2+} and membrane potential. *Whole-cell voltage-clamp recording from different HEK cells transfected with mTMEM16A. The voltage steps raging from –100 to 100 mV with a holding potential of 0 mV elicited TMEM16A currents with different steady-state current–voltage relationships in presence of different amount of free intracellular calcium (Modified from Xiao et al., 2011).*

Voltage changes the apparent affinity for calcium (Hartzell et al., 2004; Huang et al., 2012b; Pedemonte and Galietta, 2014; Xiao et al., 2011). TMEM16A and TMEM16B channels are also activated by other divalent cations, such as barium, strontium, and nickel, while zinc has instead an inhibitory effect (Stephan et al., 2009). Saturating calcium stimulation for prolonged time causes a time-dependent CaCCs decrease resulting in channels desensitization (Huang et al., 2012b; Pedemonte and Galietta, 2014). The phenomenon is called “rundown” or “desensitization” and it has been observed in both TMEM16A mediated currents (Dang et al., 2017) and also in transfected HEK-293T cells with TMEM16B (Pifferi et al., 2009), however the mechanism underlying the rundown is still unknown. It has been shown that PIP_2 regulates TMEM16A channel gating (Ta et al., 2017; Tembo et al., 2019) and it has been proposed an involvement of PIP_2 depletion in the rundown (Le et al., 2019).

By cryo-electron microscopy and complementary electrophysiological characterization of pore mutants, the structure of mouse TMEM16A was defined (Paulino et al., 2017a, 2017b). The presence of two ion conduction pores independently activated by calcium (Jeng et al., 2016; Lim et al., 2016) suggests the dimeric structure of the channel, that is confirmed by the cryo-structure which reveals the location of two pores, each contained within a single subunit of the dimeric protein (Paulino et al., 2017b). The entire

TMEM16 family follows the same general architecture (Brunner et al., 2014): they are homodimers, each subunit contains ten transmembrane helices, α1–α10 connected by loop regions of variable length (Brunner et al., 2014; Dang et al., 2017). Both termini are located on the cytoplasmic side of the membrane. The α-helices and β-strands of the amino-terminal domain are organized in a ferredoxin-like fold. The channel cavity consists of transmembrane α-helices 6 and 7, which are part of a conserved calcium-binding site and are involved in ion conduction influencing ion selectivity (Fig. 10) (Brunner et al., 2014; Yu et al., 2012).

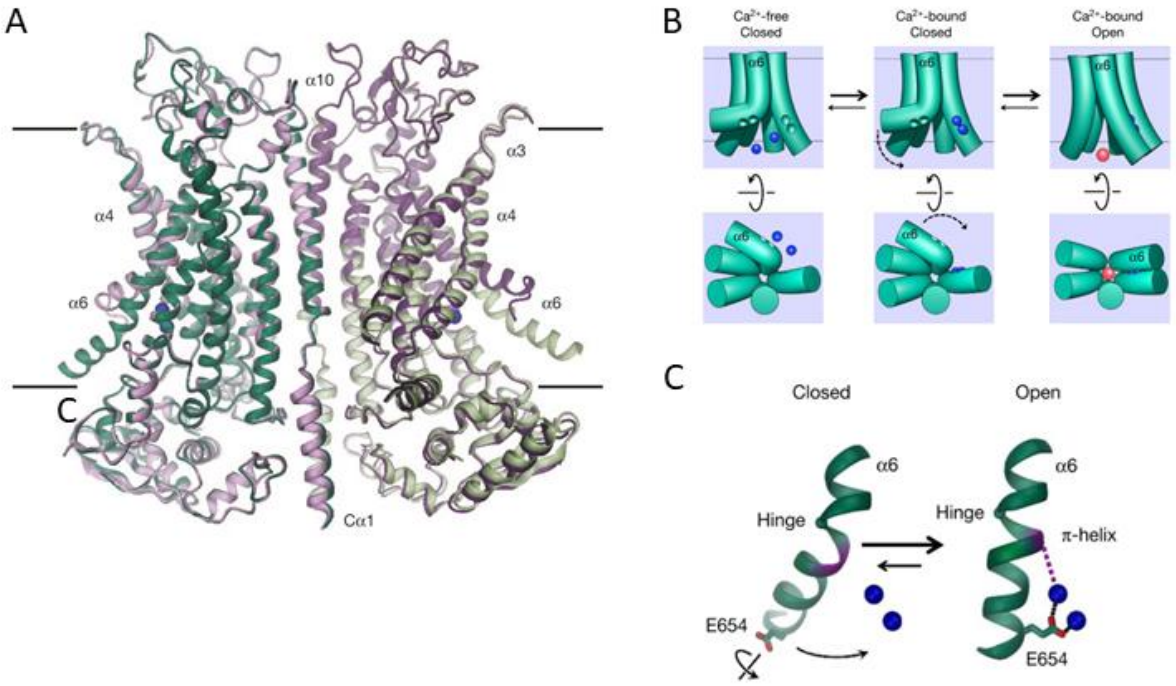


Figure 10. Structures of the mouse TMEM16A channel. ***(A)*** *Ribbon representation of a superposition of the Ca^{2+}-bound (green) and Ca^{2+}-free (violet) structures of mTMEM16A; subunits are shown in light and dark shades of the corresponding colour. The view is from within the membrane, with the extracellular side at the top. Black lines, membrane boundaries.* ***(B)*** *Schematic depiction of the activation of TMEM16A. Top panels are viewed from within the membrane, bottom panels from the intracellular side. Green cylinders, pore-lining helices; blue spheres, calcium ions; red spheres, chloride ions.* ***(C)*** *Conformational changes in α-6 on calcium binding, blue spheres, calcium ions. (From Paulino et al., 2017).*

As revealed by structures of TMEM16A in the presence of zero, one, and two calcium ions, the calcium unbinding causes the rearrangement of transmembrane α-helices 6, while the rest of the protein remains almost unchanged. In the absence of calcium, the intracellular portion of α-helix 6 moves away from the α-helix 7 resulting in a pore constriction (Fig.7). The α-helix 6 appears to serve as a key allosteric connection through which calcium, voltage, and extracellular chloride act to regulate the opening of the TMEM16A pore (Dang et al., 2017; Paulino et al., 2017a, 2017b; Peters et al., 2018). Each TMEM16A monomer forms an independent subunit cavity gated by two calcium-binding sites.

2 AIMS

Many aspects of the VNO signal transmission require further investigation and the aims of this work are in this direction. While some molecular players of the transduction machinery are known, the physiological role of many putative components of the transduction cascade remains unclear. An undefined aspect is related to the role of calcium-activated chloride currents in VSNs signaling; the other debated point is on the mechanisms underlying the peripheral sensory adaptation of the AOS. The experiments in the following sections try to elucidate some aspects of the evoked responses modulation in VSNs at peripheral level.

The first objective is to clarify the physiological role of TMEM16A and TMEM16B chloride channels in VSNs spontaneous and evoked activity.

The second goal is to establish the origin of VSNs' adaptation mechanisms and identify a molecular player involved in adaptive evoked response.

3 RESULTS

3.1 TMEM16A AND TMEM16B MODULATE PHEROMONE-EVOKED ACTION POTENTIAL FIRING IN MOUSE VOMERONASAL SENSORY NEURONS

eNeuro

Research Article: New Research

Sensory and Motor Systems

TMEM16A and TMEM16B Modulate Pheromone-Evoked Action Potential Firing in Mouse Vomeronasal Sensory Neurons

Andres Hernandez-Clavijo,[1] Nicole Sarno,[1] Kevin Y. Gonzalez-Velandia,[1] Rudolf Degen,[2] David Fleck,[2] Jason R. Rock,[3] Marc Spehr,[2] Anna Menini,[1] and Simone Pifferi[1,4]

https://doi.org/10.1523/ENEURO.0179-21.2021

[1]Neurobiology Group, SISSA, International School for Advanced Studies, Trieste 34136, Italy, [2]Department of Chemosensation, Institute for Biology II, RWTH Aachen University, Aachen D-52074, Germany, [3]Center for Regenerative Medicine, Boston University School of Medicine, Boston 02118, MA, and [4]Department of Experimental and Clinical Medicine, Università Politecnica delle Marche, Ancona 60126, Italy

Abstract

The mouse vomeronasal system controls several social behaviors. Pheromones and other social cues are detected by sensory neurons in the vomeronasal organ (VNO). Stimuli activate a transduction cascade that leads to membrane potential depolarization, increase in cytosolic Ca^{2+} level, and increased firing. The Ca^{2+}-activated chloride channels TMEM16A and TMEM16B are co-expressed within microvilli of vomeronasal neurons, but their physiological role remains elusive. Here, we investigate the contribution of each of these channels to vomeronasal neuron firing activity by comparing wild-type (WT) and knock-out (KO) mice. Performing loose-patch recordings from neurons in acute VNO slices, we show that spontaneous activity is modified by *Tmem16a* KO, indicating that TMEM16A, but not TMEM16B, is active under basal conditions. Upon exposure to diluted urine, a rich source of mouse pheromones, we observe significant changes in activity. Vomeronasal sensory neurons (VSNs) from *Tmem16a* cKO and *Tmem16b* KO mice show shorter interspike intervals (ISIs) compared with WT mice, indicating that both TMEM16A and TMEM16B modulate the firing pattern of pheromone-evoked activity in VSNs.

Key words: ion channel; sensory; TMEM16; vomeronasal

Significance Statement

Vomeronasal sensory neurons (VSNs) express two Ca^{2+}-activated chloride channels TMEM16A and TMEM16B, however their physiological role is still unclear. Using a loss of function approach, we found that TMEM16A modulates the pattern of VSN spontaneous spike activity, while TMEM16A and TMEM16B reduced the instant frequency of pheromone-evoked activity. These new findings call for a reconsideration of the patterns of the peripheral coding of sensory stimuli.

Introduction

Most mammals use at least two distinct olfactory systems to detect chemicals: the main and the accessory (vomeronasal) olfactory system. In general, pheromones affect the physiology and/or behavior of an individual by activating either one or both systems (Tirindelli et al., 2009; Touhara and Vosshall, 2009; Mohrhardt et al., 2018).

Chemical signals bind to chemosensory neurons in the vomeronasal organ (VNO), a bilateral cylindrical structure within a cartilaginous capsule located beneath the septum

Received April 22, 2021; accepted July 6, 2021; First published August 25, 2021.
The authors declare no competing financial interests.

Author contributions: A.H.-C., N.S., K.Y.G.-V., R.D., D.F., M.S., A.M., and S.P. designed research; A.H.-C., N.S., K.Y.G.-V., R.D., and D.F. performed research; J.R.R. contributed unpublished reagents/analytic tools; A.H.-C., N.S., K.Y.G.-V., R.D., D.F., M.S., A.M., and S.P. analyzed data; A.H.-C., N.S., R.D., M.S., A.M., and S.P. wrote the paper.

(Døving and Trotier, 1998). Vomeronasal sensory neurons (VSNs) are bipolar neurons with a single apical dendrite that has a terminal swelling (knob) with several microvilli, where vomeronasal receptors (V1Rs, V2Rs, FPRs) are located and sensory transduction occurs. Each VSN expresses one type or few types of vomeronasal receptors, and axons from VSNs expressing the same receptor project to various glomeruli in the accessory olfactory bulb (AOB; Rodriguez et al., 1999; Francia et al., 2014).

Vomeronasal receptor-ligand binding activates a G-protein mediated signaling pathway involving phospholipase C activation. Phosphoinositide turnover activates transient receptor potential canonical 2 (TRPC2) channels allowing the influx of Na^+ and Ca^{2+} (Liman et al., 1999; Lucas et al., 2003; Leinders-Zufall et al., 2018). In parallel, Ca^{2+} release from intracellular stores has also been described (Kim et al., 2011). Ultimately, VSN signal transduction generates membrane depolarization and action potentials that are sent to the AOB.

The increase in intracellular Ca^{2+} concentration on activation of the transduction cascade has several physiological effects, including the activation of Ca^{2+}-activated chloride channels (Yang and Delay, 2010; Kim et al., 2011; Dibattista et al., 2012; Amjad et al., 2015). At least two members of the TMEM16 family, TMEM16A and TMEM16B, form Ca^{2+}-activated chloride channels and are expressed in several different tissues (Caputo et al., 2008; Schroeder et al., 2008; Yang et al., 2008; Pifferi et al., 2009a; Stephan et al., 2009; Pedemonte and Galietta, 2014). Interestingly, although TMEM16A and TMEM16B are individually expressed in different cell types, they co-express in microvilli of VSNs (Dibattista et al., 2012; Münch et al., 2018). Not many other cell types are known to co-express TMEM16A and TMEM16B. Indeed, to our knowledge, the only other cells that have been shown to functionally express both proteins are pinealocytes (Yamamura et al., 2018). Therefore, studying the role of these channels in the VNO is helpful to understand how VSNs respond to pheromones and contributes to understanding their individual role in other cells co-expressing them.

In isolated VSNs, Amjad et al. (2015) have shown that the biophysical properties of Ca^{2+}-activated chloride currents, measured both in whole-cell and in inside-out patches from the apical neuronal region, resemble those of TMEM16A, rather than TMEM16B channels. Moreover, Ca^{2+}-activated chloride currents were abolished in VSNs from *Tmem16a* conditional knock-out mice (cKO), demonstrating that TMEM16A is a necessary component of Ca^{2+}-activated chloride channels in mouse VSNs (Amjad et al., 2015; Münch et al., 2018). Different results were obtained in *Tmem16b* KO mice, with a study reporting the lack of Ca^{2+}-activated chloride currents in VSNs (Billig et al., 2011) and another one showing that disruption of *Tmem16b* only insignificantly reduced those currents (Münch et al., 2018).

In this study, we investigated the individual roles of TMEM16A and TMEM16B in controlling physiological VSN activity. We compared spontaneous and stimulus-induced firing in wild-type (WT), cKO for *Tmem16a* or mCherry *Tmem16b* KO (Zhang et al., 2017) mice. We found that only TMEM16A is involved in spontaneous firing patterns, while both TMEM16A and TMEM16B modulate the firing pattern of pheromone-evoked activity in VSNs.

Materials and Methods

Animals

Mice were handled in accordance with the Italian Guidelines for the Use of Laboratory Animals and European Union on animal research, under a protocol approved by the ethics committee of Scuola Internazionale Superiore di Studi Avanzati (SISSA) and approved by Italian Ministry of Health.

The generation of *Tmem16a* cKO mice has been previously described in detail (Amjad et al., 2015). *Tmem16a* cKO mice were homozygous for the floxed *Tmem16a* alleles and heterozygous for *Cre* and *Omp* (Li et al., 2004; Faria et al., 2014; Schreiber et al., 2015). *Tmem16a*$^{fl/fl}$ mice were used as controls.

mCherry *Tmem16b* KO mice were kindly provided by Lily Jan (University of California, San Francisco, Zhang et al., 2017) and were generated by inserting *mCherry* sequence with a farnesylation signal at the C terminus (mCherry-F) in frame with the alternative start ATG codon in the third exon of *Tmem16b*, therefore membrane associated mCherry marks neurons that normally express *Tmem16b* (Zhang et al., 2017; see their Fig. S2C).

V2r1b-tau-GFP mice were provided by Peter Mombaerts (Max Planck Research Unit Neurogenetics, Frankfurt, Germany; Rodriguez et al., 1999).

All experiments were performed on tissues from two to three months old mice of either sex. All experiments and data analysis were performed by researchers who were blind to the mouse genotype.

Immunohistochemistry

VNO sections and immunohistochemistry were obtained as described previously (Dibattista et al., 2012; Amjad et al., 2015). The following primary antibodies were used: polyclonal goat anti-TMEM16A (1:200; sc-69 343, Santa Cruz), polyclonal rabbit anti-TMEM16B (1:500; NBP1-90739, Novus), rabbit anti-RFP (1:500;

This work was supported by Deutsche Forschungsgemeinschaft (DFG; German Research Foundation) Grants 368482240/GRK2416 (to R.D. and M. S.) and the German Academic Scholarship Foundation (to R.D.).

Acknowledgements: We thank Anna Boccaccio (CNR, Genova), Michele Dibattista (University of Bari A. Moro), and all members of the laboratory for discussions; Elettra Grdina, Angel Pascual Camerota, Lorenzo Maschietto, Giovanni Tamburin, and Cristina Degrassi (SISSA) for mice handling and Helena Krmac and Christina Vlachouli for mice genotyping; Corinna H. Engelhardt, Stefanie Kurth, and Jessica von Bongartz (RWTH-Aachen University) for excellent technical assistance; and Paul A. Heppenstall (SISSA, Trieste) for providing mCherry antibody.

Correspondence should be addressed to Anna Menini at menini@sissa.it or Marc Spehr at m.spehr@sensorik.rwth-aachen.de.

https://doi.org/10.1523/ENEURO.0179-21.2021

Copyright © 2021 Hernandez-Clavijo et al.

This is an open-access article distributed under the terms of the Creative Commons Attribution 4.0 International license, which permits unrestricted use, distribution and reproduction in any medium provided that the original work is properly attributed.

600-401-379, Rockland), goat anti-OMP (1:1000; 544-1001, Wako). The following secondary antibodies obtained from Life Technologies (dilution; catalog number) were used: donkey anti-rabbit Alexa Fluor 594 Plus (1:500; A32754), donkey anti-goat Alexa Fluor 488 Plus (1:500; A32814). Immunoreactivity was visualized with a confocal laser scanning microscope (Nikon A1R). Images were acquired using NIS-Elements Nikon software (at 1024-$\times$1024-pixel resolution) and were not modified other than to balance brightness and contrast. Nuclei were stained by DAPI. Control experiments without the primary antibodies gave no signal.

Clarity and imaging

Brains and VNOs from adult mice (V2R1b-GFP-TMEM16A$^{fl/fl}$-OMP/OMP and V2R1b-GFP-TMEM16A$^{fl/fl}$-OMP/Cre) of both sexes were dissected. Brains were further sliced in 3 mm coronal sections including the AOB. To maintain structural integrity, the tissue was fixed overnight at 4°C in hydrogel fixation solution containing 4% acrylamide, 0.05% bis-acrylamide, 0.25% VA-044 Initiator (Wako Chemicals), 4% PFA in PBS. After polymerization, lipids were removed by passive clearing. The samples were incubated at 37°C for two months in 4% SDS and 200 mM boric acid at pH 8.5. The buffer was changed every other week. During the last clearing cycle, the nuclear marker DRAQ5 (1:1000, Thermo Fisher Scientific) was added to each sample. After washing steps, samples were incubated for 24 h in RIMS80, containing 80 g Nycodenz (PROGEN Biotechnik), 20 mM PS (phosphate buffer, pH 7.5), 0.1% Tween 20, and 0.01% sodium azide. Imaging was performed using a Leica SP8 DLS microscope equipped with a 488 and 633 nm diode laser, an HC PL FLUOTAR 5$\times$/0.15 IMM DLS observing objective, an L 1.6$\times$/0.05 DLS illuminating objective and a DLS TwinFlect 7.8 mm Gly mirror cap that creates the lightsheet. Specimens were positioned in a custom-made 3D-printed chamber.

Data were analyzed using IMARIS 9.5.1 (Oxford Instruments). AOB glomerular volume was determined by measuring the volume of all fluorescently labeled glomerular structures within the AOB. VNO cell density was measured by counting the number of fluorescently labeled cells in a defined volume of vomeronasal sensory epithelium (VNE). MATLAB R2019b (MathWorks) was used for plotting and statistical analysis. CorelDRAW 2019 (Corel Corporation) was used for figure preparation.

Preparation of acute slices of mouse VNO

Acute slices of mouse VNO were prepared as previously described (Shimazaki et al., 2006; Dibattista et al., 2008; Wong et al., 2018). In brief, the VNO was removed and transferred to ice-cold artificial CSF (ACSF) containing the following: 120 mM NaCl, 20 mM $NaHCO_3$, 3 mM KCl, 2 mM $CaCl_2$, 1 mM $MgSO_4$, 10 mM HEPES, and 10 mM glucose, pH 7.4. The capsule and all cartilaginous tissues were carefully removed and the two halves of the VNO were isolated from the vomer bone. Each half of the VNO was then separately treated. The VNO was embedded in 3% Type I-A agarose (Sigma) prepared in ACSF once the agar had cooled to 38°C. Upon solidification, the agar block was fixed in a glass Petri dish and sliced with a vibratome (Vibratome 1000 Plus Sectioning System) at 200 to 250 μm thickness in oxygenated ACSF solution. Slices were then left to recover for $>$30 min in chilled and oxygenated ACSF before electrophysiological experiments were initiated.

Electrophysiological recordings from VSNs and stimuli presentation

Slices were viewed with an upright microscope (Olympus BX51WI) by infrared differential contrast optics with water immersion 20$\times$ or 60$\times$ objectives. The slice preparation maintained the VNO cross-sectional structure and many individual VSNs could be clearly distinguished by their morphology. Whole-cell or loose-patch recordings were obtained using patch pipettes pulled from borosilicate capillaries (WPI) with a PC-10 puller (Narishige) with a resistance of 3–6 MΩ. Recordings were obtained with a Multiclamp 700B amplifier controlled by Clampex 10 via a Digidata 1440 (Molecular Devices). Data were low-pass filtered at 2 kHz and sampled at 10 kHz. Experiments were performed at room temperature (20–25°C). The recording chamber was continuously perfused with oxygenated (95% O_2, and 5% CO_2) ACSF by gravity flow. The slice was anchored to the base of the recording chamber using a homemade U-shaped silver wire, holding down the agar support without touching the slice itself.

Membrane properties and inward and outward voltage-gated currents were measured in the whole-cell configuration with a KCl based intracellular solution containing the following: 80 mM K-gluconate, 60 mM KCl, 10 mM NaCl, 1 mM $MgCl_2$, 0.023 mM $CaCl_2$, 10 mM HEPES, and 10 mM EGTA, adjusted to pH 7.2 with KOH.

For recordings of Ca^{2+}-activated currents, we used a CsCl based intracellular solution containing the following: 140 mM CsCl, 10 mM HEPES, and 10 mM HEDTA, adjusted to pH 7.2 with CsOH. The nominally 0 Ca^{2+} solution contained no added Ca^{2+}. The 1.5 μM free Ca^{2+} solution was obtained by adding 3.209 mM $CaCl_2$. The added concentration was the same as that previously used to obtain 1.5 μM free Ca^{2+} experimentally determined by Fura-4F (Invitrogen) measurements by using a LS-50B luminescence spectrophotometer (PerkinElmer; Pifferi et al., 2006, 2009a, b) and based on calculation with the program WinMAXC (C. Patton, Stanford University, Stanford, CA; Patton et al., 2004).

Extracellular recordings from the soma of VSNs were obtained in the on-cell loose-patch configuration with seal resistances of 40–100 MΩ. Pipette solution was ACSF, as the bath solution, and the recordings were made in voltage-clamp mode with a holding potential of 0 mV.

Stimuli were focally delivered through a gravity-fed multivalve perfusion system (ALA-VM8, ALA Scientific Instruments). The tip of the perfusion head, with a diameter of 360 μm, was placed $\sim$500 μm away from the slice. The time delay of the stimulus was measured using a

high-K^+ ACSF solution. To avoid mechanical artifacts, the slice was constantly perfused with ACSF and the flow out of the pipette was switched between ACSF and stimulus solutions. This results in a constant flow across the epithelium and sharp concentration transients, undiluted by the bath ACSF.

Urine collection and stimulus solutions

Urine was collected from both sexes C57BL/6 mice, filtered with a 0.2-μm filter, and frozen at −80°C. Before use, male and female urines were mixed in a 1:1 ratio, and the mixture was diluted to 1:50 in ACSF (pH 7.4). As mouse urine contains urea and K^+, which could potentially cause neurons to fire by direct membrane depolarization, we used artificial urine diluted 1:50 in ACSF as a negative control. Artificial urine contained the following: 100 mM NaCl, 40 mM KCl, 20 mM NH_4OH, 4 mM $CaCl_2$, 2.5 mM $MgCl_2$,15 mM NaH_2PO_4, 20 mM $NaHSO_4$, and 333 mM urea, pH 7.4 adjusted with NaOH (Holy et al., 2000). To test cell viability, we used a high K^+ solution (25 mM KCl) by replacing equimolar amounts of NaCl with KCl in ACSF. Diluted urine or artificial urine stimuli were applied in 10-s pulses with an interstimulus interval of at least 4 min to avoid desensitization or adaptation processes (Spehr et al., 2009; Wong et al., 2018). High K^+ solution was applied in 5-s pulses. All compounds and chemicals were obtained from Sigma-Aldrich, unless otherwise stated.

Analysis of electrophysiological data

IgorPro software (WaveMetrics) and Clampfit (Molecular Devices) were used for data analysis and figure preparation. In loose-patch, slow changes in the baseline were corrected by filtering the recordings offline with a high-pass filter at 2 Hz. Spikes were initially detected using an event detection tool using an arbitrary threshold, and then confirmed by shape inspection. For spontaneous activity, the mean firing activity was estimated by dividing the number of spontaneous spikes by the duration of recordings in the absence of stimuli. Interspike interval (ISI) was calculated by measuring the time between each consecutive spike. Each ISI distribution was obtained by grouping the ISIs in bins, as indicated in the figures, and normalized by dividing the value for each bin by the total number of ISIs. The values in *y*-axes represent the percentage of spikes in each bin and the area under the curve is 100%.

For VSNs showing a high spontaneous activity, it was difficult to identify a urine response from a single recording. To avoid false positives, we applied at least three repetitive stimulations. Each recording was 90 s long divided into 40 s of prestimulus, 10 s of stimulus, and 40 s of poststimulus. To analyze the response to urine for a single cell we took the basal period (40 s prestimulation) and stimulus period (10 s of stimulation), and we calculated the basal and the stimulation frequency for each trace. We defined a threshold level as: $BF + 2^*\sigma^2$, where BF is the average of basal frequency for all the traces and σ^2 is the SD of the basal frequency. A cell was considered responsive to urine if: (1) the average spike frequency was above threshold during stimulation; and (2) there was no response to diluted artificial urine.

Statistical analysis

Data are presented as mean ± SEM, with *n* indicating the number of neurons. VSNs were obtained from at least five (whole-cell recordings) or 10 (loose-patch recordings) different WT or mutant mice. Normal distribution of the data was tested with the Shapiro–Wilk test or with the Jarque–Bera test. For normally distributed data, statistical significance was determined using unpaired Student's *t* tests. For multiple comparison of the data, we used Dunn–Hollander–Wolfe test after Kruskal–Wallis analysis. Kolmogorov–Smirnov test was used to compare cumulative distributions. *p*-values <0.05 were considered significant. Statistical analysis was performed with IgorPro software (Wavemetrics).

Results

TMEM16A and TMEM16B expression in the vomeronasal epithelium

TMEM16A and TMEM16B are co-expressed in microvilli of mouse VSNs (Dibattista et al., 2012; Münch et al., 2018) but their functional role is unclear. By immunohistochemistry, we confirmed that TMEM16A and TMEM16B are expressed at the apical surface of the vomeronasal epithelium of WT mice (Fig. 1*A*), whereas TMEM16A or TMEM16B immunoreactivity was absent, as expected, in *Tmem16a* cKO and *Tmem16b KO* mice, respectively.

mCherry *Tmem16b* KO mice (Zhang et al., 2017) allow visualization of those cells that normally express TMEM16B by membrane staining with farnesylated mCherry. Figure 1*B* clearly shows co-expression of OMP and mCherry in VSNs, confirming the expression of TMEM16B in VSNs and excluding TMEM16B expression in supporting cells of the VNO.

Ca^{2+}-activated chloride currents in VSNs from WT, *Tmem16a* cKO, and *Tmem16b* KO mice

To determine the respective contributions of TMEM16A and TMEM16B to Ca^{2+}-activated chloride currents in VSNs, we used intracellular solutions with nominally 0 Ca^{2+} or with 1.5 μM free Ca^{2+} and obtained whole-cell voltage-clamp recordings from the soma of neurons in acute VNO slices from WT, *Tmem16a* cKO, and *Tmem16b* KO mice (Fig. 2). To avoid contributions from K^+ currents (Ca^{2+}-activated or voltage-activated), the pipette solution contained Cs^+ instead of K^+. Figure 2*A* shows representative VSN recordings (holding potential V_{hold} = 0 mV) from each mouse line at voltage steps between −100 and +100 mV, followed by a step to −100 mV. In agreement with previous results (Amjad et al., 2015), we confirmed that VSNs from *Tmem16a* cKO mice lacked a significant Ca^{2+}-activated chloride current in the presence of 1.5 μM Ca^{2+}. Indeed, the average currents measured at steady state in 0 Ca^{2+} (−15 ± 3 pA at −100 mV and 326 ± 38 pA at +100 mV, $n = 6$) or in 1.5 μM Ca^{2+} (−62 ± 13 pA at −100 mV and 236 ± 41 pA at +100 mV, $n = 14$) were not significantly different (Fig. 2*B*). Furthermore, VSN currents activated by voltage steps in *Tmem16a* cKO mice did not show any time dependence (red and green traces), whereas WT currents in 1.5 μM Ca^{2+} (black traces) showed the typical kinetics characterized by an

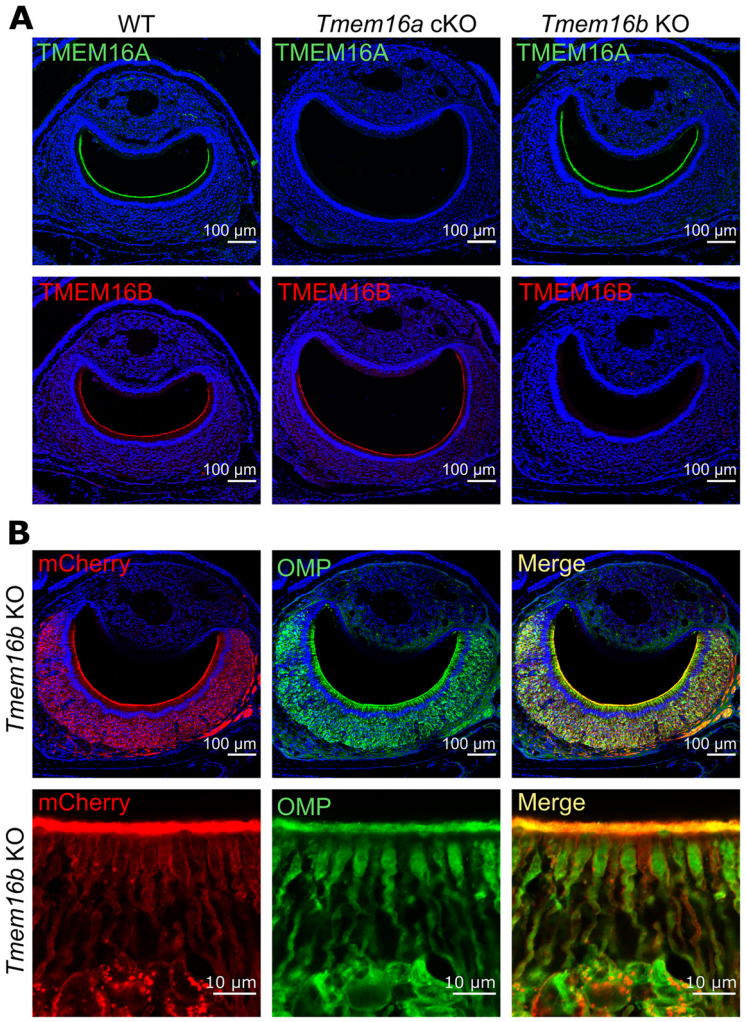


Figure 1. TMEM16A and TMEM16B are expressed at the apical surface of the vomeronasal epithelium. ***A***, Confocal micrographs of coronal sections of the VNO from WT, *Tmem16a* cKO, or *Tmem16b* KO mice, as indicated, immunostained with antibody against TMEM16A (green) and TMEM16B (red). No immunoreactivity to TMEM16A or TMEM16B was detectable in *Tmem16a* cKO or *Tmem16b* KO mice, respectively. ***B***, Confocal micrographs of VNO sections from *Tmem16b* KO mice expressing mCherry in the membrane of cells that normally express TMEM16B, immunostained with antibody against mCherry (red) and OMP (green). At the bottom, a magnification showing the co-expression of mCherry and OMP. Note that mCherry is expressed, as expected, in the membrane of entire VSNs and not only at the apical side. Cell nuclei were stained by DAPI (blue).

instantaneous current followed by an outward or inward relaxation at the most depolarizing or hyperpolarizing voltage steps, respectively. Recordings from VSNs of *Tmem16b* KO mice (brown traces; -157 ± 20 pA at -100 mV and 805 ± 79 pA at $+100$ mV, $n = 8$) revealed Ca^{2+}-activated chloride currents similar to WT mice (-105 ± 14 pA at -100 mV and 666 ± 55 pA at $+100$ mV, $n = 10$), further corroborating previous findings that TMEM16A largely contributes to Ca^{2+}-activated chloride currents in VSNs (Fig. 2*B*).

Membrane properties and voltage-gated currents of VSNs from KO mice are not altered

To test whether *Tmem16a* or *Tmem16b* deletion changes VSN passive membrane properties and/or voltage-gated currents, we performed whole-cell recordings in the presence of K^+ in the patch pipette.

Representative recordings of voltage-activated inward and outward currents from each mouse line are shown in Figure 3*A*. For I-V relations, we plotted the minimum values of inward currents during the first 20 ms after each voltage pulse (Fig. 3*B*, circles) and the outward current value at the end of each voltage pulse (Fig. 3*B*, triangles). Figure 3*B* shows that I-V relations of voltage-gated currents were similar in VSNs from WT, *Tmem16a* cKO, and *Tmem16b* KO mice.

Membrane input resistance was evaluated in voltage-clamp mode with a negative pulse of 20 mV from a holding potential of -90 mV, as in these conditions voltage-gated currents are not activated (Dibattista et al., 2008). The average membrane input resistances of VSNs from WT, *Tmem16a* cKO, and *Tmem16b* KO mice were 3.2 ± 0.3 GΩ ($n = 31$), 3.2 ± 0.2 GΩ ($n = 23$), and 2.9 ± 0.4 GΩ ($n = 23$), respectively (Fig. 3*C*). These values were not

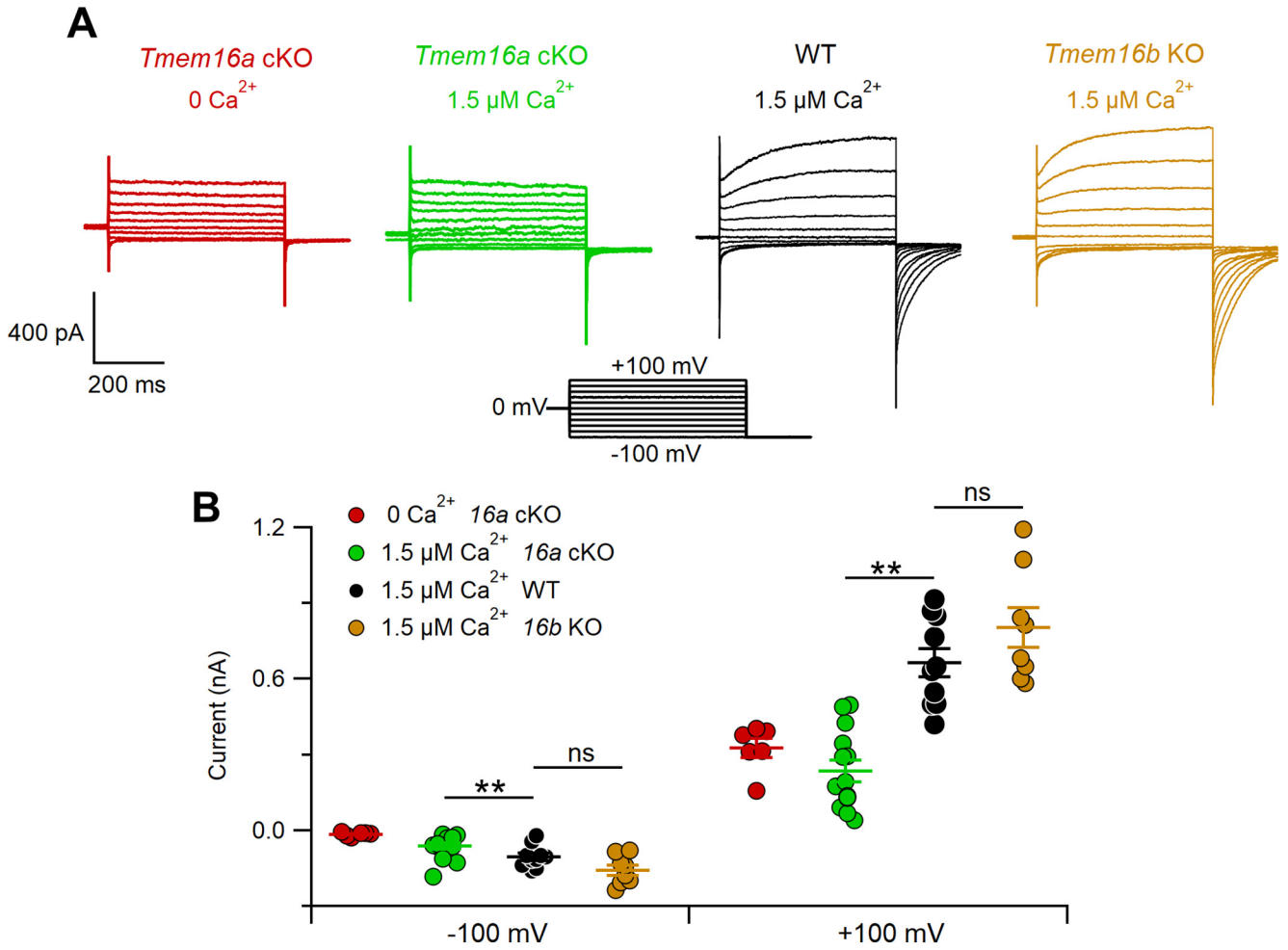


Figure 2. Ca^{2+}-activated chloride currents in VSNs. ***A***, Representative whole-cell recordings obtained with an intracellular solution containing 0 or 1.5 μM Ca^{2+} from VSNs from WT, *Tmem16a* cKO, or *Tmem16b* KO mice, as indicated. The voltage protocol is in the center of the figure. ***B***, Scatter dot plot with average ± SEM of steady-state current amplitudes measured at −100 or +100 mV with intracellular pipette solution containing nominally 0 Ca^{2+} from *Tmem16a* cKO (red, $n = 6$), or 1.5 μM free Ca^{2+} from *Tmem16a* cKO (green, $n = 14$), WT (black, $n = 10$), and *Tmem16b* KO (brown, $n = 8$) mice (**$p < 0.01$; Dunn–Hollander–Wolfe test after Kruskal–Wallis analysis at –100 and +100 mV), ns: not significant.

statistically different, indicating that membrane input resistance is not altered by either the lack of TMEM16A or TMEM16B.

The resting membrane potential was measured in current-clamp mode (I_{inject} = 0 pA) and was not statistically different between genotypes (Fig. 3*D*), with values of −69 ± 1 mV ($n = 28$) for WT, −68 ± 2 mV ($n = 22$) for *Tmem16a* cKO, and −71 ± 2 mV ($n = 20$) for *Tmem16b* KO VSNs.

These results indicate that the Ca^{2+}-activated chloride channels TMEM16A and TMEM16B do not contribute to passive membrane properties of mouse VSNs and do not alter major voltage-gated inward and outward currents in the range from −100 up to +40 mV. As TMEM16A can also be activated by high positive voltages in absence of intracellular Ca^{2+} (Xiao et al., 2011; Segura-Covarrubias et al., 2020), these results show that TMEM16A does not alter passive properties at membrane potentials up to +40 mV.

Spontaneous firing pattern is altered in VSNs from *Tmem16a* cKO

It is well known that VSNs display spontaneous firing activity in the absence of stimuli (Holy et al., 2000; Arnson and Holy, 2011) and that changes in sensory transduction components may modify this activity, as for example VSNs from *Trpc2* KO mice showed reduced spontaneous firing (Arnson and Holy, 2011). Moreover, experiments in the main olfactory epithelium have shown that deletion of TMEM16B, which is highly expressed in the cilia of olfactory sensory neurons (OSNs), caused a reduction of spontaneous firing activity in those neurons (Pietra et al., 2016). Based on these findings, we hypothesized that TMEM16A and TMEM16B might play a role in the spontaneous VSN firing.

By performing extracellular loose patch recordings from individual neurons in VNO slices from WT and mutant mice, we found that VSNs have a highly variable spontaneous activity among neurons of the same

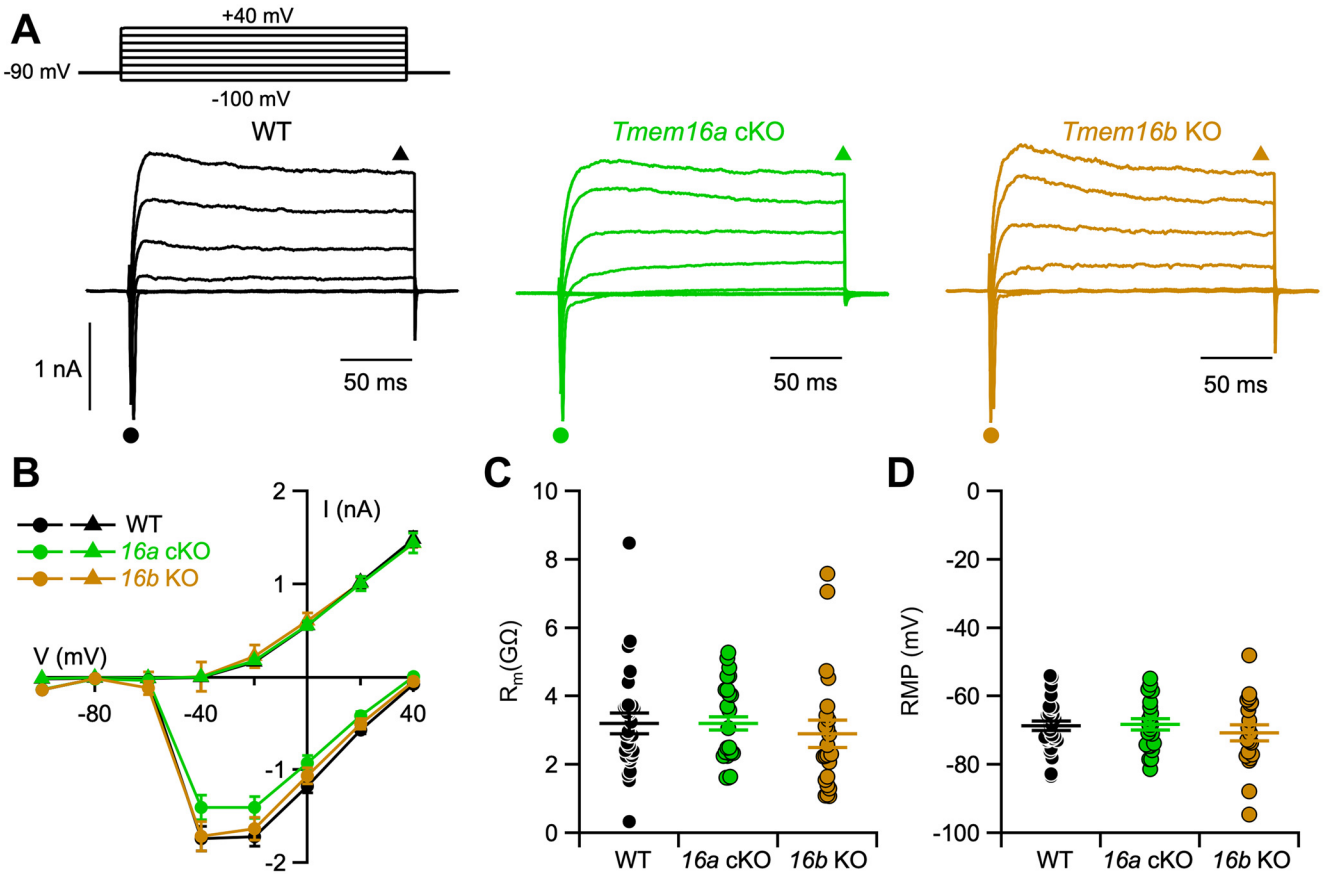


Figure 3. *Tmem16a* or *Tmem16b* deletion does not affect voltage-gated currents and membrane properties of VSNs. ***A***, Representative whole-cell recordings of VSNs obtained from the indicated mouse lines. The holding potential was −90 mV and voltage steps from −110 to +30 mV with 20-mV increment were applied. ***B***, Average ± SEM of the IV relationships of inward currents (circles) and steady-state outward currents (triangles) from WT (black, $n = 31$), *Tmem16a* cKO (green, $n = 23$), or *Tmem16b* KO (brown, $n = 23$) VSNs. Values were taken at the negative peak and at the end of voltage step as indicated by the symbols in ***A***. ***C***, Scatter dot plot with average ± SEM of the membrane resistance (R_m) recorded in voltage-clamp mode (WT, $n = 31$; *Tmem16a* cKO, $n = 23$; *Tmem16b* KO, $n = 23$. Kruskal–Wallis analysis $p = 0.21$). ***D***, Scatter dot plot with average ± SEM of resting membrane potential (RMP) recorded in current-clamp configuration (WT, $n = 28$; *Tmem16a* cKO, $n = 22$; *Tmem16b* KO, $n = 20$. Kruskal–Wallis analysis $p = 0.68$).

genotype with frequencies varying from 0 Hz (no spontaneous activity) to ~4 Hz (Fig. 4*A*). The viability of each neuron was tested by depolarization with a high K^+ solution to verify the neurons firing capability, and only VSNs responding to high K^+ were included in the analysis. VSNs that did not show spontaneous activity were: six out of 50 for WT, five out of 52 for *Tmem16a* cKO, and one out of 34 for *Tmem16b* KO. Thus, at least 88% VSNs from each genotype showed spontaneous activity.

Although the average spontaneous frequency was not significantly different among the three genotypes (0.32 ± 0.08 Hz, $n = 50$ for WT; 0.16 ± 0.04 Hz, $n = 52$ for *Tmem16a* cKO, and 0.65 ± 0.18 Hz, $n = 34$ for *Tmem16b* KO; Fig. 4*B*), we measured differences in firing patterns. To analyze activity patterns, we calculated ISI distributions from neurons with a mean frequency >0.1 Hz and plotted the distributions for each mouse line (Fig. 4*C*). To avoid overrepresentation of neurons with higher versus those with lower spontaneous activity, we normalized the ISI distribution by dividing the number of spikes for each bin by the total number of spikes for each single VSN before adding it to create the ISI distribution for each genotype. Moreover, to compare data from the three genotypes, data were normalized to the area under the curve (Fig. 4*C*). Corresponding cumulative fraction plots are shown in Figure 4*D*. We found that ISI distributions of spontaneous firing were statistically different ($p < 0.01$) between WT and *Tmem16a* cKO VSNs, while they did not differ between WT and *Tmem16b* KO VSNs. Indeed, in WT and *Tmem16b* KO VSNs, ~80% of ISIs range between 50 and 200 ms (black and brown traces, respectively). By contrast, the ISI distribution for *Tmem16a* cKO neurons is broader showing only ~50% of activity in the 50- to 200-ms ISI range (green traces). These results show that short ISIs were reduced in *Tmem16a* cKO compared with WT neurons (Fig. 4*C*,*D*), indicating that TMEM16A, but not TMEM16B, exerts firing pattern control during spontaneous activity of VSNs.

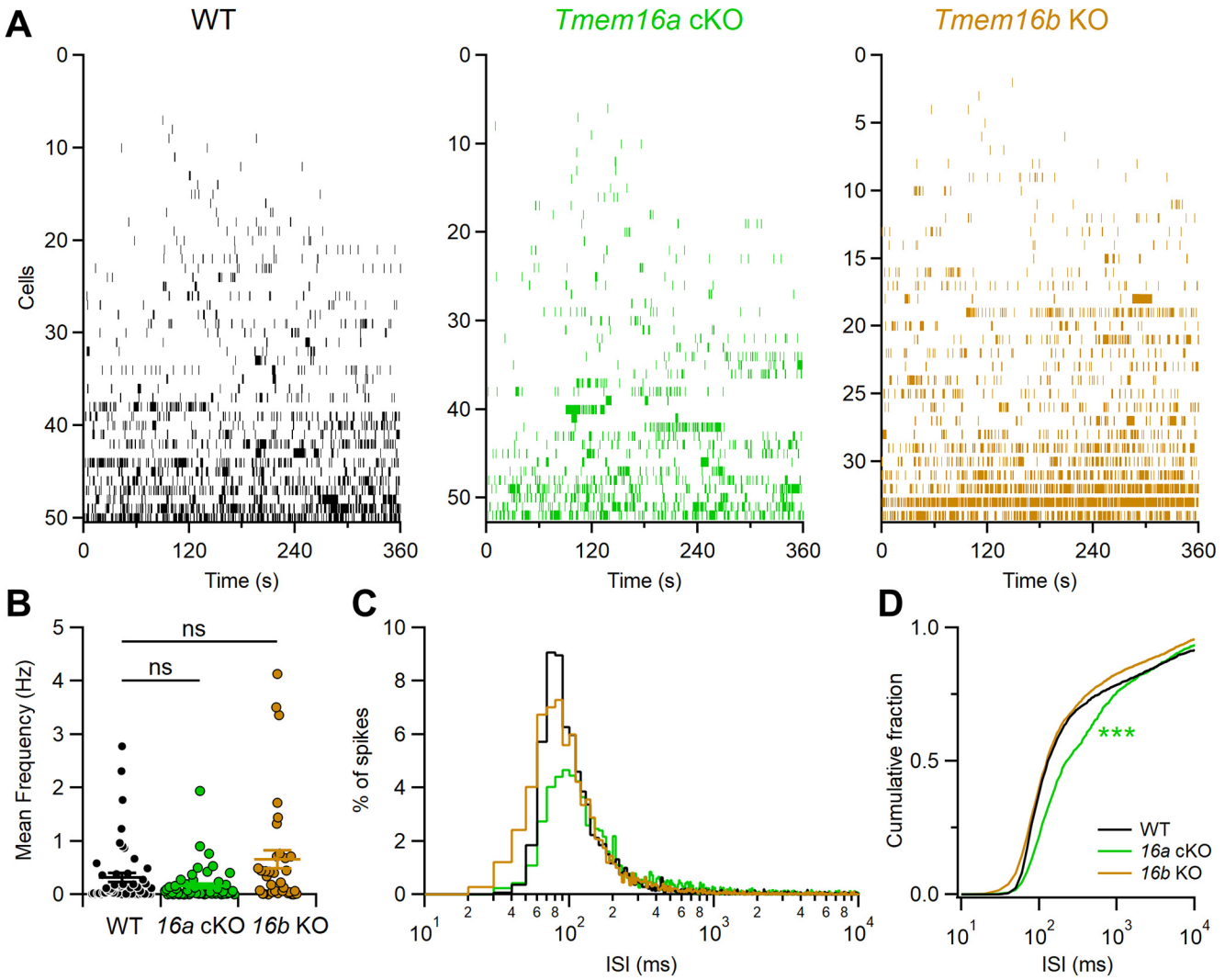


Figure 4. *Tmem16a* deletion modifies VSNs spontaneous firing activity. ***A***, Raster plots of recordings of the spontaneous activity of VSNs from WT (black, $n = 50$), *Tmem16a* cKO (green, $n = 52$), or *Tmem16b* KO (brown, $n = 34$) mice. Each row shows spike activity from a different VSN. ***B***, Mean frequency of spontaneous activity from the cells shown in ***A***. ***C***, ISI distributions of spontaneous firing from a subset of cells with mean frequency >0.1 Hz (bin = 10 ms). Values were normalized to the area under each curve to show the spike percentages for WT (black, $n = 25$), *Tmem16a* cKO (green, $n = 18$), or *Tmem16b* KO (brown, $n = 20$) mice. ***D***, Cumulative fraction of ISI distributions (***$p < 0.001$, Kolmogorov–Smirnov test).

Deletion of TMEM16A and resulting changes in spontaneous firing do not modify axonal targeting to AOB glomeruli

In the main olfactory epithelium, spontaneous activity of OSNs is essential for both formation and maintenance of the glomerular map in the OB (Yu et al., 2004; Lodovichi and Belluscio, 2012; Lorenzon et al., 2015). Furthermore, deletion of TMEM16B, the Ca^{2+}-activated chloride channel in OSNs, altered spiking and affected the glomerular formation of I7-expressing OSNs (Pietra et al., 2016). While the relation between spiking pattern and glomerular formation has been investigated in the OB, similar studies in the AOB were missing. To investigate whether spontaneous firing pattern alteration, resulting from TMEM16A deletion, affects VSN density or glomeruli formation in the AOB, we crossed *Tmem16a* cKO with V2R1b-GFP (Del Punta et al., 2002) mice to generate a mouse line in which V2R1b expressing VSNs were fluorescently labeled, but lack TMEM16A (V2R1b-GFP-TMEM16A-cKO). V2R1b-GFP-TMEM16A cKO mice were homozygous for V2R1b-GFP and *Tmem16a*-Flox genes, and heterozygous for OMP/Cre, while control animals were homozygous for V2R1b-GFP, *Tmem16a*-Flox and OMP genes, lacking the expression of Cre recombinase. We performed VNO and forebrain tissue clearing to quantify and compare (1) the number of fluorescently labeled neurons per VNO, and (2) the V2R1b-specific axonal glomerular architecture in the AOB, between TMEM16A-deficient V2R1b-GFP mice and corresponding controls (Fig. 5). Figure 5*A–C* shows an example of a cleared VNE observed with a light sheet microscope and the corresponding 3D reconstruction (Movie 1). Single VSNs were readily observed, and cellular

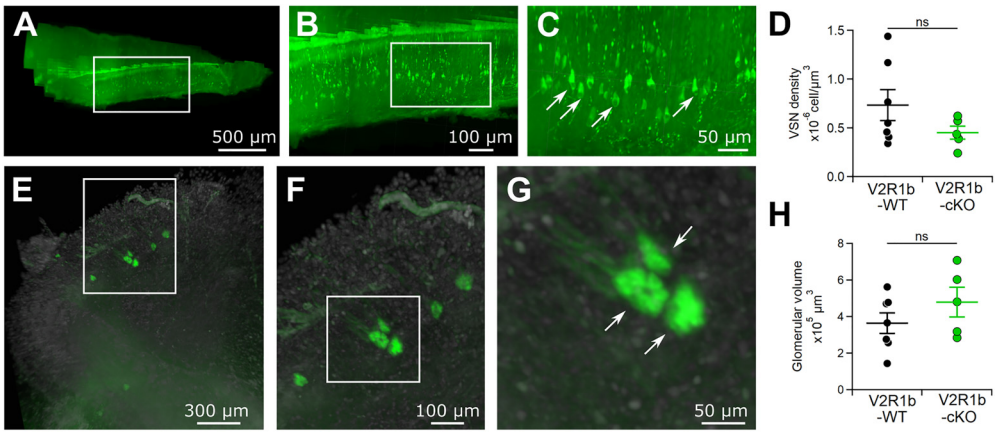


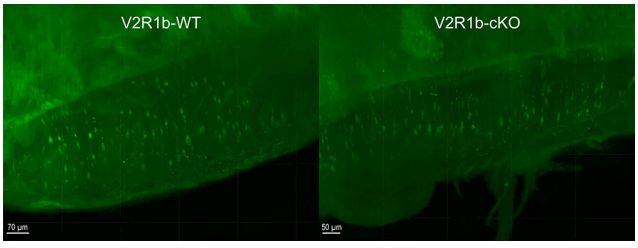
Figure 5. *Tmem16a* cKO effect on VSN density and glomerular volume. ***A–C***, top, Representative 3D projection image of a VNE from a V2R1b-WT mouse. Zoom-in indicated by white rectangles. Arrows indicate example fluorescently labeled V2R1b neurons. ***D***, Scatter dot plot (average ± SEM) of VSN density in V2R1b-WT and V2R1b-*Tmem16a* cKO mice (Student's *t* test, $p = 0.1876$). ***E–G***, top, Representative 3D projection image of AOB from V2R1b-WT mouse. Zoom-in indicated by white rectangles. Arrows indicate exemplary fluorescently labeled V2R1b glomerular structures. ***H***, Scatter dot plot with average ± SEM of glomerular volume in V2R1b-WT and V2R1b-*Tmem16a* cKO mice (Student's *t* test, $p = 0.2573$).

density was calculated (Fig. 5*D*). We found no significant statistical difference in VSN density between V2R1b-GFP-WT and V2R1b-GFP-TMEM16A-cKO mice (Fig. 5*D*, $n = 5–7$). These results indicate that deletion of TMEM16A does not affect the number of V2R1b-expressing VSNs.

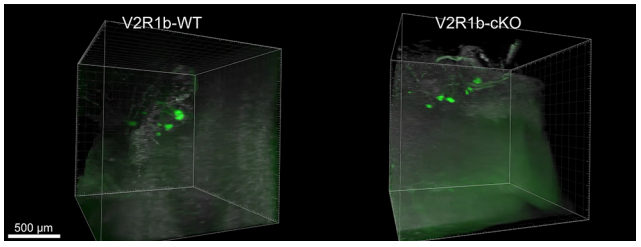
Next, we evaluated the glomerular architecture in the AOB. We identified several glomeruli innervated by V2R1b axons, confirming previous reports (Del Punta et al., 2002). Given the variability in glomerular number between animals from the same mouse line, ranging between 2 and 10 glomeruli per AOB (Del Punta et al., 2002), we decided to evaluate whether the total volume of AOB glomeruli was affected by TMEM16A deletion. Figure 5*E–G* shows a representative 3D reconstruction of the AOB with glomeruli formed by V2R1b-GFP axons (Movie 2). Single glomeruli were discernable (Fig. 5*G*, white arrows). A comparison of GFP-positive glomerular volume between V2R1b-WT and V2R1b-cKO mice show no significant statistical difference (Fig. 5*H*, $n = 5–6$). These results indicate that deletion of TMEM16A protein in VSNs and resulting alterations in firing do not affect general glomerular development in the AOB.

Response to sensory stimulation is altered in VSNs from KO mice

Next, we asked whether TMEM16A or TMEM16B deletion affects VSN responses to sensory stimulation. Thus, we stimulated VSNs with diluted mouse urine, a natural source of pheromones that has been frequently used to activate VSNs (Mohrhardt et al., 2018). While recording in loose-patch configuration, we stimulated VSNs with diluted urine and recorded the evoked firing activity. Stimulus application was repeated at least three times to avoid the detection of false-positive responses in spontaneously active neurons (Fig. 5). The viability of each VSN was tested by using a short depolarizing high K^+ solution stimulus (Fig. 6*A*), where unresponsive neurons were discarded. Furthermore, as urine also contains various ions including K^+ that could depolarize neurons (see Materials and Methods), we stimulated VSNs with diluted artificial urine (Fig. 6*B*) Neurons responding to the artificial urine control stimulus were excluded from the analysis. Finally, as VSNs display spike frequency adaptation to repetitive



Movie 1. Light-sheet fluorescence microscopy of cleared VNOs. Examples show intact transparent organs from wild type control (V2R1b-GFP - TMEM16Afl/fl - OMP/OMP; left) and TMEM16A knockout (V2R1bGFP - TMEM16Afl/fl - OMP/Cre; right) animals. Three-dimensional rendering displays the VNOs rotating around their longitudinal axes. [View online]



Movie 2. Light-sheet fluorescence imaging of cleared AOBs. Examples show intact transparent olfactory bulb samples from wild type control (V2R1b-GFP - TMEM16Afl/fl - OMP/OMP; left) and TMEM16A knockout (V2R1bGFP - TMEM16Afl/fl - OMP/Cre; right) mice. Nuclei are stained with DRAQ5 (grey scale). Green fluorescence of V2R1b-positive vomeronasal sensory neuron axons becomes apparent upon fiber coalescence and convergence in AOB glomeruli. [View online]

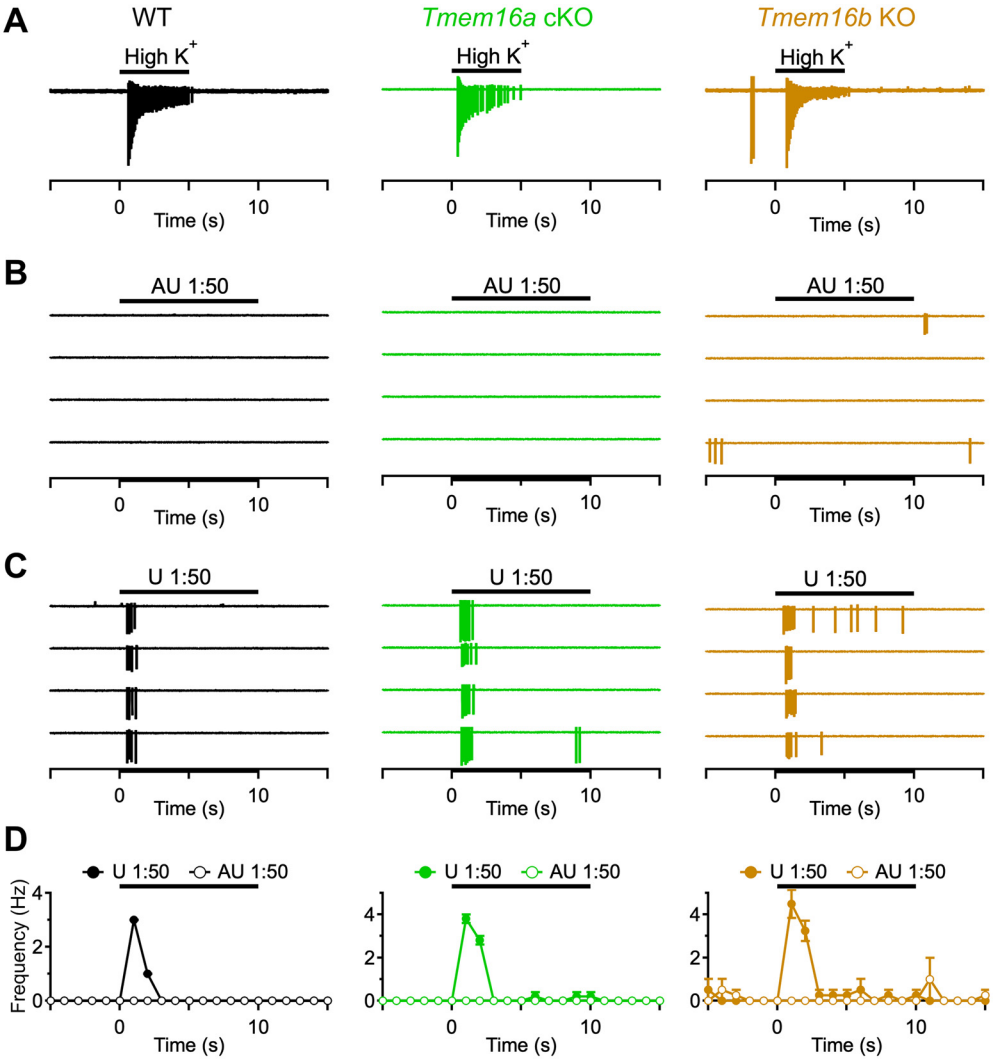


Figure 6. Evoked firing activity. ***A–C***, Representative loose-patch recordings of a VSN from each indicated mouse line stimulated with high K^+ (***A***), diluted artificial urine as control (***B***), or diluted urine (***C***). Black bars indicate the time of stimulus presentation. ***D***, Average firing activity (1-s bin width) for the responses to diluted artificial urine (empty circles) or urine (filled circles) from ***B***, ***C***. Error bars represent SEM.

stimulation (Wong et al., 2018), we selected an interstimulus interval between urine application of 4 min to avoid adaptation.

Figure 6 shows representative responses of single VSNs from WT or mutant mice. A 10-s stimulus of diluted urine was applied four times and, each time, clearly elicited an increase in firing frequency (Fig. 6*C*), whereas application of diluted artificial urine did not alter spiking activity (Fig. 6*B*). The plot of average firing frequency (1-s-bin width) shows a clear frequency increase during urine application in VSNs from either genotype (Fig. 6*D*).

Figure 7 shows reliable responses to repeated urine stimulation in 17 out of 30 WT, 22 out of 30 *Tmem16a* cKO, and 15 out of 34 *Tmem16b* KO VSNs, indicating that >45% VSNs from each genotype can respond to urine (Fig. 7*A*,*B*).

Although the mean firing frequency and response duration to urine were not significantly different among genotypes (Fig. 7*C*,*D*) a more detailed analysis showed that patterns of firing responses were altered by deletion of TMEM16A or TMEM16B (Fig. 7*E*,*F*). Indeed, ISI distributions and cumulative fractions of mutant mice were different from those of WT. ISI distribution for WT showed a peak ~200 ms, while in the ISI distribution from *Tmem16a* cKO and *Tmem16b* KO the peak was shifted to a shorter ISI of ~100 ms. These results indicate that both TMEM16A and TMEM16B modulate firing activity during signal transduction in mouse VSNs.

Discussion

In this study, we investigated the individual roles of TMEM16A and TMEM16B in regulating the physiological activity of VNO neurons. We found that TMEM16A, but not TMEM16B, modulates spontaneous spike patterns by increasing activity, while both channels shape pheromone-mediated spike activity by increasing ISIs.

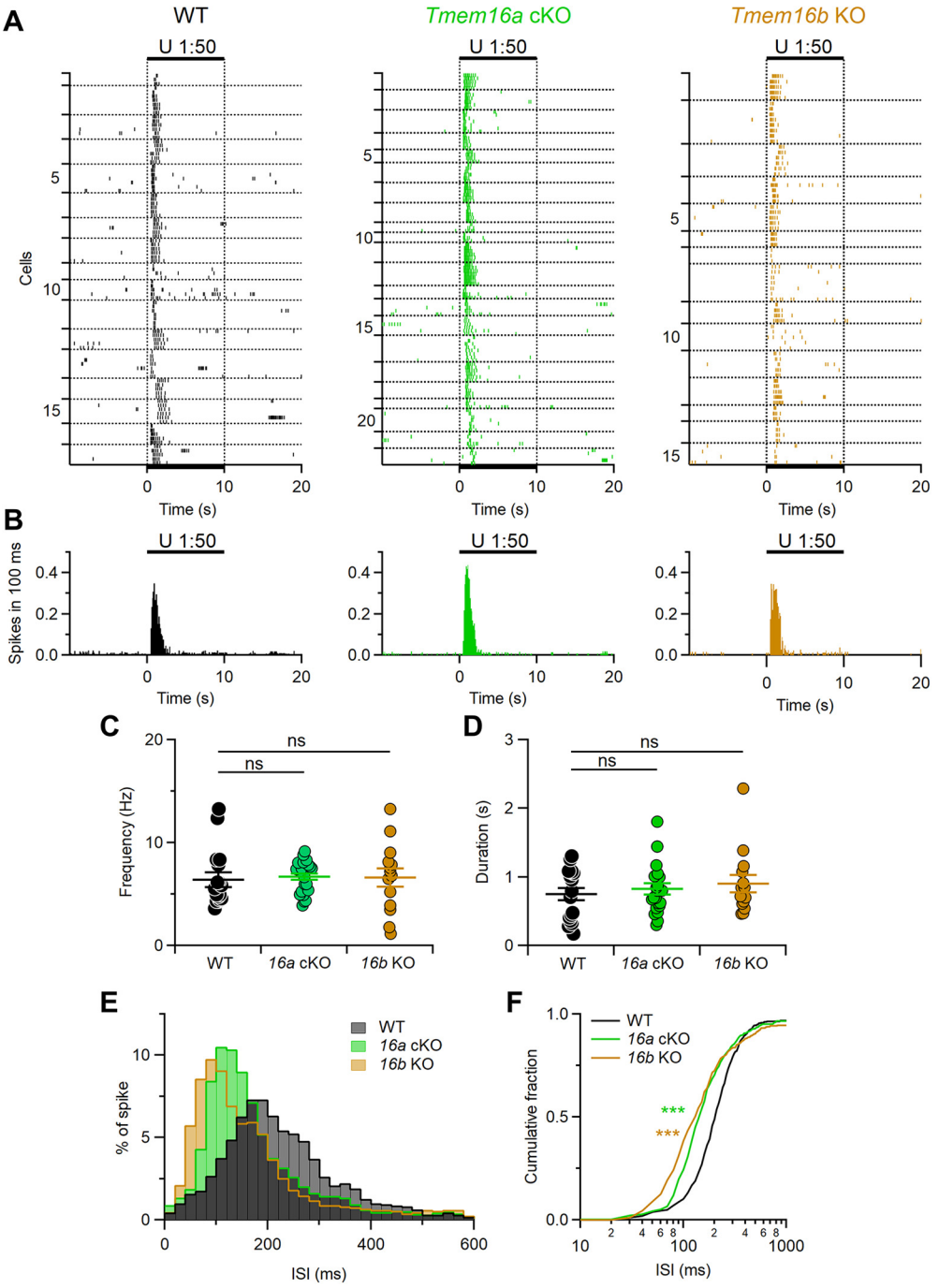


Figure 7. Patterns of evoked firing activity are modulated by TMEM16A and TMEM16B. ***A***, Raster plots showing the responses of VSNs from each indicated mouse line to diluted urine. Black bars indicate the time of stimulus presentation (10 s). Every neuron was tested at least three times. Horizontal dotted lines delimit multiple recordings from each VSNs. Numbers on the left indicate the neuron number. ***B***, Histograms of the number of spikes from neurons in ***A*** (100-ms bin width). Each neuron was averaged to equally contribute to spikes count. ***C***, ***D***, Scatter dot plots with average ± SEM of the mean frequency (***C***, Kruskal–Wallis analysis $p = 0.37$) and duration (***D***, Kruskal–Wallis analysis $p = 0.79$) of the responses to urine of VSNs from WT (black, $n = 17$), *Tmem16a* cKO (green, $n = 22$), or *Tmem16b* KO (brown, $n = 15$) mice. ***E***, Normalized ISI distributions of firing activity (20-ms bin width). ***F***, Cumulative fraction of the ISI distributions shown in ***D*** (***$p < 0.001$, Kolmogorov–Smirnov test).

Expression of TMEM16A and TMEM16B in olfactory systems

While the presence of Ca^{2+}-activated chloride currents in neurons of the main olfactory system is known since the early 1990s (Kleene and Gesteland, 1981; Kleene, 1993; Kurahashi and Yau, 1993; Lowe and Gold, 1993; Boccaccio and Menini, 2007; Pifferi et al., 2012; Dibattista et al., 2017), the first recordings of Ca^{2+}-activated currents from VSNs have been obtained more recently (Yang and Delay, 2010; Kim et al., 2011; Dibattista et al., 2012; Amjad et al., 2015).

Ca^{2+}-activated chloride channels encoded by TMEM16A and TMEM16B are characterized by functional differences. These include slower activation kinetics and higher Ca^{2+} sensitivity for TMEM16A compared with TMEM16B. The complexity is further increased by the existence of several spice variants with different properties (Ferrera et al., 2009; Huang et al., 2012; Ponissery Saidu et al., 2013; Pedemonte and Galietta, 2014).

In the main olfactory epithelium, TMEM16A and TMEM16B are expressed in different cell types: TMEM16B is expressed in the dendritic ends and cilia of OSNs (Stephan et al., 2009; Sagheddu et al., 2010; Billig et al., 2011), whereas TMEM16A is present in apical membranes and microvilli of a subpopulation of supporting cells (Henriques et al., 2019; Maurya and Menini, 2014). In the vomeronasal epithelium, however, both TMEM16A and TMEM16B are found in VSNs (Billig et al., 2011; Dibattista et al., 2012; Amjad et al., 2015; Münch et al., 2018), where they co-express in microvilli (Dibattista et al., 2012; Münch et al., 2018). Here, we confirmed previous results that TMEM16A is present only in mature VSNs, but not in VNO supporting cells (Amjad et al., 2015; Münch et al., 2018). By taking advantage of *mCherry Tmem16b* KO mice (Zhang et al., 2017), we showed that TMEM16B is also selectively expressed in mature VSNs. Thus, vomeronasal TMEM16A and TMEM16B are exclusively expressed in mature VSNs. The relative expression level of the two channels has been evaluated in the transcriptomic study of Ibarra-Soria et al. (2014). They found high expression for both transcripts, with *Tmem16a* levels about twice that of *Tmem16b*, without significant difference between males and females (Ibarra-Soria et al., 2014; see their Dataset S1 and Dataset S3).

In OSNs, deletion of TMEM16B completely abolished Ca^{2+}-activated chloride currents measured in whole-cell recordings (Billig et al., 2011; Pietra et al., 2016). In VSNs, the deletion of TMEM16A also completely abolished the current activated by 1.5 μM Ca^{2+} and measured with voltage steps up to +100 mV. As VSNs also express TMEM16B we expected to measure substantial residual current in the absence of TMEM16A. Indeed, although TMEM16B is less sensitive to Ca^{2+} than TMEM16A, it should be activated by 1.5 μM Ca^{2+} at +100 mV, as an EC_{50} of ~2 μM has been reported at high voltages (Cenedese et al., 2012; Adomaviciene et al., 2013). We also attempted to increase intracellular Ca^{2+} to 13 and 100 μM, respectively, but VSNs in slices became leaky with these solutions. However, previous experiments in isolated VSNs successfully increased intracellular Ca^{2+} up to 2 mM without finding any measurable Ca^{2+}-activated chloride current in VSNs from *Tmem16a* cKO mice (Amjad et al., 2015). Yet, as the average whole-cell leak current at +100 mV was ~300 pA, we cannot exclude that we missed a small current activated by TMEM16B. Lack of current in *Tmem16a* cKO mice was also measured by Münch et al. (2018) who suggested the possibility that Ca^{2+} concentration in the microvilli does not reach the concentration necessary to activate TMEM16B. We found that deletion of TMEM16B did not significantly reduce Ca^{2+}-activated chloride currents in VSNs confirming that most current results from TMEM16A activation. Our result thus agrees with recently published findings (Münch et al., 2018). By contrast, our data contradict a previous report showing a lack of Ca^{2+}-activated chloride currents in VSNs from *Tmem16b* KO mice (Billig et al., 2011).

It is of interest to note that TMEM16A and TMEM16B are co-expressed in pinealocytes where they can form both homomeric and heteromeric channels (Yamamura, 2018), raising the possibility that VSNs also express heteromeric channels.

Spontaneous and stimulus-evoked spike activity

In both OSNs and VSNs, Ca^{2+}-activated chloride channels are expected to play a role in the response to odorants or pheromones, as they are located close to transduction sites, i.e., in OSN cilia and VSN microvilli. This subcellular distribution is well suited to sense high Ca^{2+} concentrations produced in microdomains by transduction cascades downstream odorant or vomeronasal receptor activation (Tirindelli et al., 2009; Pifferi et al., 2010). Indeed, although the transduction cascade components in the two olfactory systems are very different, transduction currents produce an increase in intracellular Ca^{2+} in both cases. The resulting membrane depolarization triggers generation of action potentials that are conducted along OSN or VSN axons to the main or AOB, respectively. To understand the physiological role of TMEM16 channels in peripheral sensory neurons of olfactory systems, it is critical to note that both OSNs and VSNs maintain high internal chloride concentrations (Reuter et al., 1998; Kaneko et al., 2004; Kim et al., 2015; Untiet et al., 2016). Therefore, Ca^{2+}-activated chloride channels are well suited to play an excitatory transduction role by amplifying the depolarizing cation current through chloride efflux. In addition, these channels might also play a stabilizing role by setting the membrane potential close to the chloride equilibrium potential, preventing excessive depolarization.

In OSNs, extracellular loose patch recordings of spontaneous firing activity showed that TMEM16B increased spontaneous firing, as TMEM16B-deficient OSNs exhibited a reduction in instantaneous frequency (inverse of ISI) of spontaneous activity (Pietra et al., 2016). This likely results from random activation of signal transduction proteins that produces a Ca^{2+} increase sufficient to open ciliary TMEM16B channels that contribute small depolarizations and firing activity. As VSNs also display a spontaneous activity that is dependent on signal transduction cascade components (Arnson and Holy, 2011), we hypothesized that TMEM16 channels could also affect spontaneous VSN firing. Indeed, deletion of TMEM16A, but not of TMEM16B, caused differences in ISI distribution:

the percentage of ISIs between 50 and 200 ms was reduced to 50%, compared with 80% in WT VSNs. The decrease in spontaneous activity after TMEM16A deletion indicates that TMEM16A favors spike generation, probably by mediating a chloride efflux that further depolarizes the membrane after spontaneous activation of signal transduction components, similarly to TMEM16B in OSNs. As TMEM16A has a higher Ca^{2+} sensitivity than TMEM16B, a possible explanation for the lack of contribution of TMEM16B in VSNs is that the spontaneous activation of the signal transduction cascade leads to intracellular Ca^{2+} increase, which is insufficient to activate TMEM16B. Moreover, *Tmem16b* transcript expression level has been reported to be half of that of *Tmem16a* in VSNs (Ibarra-Soria et al., 2014) indicating that TMEM16B, in addition to being less sensitive to Ca^{2+}, may also have a lower expression than TMEM16A.

In the main olfactory system, TMEM16B is also involved in correct OSN glomerular targeting, as its deletion caused the formation of supernumerary glomeruli for neurons expressing the I7 odorant receptor (Pietra et al., 2016). In the vomeronasal system, deletion of TMEM16A did not produce modifications of glomerular targeting for VSNs expressing the V2R1b receptor, although we cannot exclude the possibility that this deletion may affect glomerular targeting of VSNs expressing other receptors.

In OSNs, TMEM16B has been shown to have a dual role in the control of firing, by increasing basal spiking but reducing stimulus-induced firing activity. In VSNs, we found that TMEM16A also plays a similar dual role. Indeed, individual loss of TMEM16A (or TMEM16B) strongly affected urine-evoked firing patterns by shifting the peak in the ISI distribution to ~100 ms from the value of 200 ms in WT. Thus, both TMEM16A and TMEM16B channels play a role in regulating VSN firing activity evoked by natural stimuli by doubling ISI. Stimulation of VSNs with diluted urine can forcefully activate the signal transduction cascade generating a stronger depolarization and higher cytosolic Ca^{2+} increase compared with spontaneous activation; under these conditions, TMEM16A and/or TMEM16B could first mediate a chloride efflux that amplifies the depolarization followed by a chloride influx, when the membrane potential becomes more positive than the chloride equilibrium potential, leading to membrane repolarization and increase in the ISI. Indeed, the internal chloride concentration in dendritic knobs of VSNs at rest has been estimated to be 42 mM (Untiet et al., 2016). In our experimental conditions, this would produce an equilibrium potential for chloride near −30 mV. Consequently, opening of Ca^{2+}-activated chloride channels would lead to depolarization at lower membrane potential and to repolarization at increased membrane potential.

Another study used *Tmem16a*/*Tmem16b* double KO mice (Münch et al., 2018) and reported a loss of spontaneous spiking and drastically diminished stimulus evoked spiking in VSNs indicating a relevant physiological role of these channels. Recordings and/or data analysis were somehow different from ours as they reported that only ~30% of VSNs had spontaneous activity while we measured spontaneous activity in almost 90% of VSNs from WT mice, in agreement with previous reports (Holy et al., 2000; Nodari et al., 2008; Arnson and Holy, 2011; Wong et al., 2018). This difference could stem from either sample viability, as depolarization controls were not reported, or different recording conditions. A more detailed study of firing activity should be performed in VSNs from the double KO model to better elucidate firing patterns. The same study performed a behavioral test showing that male-male territorial aggression, an innate VNO-dependent behavior in rodents, remained unaltered in double KO *Tmem16a*/*Tmem16b* mice.

It is important to note that our criteria for selecting neurons responding to urine are more stringent with respect to those of other studies (Kim et al., 2011; Münch et al., 2018) and could have excluded some VSNs with very high spontaneous firing frequencies. We argue that our method, similar to that used by Arnson and Holy (2011), is suitable to limit the analysis to a subset of clearly viable neurons.

In summary, our data provide evidence that both TMEM16A and TMEM16B modulate the pheromone-mediated spike activity of VSNs and provide the foundation for future work investigating the precise physiological role of the Ca^{2+}-activated chloride currents in VSNs.

References

Adomaviciene A, Smith KJ, Garnett H, Tammaro P (2013) Putative pore-loops of TMEM16/anoctamin channels affect channel density in cell membranes. J Physiol 591:3487–3505.

Amjad A, Hernandez-Clavijo A, Pifferi S, Maurya DK, Boccaccio A, Franzot J, Rock J, Menini A (2015) Conditional knockout of TMEM16A/anoctamin1 abolishes the calcium-activated chloride current in mouse vomeronasal sensory neurons. J Gen Physiol 145:285–301.

Arnson HA, Holy TE (2011) Chemosensory burst coding by mouse vomeronasal sensory neurons. J Neurophysiol 106:409–420.

Billig GM, Pál B, Fidzinski P, Jentsch TJ (2011) Ca2+-activated Cl− currents are dispensable for olfaction. Nat Neurosci 14:763–769.

Boccaccio A, Menini A (2007) Temporal development of cyclic nucleotide-gated and Ca2+ -activated Cl- currents in isolated mouse olfactory sensory neurons. J Neurophysiol 98:153–160.

Caputo A, Caci E, Ferrera L, Pedemonte N, Barsanti C, Sondo E, Pfeffer U, Ravazzolo R, Zegarra-Moran O, Galietta LJV (2008) TMEM16A, a membrane protein associated with calcium-dependent chloride channel activity. Science 322:590–594.

Cenedese V, Betto G, Celsi F, Cherian OL, Pifferi S, Menini A (2012) The voltage dependence of the TMEM16B/anoctamin2 calcium-activated chloride channel is modified bymutations in the first putative intracellular loop. J Gen Physiol 139:285–294.

Del Punta K, Puche A, Adams NC, Rodriguez I, Mombaerts P (2002) A divergent pattern of sensory axonal projections is rendered convergent by second-order neurons in the accessory olfactory bulb. Neuron 35:1057–1066.

Dibattista M, Mazzatenta A, Grassi F, Tirindelli R, Menini A (2008) Hyperpolarization-activated cyclic nucleotide-gated channels in mouse vomeronasal sensory neurons. J Neurophysiol 100:576–586.

Dibattista M, Amjad A, Maurya DK, Sagheddu C, Montani G, Tirindelli R, Menini A (2012) Calcium-activated chloride channels in the apical region of mouse vomeronasal sensory neurons. J Gen Physiol 140:3–15.

Dibattista M, Pifferi S, Boccaccio A, Menini A, Reisert J (2017) The long tale of the calcium activated Cl- channels in olfactory transduction. Channels (Austin) 11:399–414.

Døving KB, Trotier D (1998) Structure and function of the vomeronasal organ. J Exp Biol 201:2913–2925.

Faria D, Rock JR, Romao AM, Schweda F, Bandulik S, Witzgall R, Schlatter E, Heitzmann D, Pavenstädt H, Herrmann E, Kunzelmann

K, Schreiber R (2014) The calcium-activated chloride channel anoctamin 1 contributes to the regulation of renal function. Kidney Int 85:1369–1381.
Ferrera L, Caputo A, Ubby I, Bussani E, Zegarra-Moran O, Ravazzolo R, Pagani F, Galietta LJ (2009) Regulation of TMEM16A chloride channel properties by alternative splicing. J Biol Chem 284:33360–33368.
Francia S, Pifferi S, Menini A, Tirindelli R (2014) Vomeronasal receptors and signal transduction in the vomeronasal organ of mammals. In: Neurobiology of chemical communication, frontiers in neuroscience. (Mucignat-Caretta C, ed). Boca Raton: CRC/Taylor and Francis.
Henriques T, Agostinelli E, Hernandez-Clavijo A, Maurya DK, Rock JR, Harfe BD, Menini A, Pifferi S (2019) TMEM16A calcium-activated chloride currents in supporting cells of the mouse olfactory epithelium. J Gen Physiol 151:954–966.
Holy TE, Dulac C, Meister M (2000) Responses of vomeronasal neurons to natural stimuli. Science 289:1569–1572.
Huang WC, Xiao S, Huang F, Harfe BD, Jan YN, Jan LY (2012) Calcium-activated chloride channels (CaCCs) regulate action potential and synaptic response in hippocampal neurons. Neuron 74:179–192.
Ibarra-Soria X, Levitin MO, Saraiva LR, Logan DW (2014) The olfactory transcriptomes of mice. Plos Genet 10:e1004593.
Kaneko H, Putzier I, Frings S, Kaupp UB, Gensch T (2004) Chloride accumulation in mammalian olfactory sensory neurons. J Neurosci 24:7931–7938.
Kim S, Ma L, Yu CR (2011) Requirement of calcium-activated chloride channels in the activation of mouse vomeronasal neurons. Nat Commun 2:365.
Kim S, Ma L, Unruh J, McKinney S, Yu CR (2015) Intracellular chloride concentration of the mouse vomeronasal neuron. BMC Neurosci 16:90.
Kleene SJ (1993) Origin of the chloride current in olfactory transduction. Neuron 11:123–132.
Kleene SJ, Gesteland RC (1981) Dissociation of frog olfactory epithelium with N-ethylmaleimide. Brain Res 229:536–540.
Kurahashi T, Yau KW (1993) Co-existence of cationic and chloride components in odorant-induced current of vertebrate olfactory receptor cells. Nature 363:71–74.
Leinders-Zufall T, Storch U, Bleymehl K, Mederos Y Schnitzler M, Frank JA, Konrad DB, Trauner D, Gudermann T, Zufall F (2018) PhoDAGs enable optical control of diacylglycerol-sensitive transient receptor potential channels. Cell Chem Biol 25:215–223.e3.
Li J, Ishii T, Feinstein P, Mombaerts P (2004) Odorant receptor gene choice is reset by nuclear transfer from mouse olfactory sensory neurons. Nature 428:393–399.
Liman ER, Corey DP, Dulac C (1999) TRP2: a candidate transduction channel for mammalian pheromone sensory signaling. Proc Natl Acad Sci USA 96:5791–5796.
Lodovichi C, Belluscio L (2012) Odorant receptors in the formation of the olfactory bulb circuitry. Physiology (Bethesda) 27:200–212.
Lorenzon P, Redolfi N, Podolsky MJ, Zamparo I, Franchi SA, Pietra G, Boccaccio A, Menini A, Murthy VN, Lodovichi C (2015) Circuit formation and function in the olfactory bulb of mice with reduced spontaneous afferent activity. J Neurosci 35:146–160.
Lowe G, Gold GH (1993) Nonlinear amplification by calcium-dependent chloride channels in olfactory receptor cells. Nature 366:283–286.
Lucas P, Ukhanov K, Leinders-Zufall T, Zufall F (2003) A diacylglycerol-gated cation channel in vomeronasal neuron dendrites is impaired in TRPC2 mutant mice: mechanism of pheromone transduction. Neuron 40:551–561.
Maurya DK, Menini A (2014) Developmental expression of the calcium-activated chloride channels TMEM16A and TMEM16B in the mouse olfactory epithelium. Dev Neurobiol 74:657–675.
Mohrhardt J, Nagel M, Fleck D, Ben-Shaul Y, Spehr M (2018) Signal detection and coding in the accessory olfactory system. Chem Senses 43:667–695.
Münch J, Billig G, Hübner CA, Leinders-Zufall T, Zufall F, Jentsch TJ (2018) Ca2+-activated Cl- currents in the murine vomeronasal organ enhance neuronal spiking but are dispensable for male-male aggression. J Biol Chem 293:10392–10403.
Nodari F, Hsu FF, Fu X, Holekamp TF, Kao LF, Turk J, Holy TE (2008) Sulfated steroids as natural ligands of mouse pheromone-sensing neurons. J Neurosci 28:6407–6418.
Patton C, Thompson S, Epel D (2004) Some precautions in using chelators to buffer metals in biological solutions. Cell Calcium 35:427–431.
Pedemonte N, Galietta LJV (2014) Structure and function of TMEM16 proteins (anoctamins). Physiol Rev 94:419–459.
Pietra G, Dibattista M, Menini A, Reisert J, Boccaccio A (2016) The Ca2+-activated Cl- channel TMEM16B regulates action potential firing and axonal targeting in olfactory sensory neurons. J Gen Physiol 148:293–311.
Pifferi S, Pascarella G, Boccaccio A, Mazzatenta A, Gustincich S, Menini A, Zucchelli S (2006) Bestrophin-2 is a candidate calcium-activated chloride channel involved in olfactory transduction. Proc Natl Acad Sci USA 103:12929–12934.
Pifferi S, Dibattista M, Menini A (2009a) TMEM16B induces chloride currents activated by calcium in mammalian cells. Pflugers Arch 458:1023–1038.
Pifferi S, Dibattista M, Sagheddu C, Boccaccio A, Al Qteishat A, Ghirardi F, Tirindelli R, Menini A (2009b) Calcium-activated chloride currents in olfactory sensory neurons from mice lacking bestrophin-2. J Physiol 587:4265–4279.
Pifferi S, Menini A, Kurahashi T (2010) Signal transduction in vertebrate olfactory cilia. In: Neurobiology of olfaction (Menini A, ed), pp 203–224. Boca Raton: CRC/Taylor and Francis.
Pifferi S, Cenedese V, Menini A (2012) Anoctamin 2/TMEM16B: a calcium-activated chloride channel in olfactory transduction. Exp Physiol 97:193–199.
Ponissery Saidu S, Stephan AB, Talaga AK, Zhao H, Reisert J (2013) Channel properties of the splicing isoforms of the olfactory calcium-activated chloride channel anoctamin 2. J Gen Physiol 141:691–703.
Reuter D, Zierold K, Schröder WH, Frings S (1998) A depolarizing chloride current contributes to chemoelectrical transduction in olfactory sensory neurons in situ. J Neurosci 18:6623–6630.
Rodriguez I, Feinstein P, Mombaerts P (1999) Variable patterns of axonal projections of sensory neurons in the mouse vomeronasal system. Cell 97:199–208.
Sagheddu C, Boccaccio A, Dibattista M, Montani G, Tirindelli R, Menini A (2010) Calcium concentration jumps reveal dynamic ion selectivity of calcium-activated chloride currentsin mouse olfactory sensory neurons and TMEM16b-transfected HEK 293T cells. J Physiol 588:4189–4204.
Schreiber R, Faria D, Skryabin BV, Wanitchakool P, Rock JR, Kunzelmann K (2015) Anoctamins support calcium-dependent chloride secretion by facilitating calcium signaling in adult mouse intestine. Pflugers Arch 467:1203–1213.
Schroeder BC, Cheng T, Jan YN, Jan LY (2008) Expression cloning of TMEM16A as a calcium-activated chloride channel subunit. Cell 134:1019–1029.
Segura-Covarrubias G, Aréchiga-Figueroa IA, De Jesús-Pérez JJ, Sánchez-Solano A, Pérez-Cornejo P, Arreola J (2020) Voltage-dependent protonation of the calcium pocket enable activation of the calcium-activated chloride channel anoctamin-1 (TMEM16A). Sci Rep 10:6644.
Shimazaki R, Boccaccio A, Mazzatenta A, Pinato G, Migliore M, Menini A (2006) Electrophysiological properties and modeling of murine vomeronasal sensory neurons in acute slice preparations. Chem Senses 31:425–435.
Spehr J, Hagendorf S, Weiss J, Spehr M, Leinders-Zufall T, Zufall F (2009) Ca2+ -calmodulin feedback mediates sensory adaptation and inhibits pheromone-sensitive ion channels in the vomeronasal organ. J Neurosci 29:2125–2135.
Stephan AB, Shum EY, Hirsh S, Cygnar KD, Reisert J, Zhao H (2009) ANO2 is the cilial calcium-activated chloride channel that may mediate olfactory amplification. Proc Natl Acad Sci USA 106:11776–11781.

Tirindelli R, Dibattista M, Pifferi S, Menini A (2009) From pheromones to behavior. Physiol Rev 89:921–956.
Touhara K, Vosshall LB (2009) Sensing odorants and pheromones with chemosensory receptors. Annu Rev Physiol 71:307–332.
Untiet V, Moeller LM, Ibarra-Soria X, Sánchez-Andrade G, Stricker M, Neuhaus EM, Logan DW, Gensch T, Spehr M (2016) Elevated cytosolic Cl- concentrations in dendritic knobs of mouse vomeronasal sensory neurons. Chem Senses 41:669–676.
Wong WM, Nagel M, Hernandez-Clavijo A, Pifferi S, Menini A, Spehr M, Meeks JP (2018) Sensory adaptation to chemical cues by vomeronasal sensory neurons. eNeuro 5:ENEURO.0223-18.2018.
Xiao Q, Yu K, Perez-Cornejo P, Cui Y, Arreola J, Hartzell HC (2011) Voltage- and calcium-dependent gating of TMEM16A/Ano1 chloride channels are physically coupled by the first intracellular loop. Proc Natl Acad Sci USA 108:8891–8896.
Yamamura H, Nishimura K, Hagihara Y, Suzuki Y, Imaizumi Y (2018) TMEM16A and TMEM16B channel proteins generate Ca2+-activated Cl- current and regulate melatonin secretion in rat pineal glands. J Biol Chem 293:995–1006.
Yang C, Delay RJ (2010) Calcium-activated chloride current amplifies the response to urine in mouse vomeronasal sensory neurons. J Gen Physiol 135:3–13.
Yang YD, Cho H, Koo JY, Tak MH, Cho Y, Shim WS, Park SP, Lee J, Lee B, Kim BM, Raouf R, Shin YK, Oh U (2008) TMEM16A confers receptor-activated calcium-dependent chloride conductance. Nature 455:1210–1215.
Yu CR, Power J, Barnea G, O'Donnell S, Brown HEV, Osborne J, Axel R, Gogos JA (2004) Spontaneous neural activity is required for the establishment and maintenance of the olfactory sensory map. Neuron 42:553–566.
Zhang Y, Zhang Z, Xiao S, Tien J, Le S, Le T, Jan LY, Yang H (2017) Inferior olivary TMEM16B mediates cerebellar motor learning. Neuron 95:1103–1111.e4.

1.1 VOLTAGE-GATED SODIUM CHANNELS SLOW INACTIVATION CONTRIBUTES TO PHEROMONE SHORT-TERM ADAPTATION IN VOMERONASAL SENSORY NEURONS

Slow inactivation of sodium channels contributes to short-term adaptation in vomeronasal sensory neurons

Manuscript in preparation

Nicole Sarno performed and analyzed all the experiments and contributed and writing of the manuscript.

Andres Hernandez-Clavijo, Anna Boccaccio (Institute of Biophysics, CNR, National Research Council, Genova, Italy), Anna Menini, Simone Pifferi designed research, contributed to data analysis, and writing of the manuscript.

Key Points

- Sensory adaptation reduces the responsiveness to a stimulus to allow the detection of changes in stimulus intensity.

- Most mammals use neurons of the vomeronasal organ for the detection of pheromones but whether these neurons adapt to stimuli is still subject of debate.

- Here, we used diluted urine, which contains a rich mixture of pheromones, as a repeated stimulus to elicit spike activity in neurons of the vomeronasal organ.

- We measured spike frequency adaptation to repeated identical pulses of urine from 2 to 10 s duration applied at short time intervals (short-term adaptation).

- Here we report a novel finding that short-term spike frequency adaptation also occurred when spiking activity was induced by current steps, bypassing the transduction cascade.

- Slow inactivation of Na^+ channels partially contributes to short-term spike frequency adaptation to repeated stimuli.

- These results show that neurons of the vomeronasal organ do adapt to repeated natural stimuli and that slow inactivation of Na^+ channels partially contribute to short-term adaptation.

Abstract

Adaptation plays an important role in sensory systems as it dynamically modifies sensitivity to allow the detection of stimulus changes. The vomeronasal system controls many social behaviors in most mammals by detecting pheromones released by conspecifics. Stimuli activate a transduction cascade in vomeronasal neurons that leads to spiking activity. Whether and how these neurons adapt to stimuli is still debated and largely unknown. Here, we measured short-term adaptation performing current-clamp whole-cell recordings by using diluted urine as a stimulus, as it contains many pheromones. We measured spike-frequency adaptation in response to repeated identical stimuli from 2 to 10 s duration that was dependent on the time interval between stimuli. Responses to paired current steps also showed spike-frequency adaptation. We found that recovery from slow inactivation of voltage-gated Na^+ channels occurs in several seconds, a time scale similar to that measured during paired pulses adaptation protocols, suggesting that it partially contributes to short-term spike frequency adaptation. We conclude that vomeronasal neurons do exhibit a time dependent short-term spike frequency adaptation to repeated natural stimuli and that slow inactivation of Na^+ channels contributes to this form of adaptation. These findings not only increase our knowledge about adaptation in the vomeronasal system, but also raise the question of whether slow inactivation of Na^+ channels may play a role in other sensory systems.

INTRODUCTION

In sensory systems, the process of adaptation plays an important physiological role as it reduces the responsiveness to a stimulus allowing the detection of additional variations in stimulus intensity. It often originates at the peripheral region of sensory systems, at the level of receptor cells and further develops in the central nervous system (Torre *et al.*, 1995; Wark *et al.*, 2007; De Palo *et al.*, 2012; Webster, 2012).

Chemosensory systems allow the organism to detect chemicals from the external world and most mammals use at least two different olfactory systems: the main and the vomeronasal olfactory system. Pheromones are proteins or small molecules released from animals that affect the physiology and/or behavior of members of the same species (Tirindelli *et al.*, 2009; Brennan, 2010; Wyatt, 2017). The vomeronasal system plays a very important role in the detection of pheromones and the regulation of several behaviors including mating, pups care, aggressive and territorial behaviors (Wysocki *et al.*, 1982; Stowers *et al.*, 2002; Touhara & Vosshall, 2009; Tirindelli *et al.*, 2009; Kaur *et al.*, 2014; Mohrhardt *et al.*, 2018; Tirindelli, 2021).

Pheromones and other natural ligands enter the vomeronasal organ (VNO) and contact receptors in vomeronasal sensory neurons (VSNs), bipolar neurons that have a dendrite ending in microvilli inside the lumen of the VNO and an axon projecting to the accessory olfactory bulb (AOB). Each VSN expresses one or a few types of G protein-coupled receptors V1Rs, V2Rs, FPRs and axons of VSNs expressing the same receptor project to various glomeruli in the AOB (Dulac & Axel, 1995; Ryba & Tirindelli, 1997; Herrada & Dulac, 1997; Matsunami & Buck, 1997; Rodriguez *et al.*, 1999; Rivière *et al.*, 2009; Liberles *et al.*, 2009; Tirindelli *et al.*, 2009; Francia *et al.*, 2014; Mohrhardt *et al.*, 2018; Tirindelli, 2021). Ligand binding activates a phospholipase C signaling cascade that leads to activation of transient receptor potential canonical 2 (TRPC2) channels allowing the influx of Na^+ and Ca^{2+} and the subsequent activation of the Ca^{2+}-activated Cl^- channels TMEM16A and TMEM16B (Liman & Buck, 1994; Lucas *et al.*, 2003; Dibattista *et al.*, 2012; Amjad *et al.*, 2015; Leinders-Zufall *et al.*, 2018). Ligand binding also causes Ca^{2+} release from intracellular stores that may also directly activate Ca^{2+}-activated Cl^- channels (Kim *et al.*, 2011). Currents induced by the transduction cascades in response to chemical stimuli generates membrane depolarization and action potentials that are sent to the AOB (Mohrhardt *et al.*, 2018).

Although the process of adaptation in the main olfactory system has been extensively investigated both at the peripheral and central level, very little is known about adaptation in the vomeronasal system (Abbas & Vinberg, 2021; Martelli & Storace, 2021; Brandão *et al.*, 2021).

Indeed, adaptation in the vomeronasal organ has been subject of some debate (Holy *et al.*, 2000; Nodari *et al.*, 2008; Spehr *et al.*, 2009), but recent work showed additional evidence of adaptive responses of VSNs to natural stimuli (Silvotti *et al.*, 2018; Wong *et al.*, 2018). Repeated stimulations showed that VSNs present both short-term adaptation, in a time range of tens of seconds, and long-term adaptation, in a time range of tens of minutes (Wong *et al.*, 2018).

In this study, we used current-clamp whole-cell recordings to investigate short-term adaptation by measuring the effect of a first stimulus on the spiking response elicited by a second identical stimulus repeated at different time intervals. We compared both responses to paired stimuli to diluted urine and to current steps, to bypass the transduction cascade and analyze also adaptation properties of voltage-gated channels independent of stimuli. We found that slow inactivation of Na^+ channels in mouse VSNs partially contribute to spike frequency adaptation to repeated stimuli.

MATERIALS AND METHODS

Animals and ethical approval

Mice were handled according to the guidelines of the Italian Animal Welfare Act (Decreto legislativo 26/2014) and European Union guidelines on animal research (2010/63) under a protocol approved by the Italian Ministry of Health. Mice had free access to water and food. Every effort was made to reduce the number of animals used. 2-3 month-old C57BL/6 mice were anaesthetized with CO_2 and decapitated before removal of the VNO. Mice were transferred to a cage (8 x 10 x 12 cm, height/width/length) and 100% CO_2 was slowly injected into the cage until the animal stopped breathing and no longer displayed pedal reflex (near 3 min, gas flow rate was ∼20% of chamber volume per minute).

Acute slices of mouse VNO

Acute slices of mouse VNO were prepared as previously described (Shimazaki *et al.*, 2006; Dibattista *et al.*, 2012; Wong *et al.*, 2018). The VNO was removed and transferred to ice-cold artificial cerebrospinal fluid (ACSF). The capsule and all cartilaginous tissues were removed with the help of the tip of fine forceps obtaining the two clean halves of the VNO. Each half was embedded in 3% low-grade agar (A7002, Sigma, Milan, Italy) prepared in ACSF, once the agar had cooled to 38°C. Upon solidification, the agar block was fixed in a glass Petri dish filled by ice-cold oxygenated ACSF solution and sliced with a vibratome (Vibratome 1000 Plus Sectioning System) at 200 μm. Slices were then left to recover for >30 min before electrophysiological experiments were initiated.

Electrophysiological recordings and solutions

Slices were viewed with an upright microscope (Zeiss Axioscope, Germany) with water immersion 40X objective (Olympus, Japan). The slice preparation maintained the VNO cross-sectional structure and VSNs could be distinguished by their morphology. Patch pipettes, pulled from borosilicate capillaries (WPI, Friedberg, Germany) with a PC-10 puller (Narishige, Tokyo, Japan), had a resistance of 3–6 MΩ. Electrophysiological recordings were made using an Axopatch 200B amplifier controlled by Clampex 10 via a Digidata 1440A (Molecular Devices, Sunnyvale, CA, USA). Experiments were performed at room temperature (20–25°C). The recording chamber was continuously perfused by gravity flow with oxygenated (95% O_2, and 5% CO_2) ACSF containing (in mM): 120 NaCl, 20 $NaHCO_3$, 5 KCl, 2 $CaCl_2$, 1 $MgSO_4$, 10 HEPES, 10 glucose, pH 7.4. The slice was anchored to the base of the recording chamber using a home-made U-shaped silver wire, holding down the agar support without touching the slice itself.

For current-clamp recordings, the intracellular solution filling the patch pipette contained (in mM) 80 K-Gluconate, 60 KCl, 2 Mg-ATP, 10 HEPES, and 1 EGTA, adjusted to pH 7.2 with KOH. Paired-pulses experiments were carried out at a 0 pA holding current and stimulus of variable duration (from 2 to 10 s) consisted either in diluted urine application or in 5 pA current steps. Inter-pulse intervals (IPIs) varied from 2 to 60 s. The time between independent sweeps was at least 2 min to avoid cumulative adaptation (Wong *et al.*, 2018). Data were low-pass filtered at 2 kHz and sampled at 10 kHz.

Urine was collected from both sexes C57BL/6 mice, filtered with a 0.2 µm filter, and frozen at -80°C. Before use, male and female urines were mixed in a 1:1 ratio and the mixture was diluted to 1:50 in ACSF (pH 7.4). As mouse urine contains urea and K^+, which could potentially cause neurons to fire by direct membrane depolarization, we used as a negative control artificial urine diluted to 1:50 in ACSF. Artificial urine contained (in mM): 100 NaCl, 40 KCl, 20 NH_4OH, 4 $CaCl_2$, 2.5 $MgCl_2$, 15 NaH_2PO_4, 20 $NaHSO_4$, 333 urea, pH 7.4 adjusted with NaOH (Holy *et al.*, 2000; Wong *et al.*, 2018). To test cell viability, we used a high K^+ solution (25 mM KCl) by replacing equimolar amounts of NaCl with KCl in ACSF. Urine, artificial urine and high K^+ solutions were delivered through an 8-into-1 multi-barrel perfusion pencil connected to a ValveLink8.2 pinch valve perfusion system (Automate Scientific, Berkeley, CA, USA). For each experiment the response to high K^+ stimulation (Fig. 1) was used to evaluate the arrival of solution to the cell. We included in the dataset only neurons that fired in response to high K^+ solution and did not respond to artificial urine.

For voltage-clamp recordings, the intracellular solution filling the patch pipette contained (in mM): 135 CsCl, 5 NaCl, 10 HEPES, and 10 EGTA, adjusted to pH 7.2 with NaOH. 100 µM $CdCl_2$ was added to extracellular ACSF in all recordings, except otherwise stated, to block Ca^{2+} channels. 2 µM TTX (Latoxan, Portes-lès-Valence, France) was used to block Na^+ channels. Leakage and capacitive currents were subtracted. All compounds and chemicals were obtained from Sigma-Aldrich, unless otherwise stated.

Data analysis

IgorPro 6.7/8 software (WaveMetrics) was used for data analysis and figures preparation. Individual spikes were identified by a custom-written detection procedure and confirmed by shape inspection. Data are presented as mean ± standard deviation and number of cells (*n*). The voltage-gated inactivation curves were fitted to the following Boltzmann equation: $I/I_{max} = A + (1-A) / (1+ \exp((V - V_{half})/k)$ where I is the peak sodium current, I_{max} the maximal peak sodium current, V is the membrane potential, V_{half} is the membrane potential at which I is half of I_{max}, k is the slope constant and A is the asymptotic value. Statistical significance was determined using the following tests.

Shapiro-Wilk test was used to verify data normality. For data normally distributed, ANOVA for repeated measurements was used, followed by paired t-test with Bonferroni correction, while for data not normally distributed, statistical significance was determined using Friedman's test followed by Desmar test. The p values associated to Desmar test were calculated using the algorithm in R developed by Eisinga *et al*. (2017). $p<0.05$ was considered statistically significant.

RESULTS

We performed current-clamp whole-cell recordings from the soma of neurons in acute murine VNO slices. The average resting membrane potential was -65 ± 6 mV (range -84 to -53 mV), and the average input resistance was 1.3 ± 0.5 (n=34). We stimulated VSNs with a time-controlled flow of diluted mouse urine, which is very rich in natural ligands for vomeronasal receptors (Moss *et al.*, 1997; Nodari *et al.*, 2008; Tirindelli *et al.*, 2009; Doyle *et al.*, 2016), and recorded the evoked spiking activity (Fig. 1*A*, green trace). On the same neuron, we used a depolarizing high K^+ solution stimulus as a positive control to test the neuron viability and to determine the time of arrival of the solution on the neuron (Fig. 1*A*, black trace). Moreover, as urine contains K^+, we also performed a control by applying diluted artificial urine (Fig. 1*A*, grey trace), a solution with salt composition similar to urine (Holy *et al.*, 2000; Wong *et al.*, 2018) and discarded neurons responding to artificial urine. In this way we verified that spiking activity in response to urine was not due to changes in ion concentration. The raster plot in Figure 1B shows examples of responses to 5 s urine stimulation from 10 different VSNs.

VSNs show short-term spike frequency adaptation in response to repeated natural stimuli

To evaluate the time-course of adaptation, we first applied a 5 s urine pulse followed by a second pulse of the same duration at different interpulse intervals (IPIs). As we have previously reported (Wong *et al.*, 2018), we confirm that the number of spikes during the second pulse was smaller for short IPIs but recovered toward the value of the first pulse as the IPI increased (Fig. 2*A* and *B*). The recovery time between each paired pulse was at least 2 min. To quantify sensory adaptation and compare results from several neurons, we normalized the average firing frequency during the second pulse to the value during the first one (Fig. 2*C*) and found that spike frequency was significantly different at IPI of 5 s (average frequency ratio 0.72 ± 0.18, n=10), whereas for longer IPIs of 10, 20 and 60 s the frequency was not significantly different.

To further investigate the dependence of short-term adaptation on stimulus duration, we applied urine pulses of shorter (2 s) and longer (10 s) durations than 5 s (Fig. 3*A* and *B*). We found that repetitive urine stimuli of 2 s showed adaptation only at IPI of 2 s (Fig. 3*C*). On the other hand, paired pulse protocols with longer urine stimulations of 10 s resulted in spike frequency adaptation when IPIs of 2, 5 and 10 s were used (average frequency ratios 0.68 ± 0.21 for 2s, 0.79 ± 0.14 for 5 s and 0.76 ± 0.2 for 10 s, n=9; Fig. 3*B* and *D*).

These results show that short-term adaptation in VSNs depends on the duration of urine stimulation as well as on IPI.

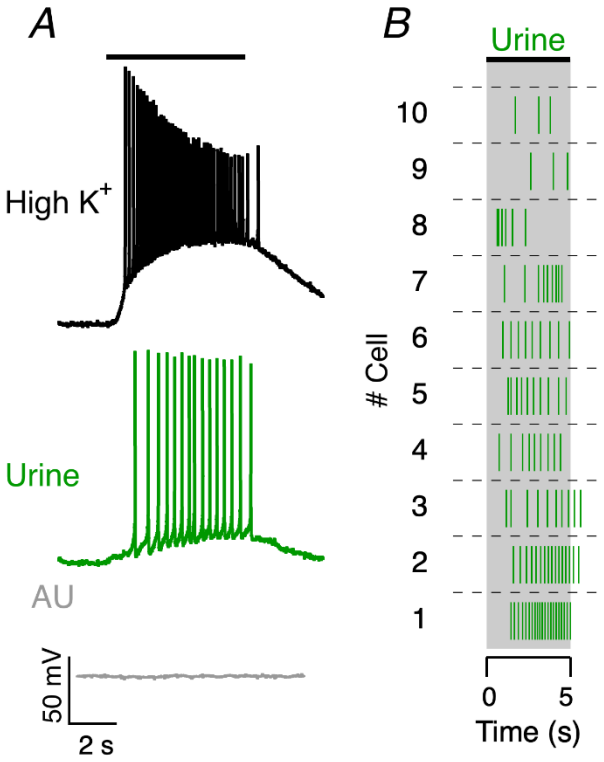


Figure 1. Diluted urine elicits spike activity in VSNs

A, whole-cell current-clamp recordings from a VSN stimulated for 5 s with high K^+ solution (25 mM KCl, black trace), diluted urine (1:50, green trace), or diluted artificial urine (1:50, grey trace). Top, the black bar indicates the arrival of the solutions to the neuron based on the response to high K^+ solution. ***B***, raster plot of urine responses of 10 different neurons stimulated for 5 s.

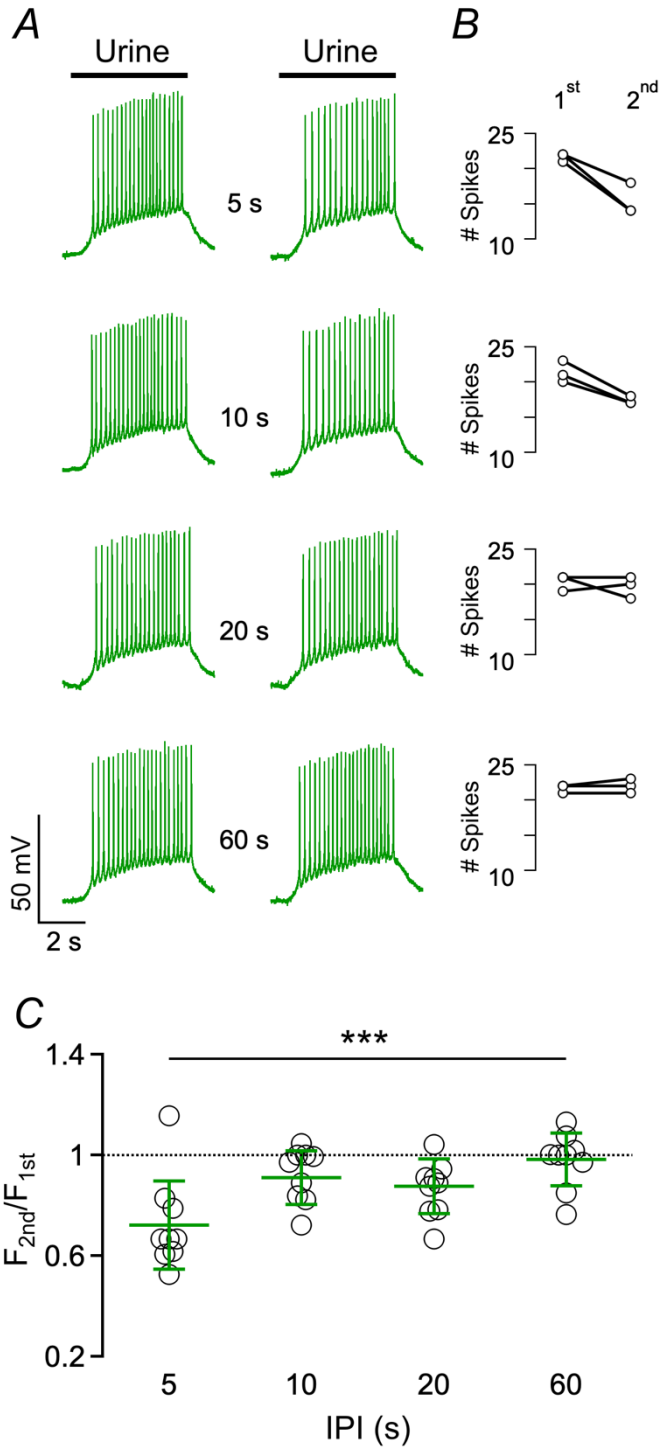


Figure 2. Spike frequency adaptation to repeated urine stimulations

A, representative whole-cell current-clamp recordings from a VSNs repetitively stimulated with diluted urine for 5 s with increasing intervals between pulses of 5, 10, 20 or 60 s, as indicated. Black bars at the top indicate the time of urine application. ***B,*** number of spikes during the first and the second stimulation at the corresponding IPI shown in the same row in *A*. The paired pulse protocol was repeated three times in the same neuron. ***C,*** scatter dot plot with averages ± SD of normalized spike frequency of the second with respect to the first stimulation for each IPI (n=10, Demsar test after Friedman test, p=0.00029).

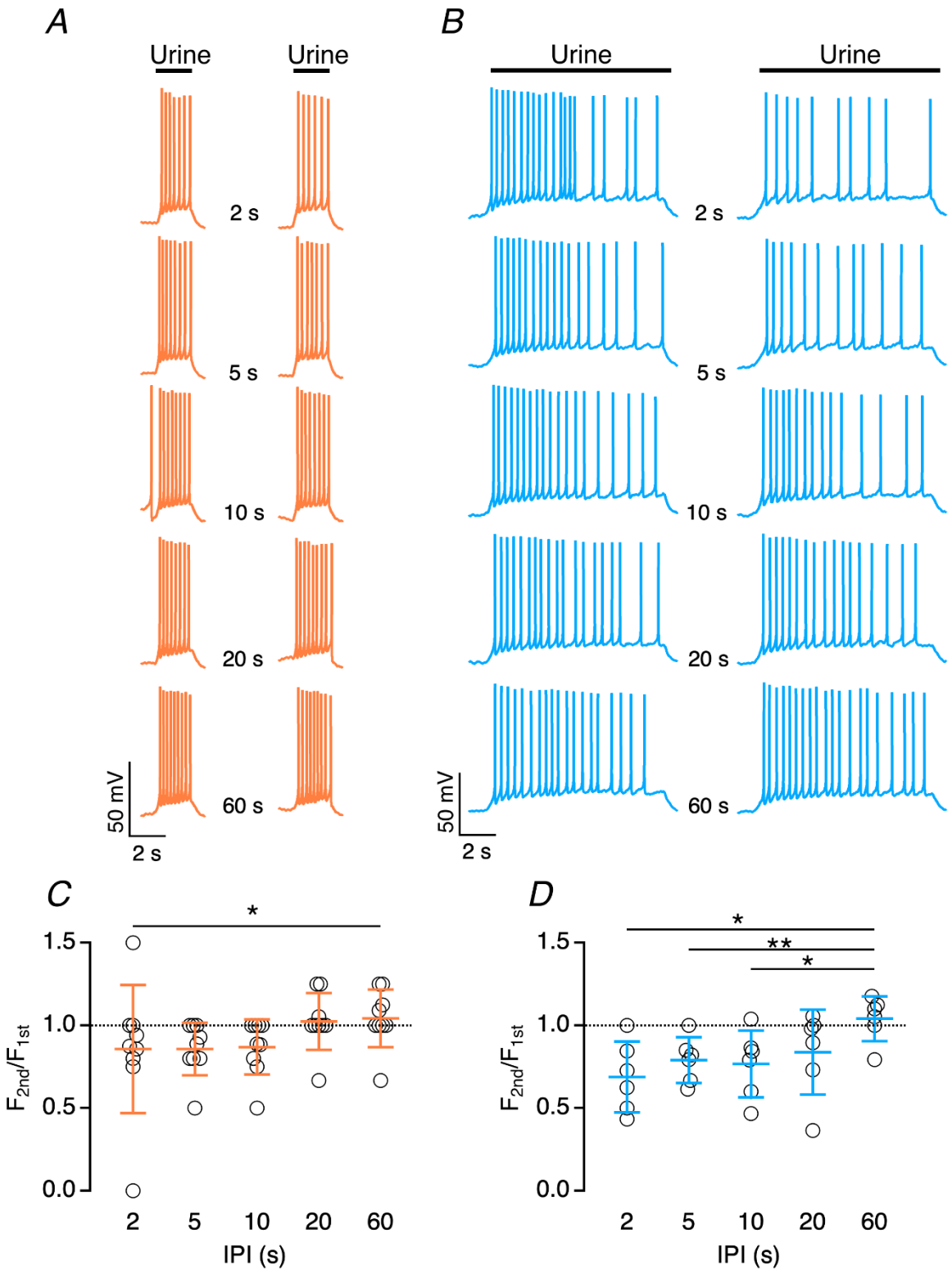


Figure 3. The duration of urine stimulation affects the extent of spike frequency adaptation

Representative whole-cell current-clamp recordings obtained stimulating VSNs with diluted urine for 2 **(*A*)** or 10 s **(*B*)**, with increasing intervals between pulses of 2, 5, 10, 20 or 60 s, as indicated. Black bars indicate the time of urine application. ***C*** and ***D***, scatter dot plots with averages ± SD of normalized spike frequencies for each IPI for urine pulses of 2 **(*C*)** or 10 s **(*D*)** (for *C:* n=9, Demsar test after Friedman test p=0.045 for IPI 2 s;

for *D:* n=6, Paired t-test with Bonferroni correction after ANOVA for repeated measurements p=0.018 for IPI 2 s, p=0.008 for IPI 5 s and p=0.036 for IPI 10 s).

VSNs show short-term spike frequency adaptation to repeated current steps

To test if short-term adaptation is due to adaptation of components of the signal transduction cascade and/or to a signal transduction-independent component, we stimulated VSNs with current steps instead of urine, thus inducing spiking activity while bypassing the activation of the signal transduction cascade.

We applied depolarizing current injections of 5 pA, a value that is sufficient to generate action potentials but does not saturate spike frequency in VSNs (Liman & Corey, 1996; Shimazaki *et al.*, 2006). We first stimulated VSNs with a current step lasting 5 s, followed by an identical stimulus at time intervals increasing from 2 to 60 s (Fig. 4*A* and *B*). Surprisingly, stimulation with paired current steps produced short-term adaptation when IPI of 2 and 5 s were used (average frequency ratios 0.8 ± 0.03 for 2 s and 0.87 ± 0.03 for 5 s, n=15).

We next examined if current step's duration affects short-term adaptation by repeating the same experiments obtained with urine stimuli (Fig. 3), i.e. we applied pairs of current steps of 2 or 10 s duration at various IPIs. We found that repetitive current steps of 2 s generated short-term adaptation with an IPI of 2 s (average frequency ratio 0.89 ± 0.09, n=13) but not when longer IPIs were used (Fig. 5*A* and *C*), while current steps of 10 s caused adaptation with IPI of 2 and 5 s (average frequency ratios 0.79 ± 0.13 for 2 s and 0.81 ± 0.12 for 5 s, n=13; Fig. 5*B* and *D*). Thus, short-term adaptation was very similar when current or urine stimulation was used in VSNs.

These data indicate that ion channels involved in the generation of action potentials, independent of signal transduction cascade components, might contribute to the development of short-term spike frequency adaptation in VSNs.

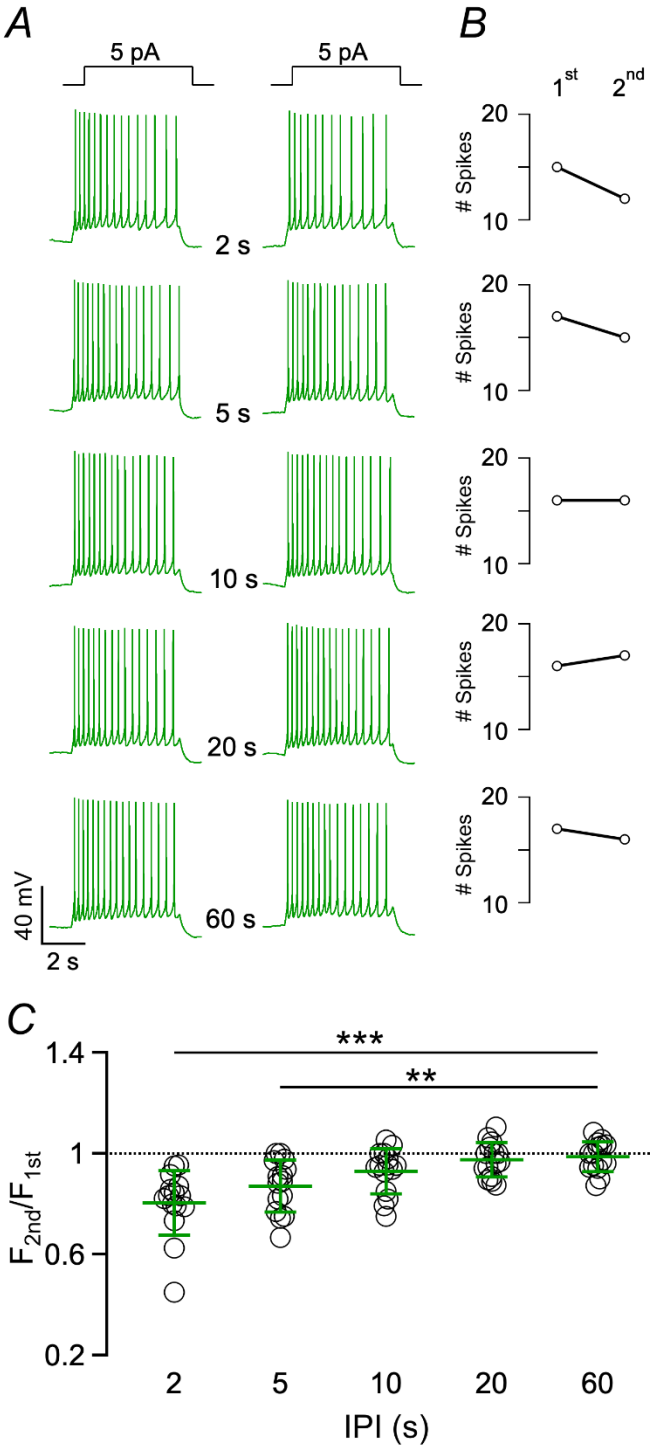


Figure 4. VSNs show spike frequency adaptation in response to repeated current steps
A, representative whole-cell current-clamp recordings of a VSNs repetitively stimulated with a 5 pA current step for 5 s with increasing intervals between steps of 2, 5, 10, 20, 60 s, as indicated. Steps at the top indicate the time of current injection. ***B,*** number of spikes during the first and the second stimulation at corresponding IPI shown in the same row in *A*. ***C,*** Scatter dot plot with averages ± SD of the normalized spike frequency of the second with respect to the first stimulation for each IPI (n=15, Demsar test after Friedman test p=7.5*10-5 for 2 s, p=0.006 for 5 s).

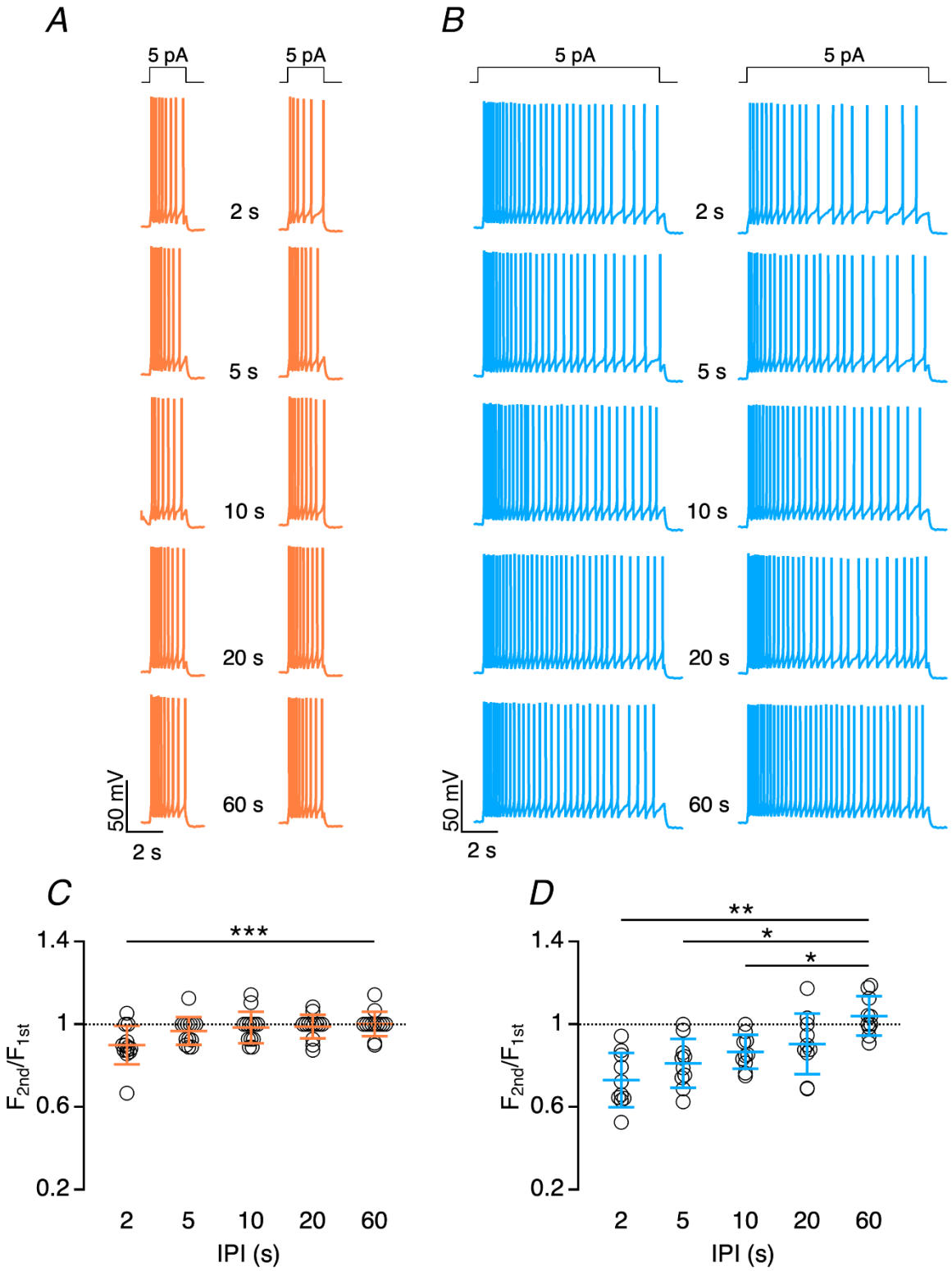


Figure 5. The duration of current step stimulation affects the extent of spike frequency adaptation

Representative whole-cell current-clamp recordings obtained stimulating VSNs with a 5 pA current step for 2 **(*A*)** or 10 s **(*B*)**, with increasing intervals between steps of 2, 5, 10, 20 or 60 s, as indicated. Steps at the top indicate the time of current injection. ***C*** and ***D***, scatter dot plots with averages ± SD of normalized spike frequencies for each IPI for current steps of 2 (*C*) or 10 s (*D*) (for *C:* n=13, Demsar test after Friedman test

p=0.005 for IPI 2 s; for *D:* n=10, Paired t-test with Bonferroni correction after ANOVA for repeated measurements p=0.0019 for IPI 2 s, p=0.01 for IPI 5 s, p=0.01 for IPI 10 s).

Phase-plane plot analysis of action potentials during repetitive stimulations

To obtain information about ion channels involved in spike frequency adaptation, we analyzed the first action potentials during the first and second paired pulses by using phase-plane plot analysis. In this type of analysis, the changes of membrane potential with time (dV/dt) are plotted as a function of membrane potential and each action potential is represented by a loop, with the upper and lower parts representing the depolarization and repolarization phases, respectively (Jenerick, 1963; Naundorf *et al.*, 2006; Bean, 2007). The maximal value of dV/dt is the maximal rising slope of the depolarization phase of the action potential, that is related to the amplitude of Na^+ currents (Bean, 2007). In Figure 6*A*, we superimposed phase-plane plots calculated from the first action potential evoked by 10 s urine pulses at different IPIs. At 2 s IPI, the maximal value of dV/dt was clearly lower for the second (46 mV/ms, dashed line) compared to the first (59 mV/ms, continuous line) urine pulse, while increasing IPIs narrowed the differences in the maximal values of dV/dt between the first action potentials of the repeated urine pulses. On average, the ratio between maximal values of dV/dt was significantly different at 2 and 5 s IPI (0.74 ± 0.12 for 2 s and 0.81 ± 0.04 for 5 s, n = 6) (Fig. 6*B*). The reduction of the maximal dV/dt value indicates a contribution of Na^+ channels to spike frequency adaptation to urine (Fig. 6*B*). Despite the trend, we did not measure any significant difference in maximal dV/dt for shorter urine paired pulses of 2 and 5 s (Fig. 6*C* and *D*).

We performed the same analysis when VSNs were stimulated with paired current steps as in Figs. 4 and 5. In a similar way to urine stimulation, phase-plane plots for current paired pulses of 10 s show a clear difference in maximal dV/dt during second stimulation when short IPIs (2, 5 s) were used, and no differences were observed at longer IPIs (Fig. 6*F*). Current pulses of 5 s also displayed difference in maximal dV/dt at short IPIs (Fig. 6*G*), while for current pulses of 2 s results were similar to those with urine stimuli (Fig. 6*H*).

Taken together, these data indicate that voltage-gated Na^+ channels involved in action potential generation contribute to short-term spike frequency adaptation in VSNs.

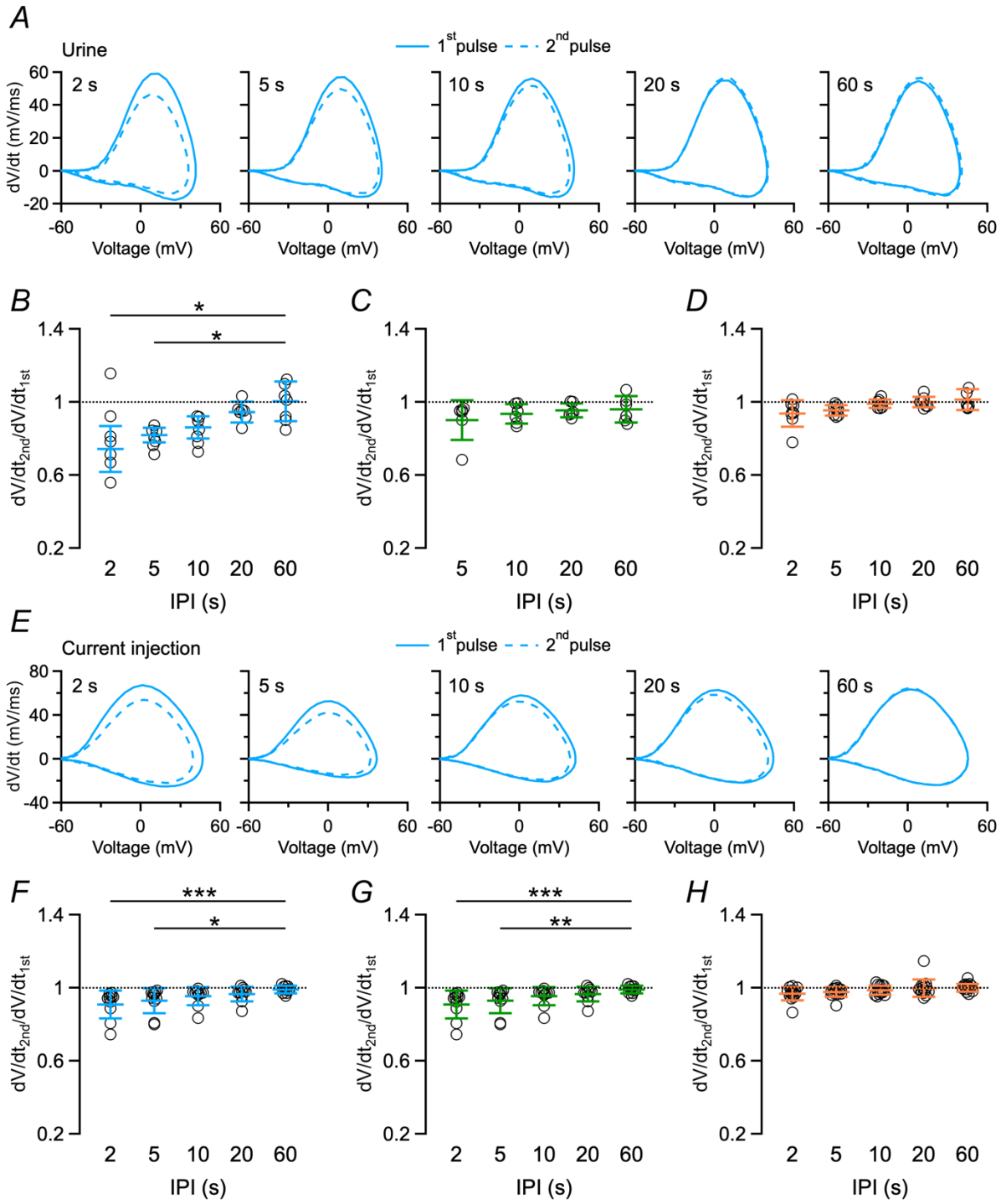


Figure 6. Phase-plane plot analysis of action potentials from repeated stimulations

A, Phase-plane plots of the first action potential in response to a repeated urine stimulation of 10 s duration with increasing IPIs ranging from 2 to 60 s, as indicated. Continuous and dashed lines were calculated from the first action potential of the first and second urine pulse, respectively. ***B-D***, scatter dot plots with averages ± SD of the ratio between the maximal dV/dt values of the first action potentials at each IPI. Urine pulse duration 10 (*B*), 5 (*C*) and 2 s (*D*). (for *B* n=6, Demsar test after Friedman test p=0.0021 for IPI 2 s and p=0.0041 for IPI 5s; for *C* n=6, Friedman test p=0.89; for *D* n=9 Friedman test p=0.051). ***E,*** Phase-plane plots of the first action potential in response to a repeated 5 pA current step of 10 s duration with increasing IPIs ranging from 2 to 60 s, as indicated. Continuous and dashed lines were calculated from the first action potential of the first and second current step,

respectively. ***F-H,*** scatter dot plots with averages ± SD of the ratio between the maximal dV/dt values of the first action potentials at each IPI. Current step duration 10 (*F*), 5 (*G*) and 2 s (*H*). (for *F* n=8, Demsar test after Friedman test p=0.00054 for IPI 2 s and p=0.018 for IPI 5 s; for *H* n=14, Friedman test p=0.126).

Inactivation properties of voltage-gated Na^+ currents in VSNs

To measure the inactivation properties of Na^+ channels in VSNs, we recorded inward currents from individual VSNs in the whole-cell voltage-clamp configuration using a Cs^+-based intracellular solution to block outward K^+ currents. Representative inward currents generated in response to a series of step depolarizations from a holding potential of -100 mV are shown in Fig. 7*A*. As both Na^+ and Ca^{2+} currents may contribute to inward currents in VSNs (Liman & Corey, 1996; Ukhanov *et al.*, 2007), we added 100 µM Cd^{2+} to the external solution to block Ca^{2+} currents. The remaining inward currents were abolished by the addition of 2 µM TTX, indicating that they were mainly carried by TTX-sensitive Na^+ channels (Fig. 7*A* and *B*). On average, the Na^+ current was 83 ± 2 % (n=8) of the total inward current at -20 mV.

To measure the voltage dependence of steady state fast and slow inactivation of Na^+ channels, we used typical voltage protocols composed of prepulses and test pulse to evaluate the non-inactivated fraction of Na^+ channels (all recordings were performed in the presence of 100 µM Cd^{2+} in the bath). For fast inactivation, we used prepulses of 30 ms at voltages from -90 to 0 mV, followed by a test potential of 30 ms at -20 mV (Fig. 7*C*). Normalized currents plotted as a function of the prepulse potential were fitted by the Boltzmann equation (Fig. 7*D*) and data from several neurons gave the following parameters: V_{half} = -46.7 ± 1.6 mV and k = 4.9 ± 1.3 mV (n=8). As Na^+ channels can also enter a slow inactivated state which might be relevant to our study of adaptation, we induced slow inactivation by applying prepulses of 30 s (Fig. 7*E*) at voltages from -90 to 0 mV, followed by a short (20 ms) hyperpolarizing step (to separate fast from slow inactivation) and by a (30 ms) test potential at 0 mV (Fig. 7*E*). The fit with a Boltzmann equation of the normalized current versus the prepulse potential (Fig. 7*F*) resulted in V_{half} = -50.6 ± 2.4 mV and k = 8.7 ±1.3 mV (n=6). These results indicate that Na^+ channels in VSNs undergo slow inactivation process after continuous depolarization.

As Na^+ channels enter a state of slow inactivation upon long depolarization from which they recover only after several seconds, we measured the time course of recovery of Na^+ channels in VSNs with a typical paired-pulse protocol with depolarizing prepulses varying from 1 to 10 s duration. A depolarizing prepulse of a selected duration was given from a holding potential of -80 mV to -20 mV to induce inactivation, followed by a second pulse (test) with IPIs varying from 1 to 15 s (top line in Fig. 8*A, B*). The neuron was kept at -80 mV during each IPI. Moreover, to allow a complete recovery

of the Na^+ current, the time between each consecutive paired-pulse was at least 1 min. The peak current measured 1 s after each prepulse (from 1 to 10 s duration) was smaller than that measured at the prepulse but as IPI increased more channels recovered from inactivation and the peak current produced by the second pulse gradually recovered toward the initial value. Figure 8*A* and *B* shows the superimposition of ratios of the peak currents evoked by the second and first pulses at IPIs from 1 to 15 s for depolarizing prepulses of 1 or 10 s, respectively. The first test pulse, applied 1s after the depolarizing prepulse, produced a Na^+ current of decreasing amplitude as the prepulse duration increased (average current ratios 0.89 ± 0.08 for 1 s, 0.77 ± 0.14 for 2 s, 0.55 ± 0.17 for 5 s, 0.44 ± 0.19 for 10 s, n=6) (Fig. 8*A*-*C*). When the IPI increased, the recovery of the Na^+ current toward its initial amplitude was slower for longer prepulse durations and the time necessary to recover to 90% of the initial peak amplitude was 2, 6, 11 or 15 s for prepulse durations of 1, 2, 5, or 10 s respectively (Fig. 8*A*, *B*, *D*).

These data show that voltage-gated Na^+ channels in VSNs present slow inactivation and that recovery from slow inactivation requires several seconds and depends on the duration of the inactivation step. The time scale of seconds for recovery from slow inactivation is similar to what measured during short-term adaptation protocols, suggesting that slow recovery from inactivation of Na^+ channels partially contribute to short-term spike frequency adaptation observed in VSNs.

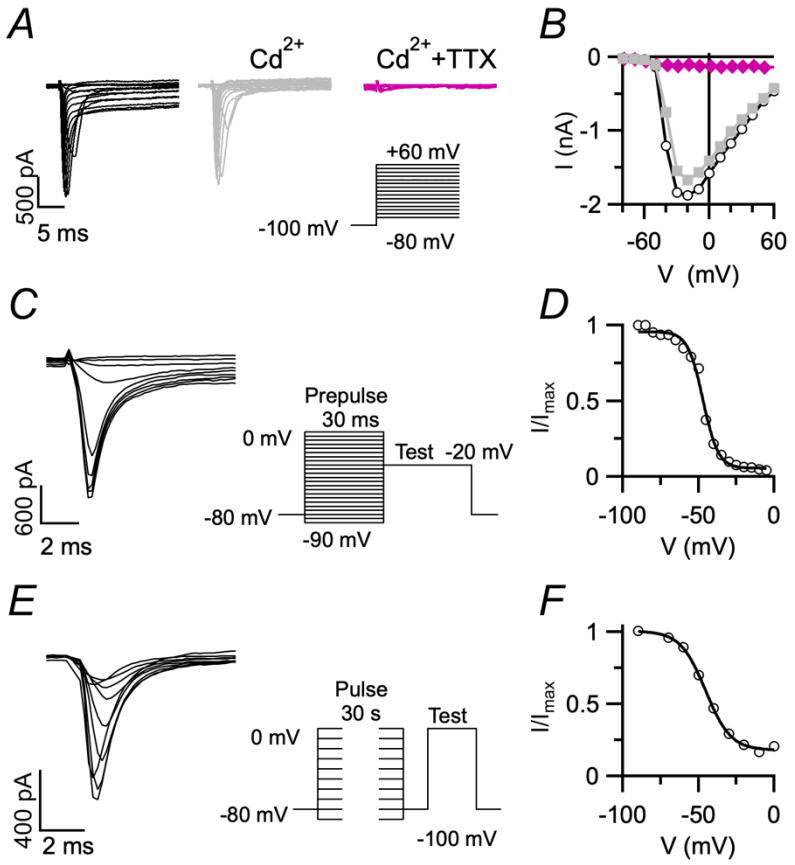


Figure 7. Inactivation of Na^+ currents in VSNs

A, Families of whole-cell voltage-gated inward currents recorded from a VSN elicited by voltage steps from -80 to +60 mV with 10 mV increment from a holding potential of -100 mV. The patch pipette contained a Cs^+-based intracellular solution. The neuron was exposed successively to bath solutions containing 100 µM Cd^{2+} and 100 µM Cd^{2+} plus 2 µM TTX, as indicated. ***B,*** current-voltage relations for the peak inward currents from the recordings in *A*. ***C*** and ***E,*** current recordings from the same VSN shown in *A* in response to stimulation protocols to measure inactivation in the presence of 100 µM Cd^{2+}. A test pulse was preceded by a prepulse at the indicated voltages of 30 ms (*C*) or 30 s (*E*) duration to measure fast and slow inactivation, respectively. In *C* one every two traces is shown. ***D*** and ***F,*** normalized currents versus membrane potential from the experiments shown in *C* and *E* were fitted with a Boltzmann equation with V_{half} = -46.9 mV, k = -6.9 mV for fast inactivation (*D*) and V_{half} = -45.2 mV, k = 8.3 mV and asymptotic value A = 0.18 for slow inactivation (*F*).

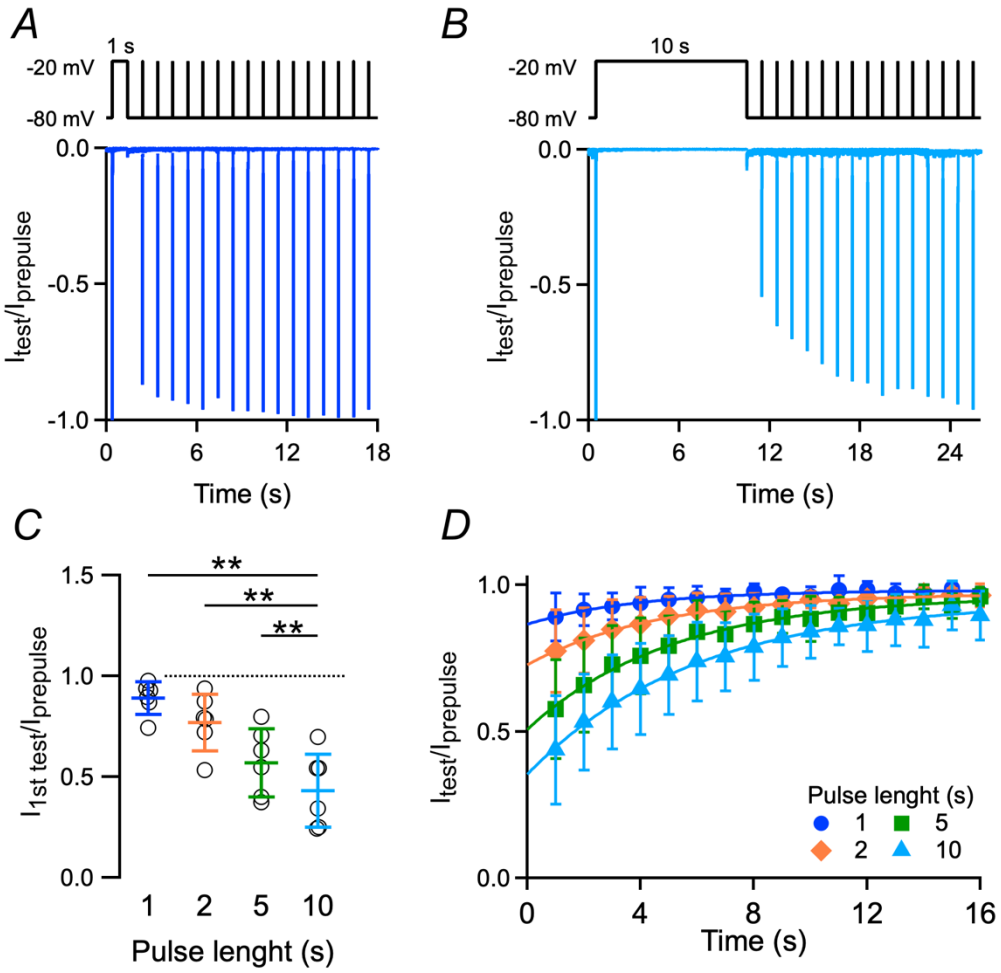


Figure 8. Time course of recovery of Na^+ channels from inactivation induced by depolarization steps varying from 1 to 10 s duration

A and ***B,*** representative whole-cell voltage-clamp recordings of Na^+ currents in a VSN in the presence of 100 µM Cd^{2+}. Currents were elicited by a paired pulse protocol consisting of a depolarization prepulse from -80 to -20 mV of 1 (*A*) or 10 s (*B*) duration followed by a short (10 ms) test pulse at increasing recovery intervals ranging from 1 to 15 s. The holding potential was -80 mV. For each IPI, the peak current measured at the test pulse was normalized to the prepulse peak current and superimposed. ***C,*** scatter dot plots with averages ± SD of the normalized peak currents measured at 1s after the prepulse of the indicated duration (Paired t-test with Bonferroni correction after ANOVA for repeated measurements p=0.0025 for 1 s, p=0.0018 for 5 s, p=0.0022 for 5 s, n=6). (*D*) recovery from inactivation as a function of IPIs at the indicated prepulse duration.

DISCUSSION

In this work we investigated the molecular mechanism underlying short-term adaptation in VSNs using whole-cell recordings from a VNO slice preparation.

We found that VSNs undergoes short-term adaptation when stimulated with a paired-pulse protocol using diluted urine as a natural source of pheromones (Fig. 2-3), confirming previous results obtained by using in situ Ca^{2+}-imaging and extracellular electrophysiology recordings (Wong *et al.*, 2018). Surprisingly, we found that short-term adaptation in VSNs was still present when they are stimulated by a current step injection independently of signal transduction activation (Fig. 4-5). The analysis of action potential firing suggested that sodium channels could be an important player during short-term adaptation (Fig. 6). We therefore isolated sodium currents in VSNs and found that these channels present slow-inactivation processes with a similar time scale of the short-term adaptation observed after paired pulse protocol (Fig. 7-8). Our results strongly suggest that slow inactivation of sodium channels is an important component of short-term adaptation during pheromone encoding by the VNO.

Sensory short-term adaptation depends on the duration of VSNs urine stimulation.

Short-term adaptation has been previously observed in VSNs using paired-pulse urine stimulations and recording the calcium dynamics or the firing activity extracellularly (Wong *et al.*, 2018). Paired urine stimulation of 5 s induced a reduction in the number of spikes in the second stimulus respect to the first one for IPI shorter than 20 s (Wong *et al.*, 2018). We performed whole-cell recordings from VSNs in slice preparation and show that short-term adaptation was present when neurons were stimulated with paired 5 s urine pulses with an IPI of 5 s. Short-term adaptation was evaluated by comparing the number of spikes of the second respect to the first response. Adaptation recovered for IPIs longer than 10 s, although in most experiment at 10 s it was still present (Fig. 2). Wong *et al.*(2018) in loose-patch extracellular recordings showed that short term adaptation recovered fully in 20 seconds, while longer times were needed for in situ-Ca imaging recordings.

We extended our investigation changing the duration of the stimulus. We found that paired 2 s long urine stimulation was less effective since short adaptation was present only at the smallest IPI of 2 s. At the contrary the 10 seconds long stimuli induced adaptation that required longer times to fully recover (Fig. 3).

Contribution of action potential machinery to short-term adaptation in VSNs.

Spehr and colleagues proposed a Ca^{2+}/Calmodulin feedback working on sensory transduction cascade as underlying mechanism of sensory adaptation in VSNs (Spehr *et al.*, 2009). In order to test if the there is an additional contribution, independent of signal transduction activation, we applied to VSNs paired pulse stimulation protocol with a current steps alternatively to urine stimulation, therefore bypassing the activation of the signal transduction cascade.

Surprisingly, paired current step stimulation of 5 pA for 5 s induced a reduction in the number of spikes in the second stimulus respect to the first one (Fig. 4), similarly to what observed with urine stimulation (normalized frequency for current step and urine stimulation at 5 s IPI is respectively 0.87 ± 0.03 and 0.72 ± 0.06). Short-term adaptation was observed also at 2 s IPI, while it was not statistically significant at longer ones (Fig 4*C*).

We changed the duration of the current step and similarly to what observed for urine stimulation, shortening of duration of the stimulus to 2 s was less effective in inducing short term adaptation, that was present only for the shorter IPI of 2 s. In contrast, a stimulus of 10 s induced short-term adaptation up to 10 s IPIs, as observed with urine stimulation.

We found that a comparable amplitude and recovery time of short-term adaptation when a physiological urine stimulus is replaced with a no-sensory stimulation, such as a current step, indicating that an additional process contribute to the adaptation independently by the modulation of the transduction machinery.

Voltage-gated sodium channels contribute to pheromone adaptation in vomeronasal sensory neurons

We performed the phase plot analysis to compare the action potential dynamics of the of the first action potentials evoked by pair-pulse stimulation. We found a significant difference in the upstroke of the action potential during the second stimulation (Fig. 6*A*, *E*) since a lower maximal dV/dt reflects the slower speed of the spike rise and it is directly proportional to the availability of voltage-gated sodium channels. Therefore, the analysis of the action potential in control and adapted state of VSNs suggest a contribution of sodium channels to short term adaptation.

Voltage-gated sodium channels undergo rapid activation to initiate the rising phase of action potential, followed by fast and slow inactivation processes. While fast inactivation attenuates inward sodium conductance on the milliseconds time scale, slow inactivation occurs when prolonged or high frequency depolarizations over the span of seconds reduce the number of channels available to provide excitatory inward currents (Silva, 2014). Therefore, slow inactivation of voltage-gated sodium channels plays a role in controlling membrane excitability, firing properties, and in particular spike frequency adaptation in the nervous system (Fleidervish *et al.*, 1996; Toib *et al.*, 1998).

Several sodium channels isoforms have been found to be expressed in VSNs either at mRNA level by RT-PCR or by immunohistochemistry (Nav1.1, Nav1.2, Nav1.3, Nav1.5, Nav1.6 and Nav1.7) and they differ as expression levels and localization in different compartments (Fieni *et al.*, 2003; Bolz *et al.*, 2017). A mixture of them is likely contributing to the generation of action potentials in VSNs and to the Na^+ current we recorded in whole-cell experiments.

Slow inactivation has similar, albeit not identical characteristics, for different sodium channels isoforms, that can differ in extent, kinetics, voltage dependence (Ulbricht, 2005; Silva, 2014). However, a hallmark is the much slower time scale respect to the fast inactivation process, seconds against milliseconds.

Our results show that sodium currents recorded in VSNs present slow inactivation that increased for longer stimulus length (Fig. 7 *E-F*) and recovered in the same time scale of recovery from short term adaptation after paired pulse protocol stimulation with urine or current step (Fig. 8).

A modulatory mechanisms of firing activity has been reported in VSNs by Ukhanov et al. (2007), that showed that prolonged depolarization obtained by current injection causes spike frequency adaptation due to the coupling of L-type calcium currents and BK large–conductance potassium currents. We observed spike frequency adaptation in most experiments when VSNs were stimulated with long stimuli either with urine or with current injection (see Fig 3 and 5, responses to 10 s). However, this mechanism cannot account for a change in the upstroke of the action potential (Fig. 6).

Many studies reported voltage gated sodium channels slow inactivation associated to activity dependent modulation of neuronal excitability. By way of example, in neocortical pyramidal cells sodium channels slow inactivation is associated to cumulative adaptation of spike firing caused by prolonged and repetitive depolarizing stimuli and to a slowing of the rising phase of the action potentials (Fleidervish *et al.*, 1996). In hippocampus CA1 pyramidal neurons cumulative inactivation is involved in regulating back-propagating action potential amplitude and can influence dendritic excitation (Mickus *et al.*, 1999; Jung *et al.*, 2013).

Interestingly, slow inactivation of sodium channels has been already associated to an adaptation process in the visual sensory system in salamander, where in retinal ganglion cells it is involved in light temporal contrast adaptation (Kim & Rieke, 2003). Increasing contrast causes an increase in input current variance and consequently of the spike rate that in turn reduces sodium channels availability through slow inactivation (Kim & Rieke, 2003).

Our work confirms former evidence of short-term adaptation in VSNs when stimulated with the urine by using the whole-cell patch clamp technique and show evidence for the contribution of a novel molecular mechanism. We show that short-term adaptation is surprisingly present also when VSNs are stimulated by paired pulse current steps, bypassing the transduction cascade. The extent

and the time course of adaptation observed in VSNs is consistent with the involvement of voltage gated sodium channel slow inactivation process, that occurs in the timescale of seconds. In conclusion our work proposes an important contribution of the intrinsic properties of individual VNSs to the sensory adaptation to natural stimuli.

REFERENCES

Abbas F & Vinberg F (2021). Transduction and Adaptation Mechanisms in the Cilium or Microvilli of Photoreceptors and Olfactory Receptors From Insects to Humans. *Front Cell Neurosci* **15,** 662453.

Amjad A, Hernandez-Clavijo A, Pifferi S, Maurya DK, Boccaccio A, Franzot J, Rock J & Menini A (2015). Conditional knockout of TMEM16A/anoctamin1 abolishes the calcium-activated chloride current in mouse vomeronasal sensory neurons. *J Gen Physiol* **145,** 285–301.

Bean BP (2007). The action potential in mammalian central neurons. *Nat Rev Neurosci* **8,** 451–465.

Bolz F, Kasper S, Bufe B, Zufall F & Pyrski M (2017). Organization and Plasticity of Sodium Channel Expression in the Mouse Olfactory and Vomeronasal Epithelia. *Front Neuroanat* **11,** 28.

Brandão SC, Silies M & Martelli C (2021). Adaptive temporal processing of odor stimuli. *Cell Tissue Res* **383,** 125–141.

Brennan PA (2010). Pheromones and Mammalian Behavior. In *The Neurobiology of Olfaction*, ed. Menini A, Frontiers in Neuroscience. CRC Press/Taylor & Francis, Boca Raton (FL). Available at: http://www.ncbi.nlm.nih.gov/books/NBK55973/ [Accessed August 22, 2021].

De Palo G, Boccaccio A, Miri A, Menini A & Altafini C (2012). A dynamical feedback model for adaptation in the olfactory transduction pathway. *Biophys J* **102,** 2677–2686.

Dibattista M, Amjad A, Maurya DK, Sagheddu C, Montani G, Tirindelli R & Menini A (2012). Calcium-activated chloride channels in the apical region of mouse vomeronasal sensory neurons. *J Gen Physiol* **140,** 3–15.

Doyle WI, Dinser JA, Cansler HL, Zhang X, Dinh DD, Browder NS, Riddington IM & Meeks JP (2016). Faecal bile acids are natural ligands of the mouse accessory olfactory system. *Nat Commun* **7,** 11936.

Dulac C & Axel R (1995). A novel family of genes encoding putative pheromone receptors in mammals. *Cell* **83,** 195–206.

Eisinga R, Heskes T, Pelzer B & Te Grotenhuis M (2017). Exact p-values for pairwise comparison of Friedman rank sums, with application to comparing classifiers. *BMC Bioinformatics* **18,** 68.

Fieni F, Ghiaroni V, Tirindelli R, Pietra P & Bigiani A (2003). Apical and basal neurones isolated from the mouse vomeronasal organ differ for voltage-dependent currents. *J Physiol* **552,** 425–436.

Fleidervish IA, Friedman A & Gutnick MJ (1996). Slow inactivation of Na+ current and slow cumulative spike adaptation in mouse and guinea-pig neocortical neurones in slices. *J Physiol* **493 (Pt 1),** 83–97.

Francia S, Pifferi S, Menini A & Tirindelli R (2014). Vomeronasal Receptors and Signal Transduction in the Vomeronasal Organ of Mammals. In *Neurobiology of Chemical Communication*, ed. Mucignat-Caretta C, Frontiers in Neuroscience. CRC Press/Taylor & Francis, Boca Raton (FL). Available at: http://www.ncbi.nlm.nih.gov/books/NBK200993/ [Accessed May 10, 2016].

Herrada G & Dulac C (1997). A novel family of putative pheromone receptors in mammals with a topographically organized and sexually dimorphic distribution. *Cell* **90,** 763–773.

Holy TE, Dulac C & Meister M (2000). Responses of vomeronasal neurons to natural stimuli. *Science* **289,** 1569–1572.

Jenerick H (1963). Phase plane trajectories of the muscle spike potential. *Biophys J* **3,** 363–377.

Jung J, Nam JH, Park HW, Oh U, Yoon J-H & Lee MG (2013). Dynamic modulation of ANO1/TMEM16A HCO3(-) permeability by Ca2+/calmodulin. *Proc Natl Acad Sci U S A* **110,** 360–365.

Kaur AW, Ackels T, Kuo T-H, Cichy A, Dey S, Hays C, Kateri M, Logan DW, Marton TF, Spehr M & Stowers L (2014). Murine pheromone proteins constitute a context-dependent combinatorial code governing multiple social behaviors. *Cell* **157,** 676–688.

Kim KJ & Rieke F (2003). Slow Na+ inactivation and variance adaptation in salamander retinal ganglion cells. *J Neurosci Off J Soc Neurosci* **23,** 1506–1516.

Kim S, Ma L & Yu CR (2011). Requirement of calcium-activated chloride channels in the activation of mouse vomeronasal neurons. *Nat Commun* **2,** 365.

Leinders-Zufall T, Storch U, Bleymehl K, Mederos Y Schnitzler M, Frank JA, Konrad DB, Trauner D, Gudermann T & Zufall F (2018). PhoDAGs Enable Optical Control of Diacylglycerol-Sensitive Transient Receptor Potential Channels. *Cell Chem Biol* **25,** 215-223.e3.

Liberles SD, Horowitz LF, Kuang D, Contos JJ, Wilson KL, Siltberg-Liberles J, Liberles DA & Buck LB (2009). Formyl peptide receptors are candidate chemosensory receptors in the vomeronasal organ. *Proc Natl Acad Sci U S A* **106,** 9842–9847.

Liman ER & Buck LB (1994). A second subunit of the olfactory cyclic nucleotide-gated channel confers high sensitivity to cAMP. *Neuron* **13,** 611–621.

Liman ER & Corey DP (1996). Electrophysiological characterization of chemosensory neurons from the mouse vomeronasal organ. *J Neurosci Off J Soc Neurosci* **16,** 4625–4637.

Lucas P, Ukhanov K, Leinders-Zufall T & Zufall F (2003). A diacylglycerol-gated cation channel in vomeronasal neuron dendrites is impaired in TRPC2 mutant mice: mechanism of pheromone transduction. *Neuron* **40,** 551–561.

Martelli C & Storace DA (2021). Stimulus Driven Functional Transformations in the Early Olfactory System. *Front Cell Neurosci* **15,** 684742.

Matsunami H & Buck LB (1997). A multigene family encoding a diverse array of putative pheromone receptors in mammals. *Cell* **90,** 775–784.

Mickus T, Jung HY & Spruston N (1999). Slow sodium channel inactivation in CA1 pyramidal cells. *Ann N Y Acad Sci* **868,** 97–101.

Mohrhardt J, Nagel M, Fleck D, Ben-Shaul Y & Spehr M (2018). Signal Detection and Coding in the Accessory Olfactory System. *Chem Senses* **43,** 667–695.

Moss RL, Flynn RE, Shen XM, Dudley C, Shi J & Novotny M (1997). Urine-derived compound evokes membrane responses in mouse vomeronasal receptor neurons. *J Neurophysiol* **77,** 2856–2862.

Naundorf B, Wolf F & Volgushev M (2006). Unique features of action potential initiation in cortical neurons. *Nature* **440,** 1060–1063.

Nodari F, Hsu F-F, Fu X, Holekamp TF, Kao L-F, Turk J & Holy TE (2008). Sulfated steroids as natural ligands of mouse pheromone-sensing neurons. *J Neurosci Off J Soc Neurosci* **28,** 6407–6418.

Rivière S, Challet L, Fluegge D, Spehr M & Rodriguez I (2009). Formyl peptide receptor-like proteins are a novel family of vomeronasal chemosensors. *Nature* **459,** 574–577.

Rodriguez I, Feinstein P & Mombaerts P (1999). Variable patterns of axonal projections of sensory neurons in the mouse vomeronasal system. *Cell* **97,** 199–208.

Ryba NJ & Tirindelli R (1997). A new multigene family of putative pheromone receptors. *Neuron* **19,** 371–379.

Shimazaki R, Boccaccio A, Mazzatenta A, Pinato G, Migliore M & Menini A (2006). Electrophysiological properties and modeling of murine vomeronasal sensory neurons in acute slice preparations. *Chem Senses* **31,** 425–435.

Silva J (2014). Slow inactivation of Na(+) channels. *Handb Exp Pharmacol* **221,** 33–49.

Silvotti L, Cavaliere RM, Belletti S & Tirindelli R (2018). In-vivo activation of vomeronasal neurons shows adaptive responses to pheromonal stimuli. *Sci Rep* **8,** 8490.

Spehr J, Hagendorf S, Weiss J, Spehr M, Leinders-Zufall T & Zufall F (2009). Ca2+ -calmodulin feedback mediates sensory adaptation and inhibits pheromone-sensitive ion channels in the vomeronasal organ. *J Neurosci Off J Soc Neurosci* **29,** 2125–2135.

Stowers L, Holy TE, Meister M, Dulac C & Koentges G (2002). Loss of sex discrimination and male-male aggression in mice deficient for TRP2. *Science* **295,** 1493–1500.

Tirindelli R (2021). Coding of pheromones by vomeronasal receptors. *Cell Tissue Res* **383,** 367–386.

Tirindelli R, Dibattista M, Pifferi S & Menini A (2009). From pheromones to behavior. *Physiol Rev* **89,** 921–956.

Toib A, Lyakhov V & Marom S (1998). Interaction between duration of activity and time course of recovery from slow inactivation in mammalian brain Na+ channels. *J Neurosci Off J Soc Neurosci* **18,** 1893–1903.

Torre V, Ashmore JF, Lamb TD & Menini A (1995). Transduction and adaptation in sensory receptor cells. *J Neurosci Off J Soc Neurosci* **15,** 7757–7768.

Touhara K & Vosshall LB (2009). Sensing odorants and pheromones with chemosensory receptors. *Annu Rev Physiol* **71,** 307–332.

Ukhanov K, Leinders-Zufall T & Zufall F (2007). Patch-clamp analysis of gene-targeted vomeronasal neurons expressing a defined V1r or V2r receptor: ionic mechanisms underlying persistent firing. *J Neurophysiol* **98,** 2357–2369.

Ulbricht W (2005). Sodium channel inactivation: molecular determinants and modulation. *Physiol Rev* **85,** 1271–1301.

Wark B, Lundstrom BN & Fairhall A (2007). Sensory adaptation. *Curr Opin Neurobiol* **17,** 423–429.

Webster MA (2012). Evolving concepts of sensory adaptation. *F1000Prime Rep*. Available at: https://facultyopinions.com/prime/reports/b/4/21/ [Accessed August 22, 2021].

Wong WM, Nagel M, Hernandez-Clavijo A, Pifferi S, Menini A, Spehr M & Meeks JP (2018). Sensory Adaptation to Chemical Cues by Vomeronasal Sensory Neurons. *eNeuro*; DOI: 10.1523/ENEURO.0223-18.2018.

Wyatt TD (2017). Pheromones. *Curr Biol CB* **27,** R739–R743.

Wysocki CJ, Nyby J, Whitney G, Beauchamp GK & Katz Y (1982). The vomeronasal organ: primary role in mouse chemosensory gender recognition. *Physiol Behav* **29,** 315–327.

2 CONCLUSIONS

The AOS has the capacity for adaptive learning, experience, and state-dependent plasticity (Dey et al., 2015; Griffiths and Brennan, 2015; Stowers and Liberles, 2016). In many case, early stages of plasticity start at peripheral level, but the mechanisms are still elusive since the physiological role of many putative components of the transduction cascade remains unclear. In the first part of my thesis, I contributed to the investigation of the peripheral modulation of spontaneous and evoked activity in VSNs defining exciting directions for future investigation.

We explored the role of calcium-activated chloride current in VSNs by using electrophysiological recordings on WT and genetically modified mice: the cKO mice for *Tmem16a* gene and the total KO mice for *Tmem16b* gene are a good model to study the role of calcium-activated chloride currents in vomeronasal physiology. The resting membrane properties and voltage-gated currents in VSNs are not altered by the absence of both TMEM16A and B channels. To check if TMEM16A and TMEM16B are involved in firing activity, we recorded spontaneous and evoked activity in loose-patch configuration. We found that VSNs from acute slices have spontaneous activity with similar mean frequencies in WT, TMEM16A cKO and TMEM16B KO, however the TMEM16A mice show a significant difference in instant frequency of spontaneous activity. Indeed, the cumulative fraction curve of inter-spike intervals (ISI) is shifted towards longer intervals in TMEM16A cKO mice, but not in TMEM16B KO mice, suggesting that TMEM16A calcium-activated chloride channels are active during spontaneous firing activity and favor spikes generation resulting in an instant frequency increase under physiological conditions. On the other hand, during urine-evoked activity the massive efflux of chloride, through both TMEM16A and TMEM16B channels, coupled with the equilibrium potential of chloride ion near -30 mV could explain the effect on ISI distribution of evoked spikes towards shorter intervals in stimulated VSNs from TMEM16A cKO and TMEM16B KO. The dynamic of chloride currents during signal transduction in VSNs is a key factor in understanding the role of TMEM16 channels in VNO signaling. We can conclude that calcium-activated chloride currents play a dual role in activity modulation of VSNs: drive the depolarization during spontaneous firing and contain/modulate the frequency of the response during evoked activity; the contribution of each channel requires further investigations.

In the second part of my thesis, I analyzed short-term adaptation properties of VSNs. We recorded the voltage changes of VSNs in whole-cell configuration using two dissimilar sources of stimuli: urine as natural activator of sensory transduction and current step as non-sensory stimulus to further investigate the differences between sensory and non-sensory information processing in VSNs. Since

we are interested on molecular mechanisms underlying short-term adaptation, we used the common double-pulse protocol with different time intervals between stimulations (Spehr et al., 2009; Wong et al., 2018). The mean spike frequency of the second response proportionally decreases depending on the duration of stimulation and on the length of the interval in between. The longer pulses result in stronger degree of adaptation for both the stimuli used suggesting the inspection of molecular mechanisms also downstream the transduction machinery. Moreover, the interval within two consecutive stimulations necessary for the recovery of former spiking properties strongly depends on the duration of previous activity as a memory-like form of plasticity. Unexpectedly, independently of signal transduction activation, short-term adaptation in VSNs is still present and the analysis of action potential firing suggests that sodium channels slow inactivation as an important player during short-term adaptation. By isolation of sodium currents in VSNs we found slow-inactivation processes in sodium channels kinetics with a similar timescale of the short-term adaptation observed after paired pulse protocol. Our results strongly suggest that slow inactivation of sodium channels is an important component of short-term adaptation during pheromone encoding by the VNO.

The modulation of VSNs activity occurs at different levels upstream and downstream the transduction machinery with the contribution of several molecular mechanisms. We suggest two additional mechanisms involved in modulation at peripheral level, the calcium-activated chloride channels TMEM16A and TMEM16B, and slow inactivation of sodium channels that might be relevant in pheromone decoding.

3 REFERENCES

Amjad, A., Hernandez-Clavijo, A., Pifferi, S., Maurya, D.K., Boccaccio, A., Franzot, J., Rock, J., and Menini, A. (2015). Conditional knockout of TMEM16A/anoctamin1 abolishes the calciumactivated chloride current in mouse vomeronasal sensory neurons. J. Gen. Physiol. *145*, 285–301.

Antunes, G., Sebastião, A.M., and Souza, F.M.S. de (2014). Mechanisms of Regulation of Olfactory Transduction and Adaptation in the Olfactory Cilium. PLoS One *9*, e105531.

Arakawa, H., Cruz, S., and Deak, T. (2011). From models to mechanisms: Odorant communication as a key determinant of social behavior in rodents during illness-associated states. Neurosci. Biobehav. Rev. *35*, 1916–1928.

Arnáiz, E., Moreno, D., and Quesada, R. (2014). Determination of Volatiles in Mouse Urine by Headspace Solid Phase Microextraction and Gas Chromatography-Mass Spectrometry. Anal. Lett. *47*, 721–729.

Balasubramanian, Lynch, and Barry (1996). Calcium-dependent modulation of the agonist affinity of the mammalian olfactory cyclic nucleotide-gated channel by calmodulin and a novel endogenous factor. J. Membr. Biol. *152*, 13–23.

Bellringer, Pratt, and Keverne (1980). Involvement of the vomeronasal organ and prolactin in pheromonal induction of delayed implantation in mice. J. Reprod. Fertil. *59*, 223–228.

Belluscio, L., Koentges, G., Axel, R., and Dulac, C. (1999). A map of pheromone receptor activation in the mammalian brain. Cell *97*, 209–220.

Berghard, A., Buck, L.B., and Liman, E.R. (1996). Evidence for distinct signaling mechanisms in two mammalian olfactory sense organs (vomeronasal organ/pheromone/sensory). Neurobiol. Commun. by Gerald D. Fischbach, Harvard Med. Sch. *93*, 2365–2369.

Beynon, R.J., and Hurst, J.L. (2003). Multiple roles of major urinary proteins in the house mouse, Mus domesticus. In Biochemical Society Transactions, (Portland Press Ltd), pp. 142–146.

Beynon, R.J., Veggerby, C., Payne, C.E., Robertson, D.H.L., Gaskell, S.J., Humphries, R.E., and Hurst, J.L. (2002). Polymorphism in major urinary proteins: Molecular heterogeneity in a wild mouse population. J. Chem. Ecol. *28*, 1429–1446.

Bezprozvanny, L., Watras, J., and Ehrlich, B.E. (1991). Bell-shaped calcium-response curves of

lns(l,4,5)P3- and calcium-gated channels from endoplasmic reticulum of cerebellum. Nat. 1991 3516329 *351*, 751–754.

Billig, G.M., Pál, B., Fidzinski, P., and Jentsch, T.J. (2011). Ca2+-activated Cl- currents are dispensable for olfaction. Nat. Neurosci. *14*, 763–769.

Boccaccio, A., Lagostena, L., Hagen, V., and Menini, A. (2006). Fast Adaptation in Mouse Olfactory Sensory Neurons Does Not Require the Activity of Phosphodiesterase. J. Gen. Physiol. *128*, 171–184.

Boillat, M., Challet, L., Rossier, D., Kan, C., Carleton, A., and Rodriguez, I. (2015). The vomeronasal system mediates sick conspecific avoidance. Curr. Biol. *25*, 251–255.

Bolz, F., Kasper, S., Bufe, B., Zufall, F., and Pyrski, M. (2017). Organization and plasticity of sodium channel expression in the mouse olfactory and vomeronasal epithelia. Front. Neuroanat. *11*, 1–15.

Boschat, C., Pélofi, C., Randin, O., Roppolo, D., Lüscher, C., Broillet, M.C., and Rodriguez, I. (2002). Pheromone detection mediated by a V1r vomeronasal receptor. Nat. Neurosci. *5*, 1261–1262.

Bossert, W.H., and Wilson, E.O. (1963). The analysis of olfactory communication among animals. J. Theor. Biol. *5*, 443–469.

Bradley, Reuter, and Frings (2001). Facilitation of calmodulin-mediated odor adaptation by cAMP-gated channel subunits. Science *294*, 2176–2178.

Bradley, J., Bönigk, W., Yau, K.-W., and Frings, S. (2004). Calmodulin permanently associates with rat olfactory CNG channels under native conditions. Nat. Neurosci. 2004 77 *7*, 705–710.

Brann, J.H., Dennis, J.C., Morrison, E.E., and Fadool, D.A. (2002). Type-specific inositol 1,4,5-trisphosphate receptor localization in the vomeronasal organ and its interaction with a transient receptor potential channel, TRPC2. J. Neurochem. *83*, 1452–1460.

Brennan, P.A. (2009). Pheromones and mammalian behavior. In The Neurobiology of Olfaction, (CRC Press), pp. 157–179.

Broillet, M.C., and Firestein, S. (1997). β Subunits of the Olfactory Cyclic Nucleotide-Gated Channel Form a Nitric Oxide Activated Ca2+ Channel. Neuron *18*, 951–958.

Bruce, H. (1959). An exteroceptive block to pregnancy in the mouse. Nature *184*, 105.

Brunner, J.D., Lim, N.K., Schenck, S., Duerst, A., and Dutzler, R. (2014). X-ray structure of a

calcium-activated TMEM16 lipid scramblase. Nat. 2014 5167530 *516*, 207–212.

Buck, L., and Axel, R. (1991). A novel multigene family may encode odorant receptors: A molecular basis for odor recognition. Cell *65*, 175–187.

Bufe, B., Schumann, T., and Zufall, F. (2012). Formyl peptide receptors from immune and vomeronasal system exhibit distinct agonist properties. J. Biol. Chem. *287*, 33644–33655.

Caputo, A., Caci, E., Ferrera, L., Pedemonte, N., Barsanti, C., Sondo, E., Pfeffer, U., Ravazzolo, R., Zegarra-Moran, O., and Galietta, L.J.V. (2008). TMEM16A, a membrane protein associated with calcium-dependent chloride channel activity. Science (80-.). *322*, 590–594.

Celsi, F., D'errico, A., and Menini, A. (2012). Responses to Sulfated Steroids of Female Mouse Vomeronasal Sensory Neurons. Chem. Senses *37*, 849–858.

Chamero, P., Marton, T.F., Logan, D.W., Flanagan, K., Cruz, J.R., Saghatelian, A., Cravatt, B.F., and Stowers, L. (2007). Identification of protein pheromones that promote aggressive behaviour. Nature *450*, 899–902.

Chamero, P., Leinders-Zufall, T., and Zufall, F. (2012). From genes to social communication: molecular sensing by the vomeronasal organ. Trends Neurosci. *35*, 597–606.

Chamero, P., Weiss, J., Alonso, M.T., Rodríguez-Prados, M., Hisatsune, C., Mikoshiba, K., Leinders-Zufall, T., and Zufall, F. (2017). Type 3 inositol 1,4,5-trisphosphate receptor is dispensable for sensory activation of the mammalian vomeronasal organ. Sci. Rep. *7*, 1–15.

Cherian, S., Wai Lam, Y., McDaniels, I., Struziak, M., and Delay, R.J. (2014). Estradiol rapidly modulates odor responses in mouse vomeronasal sensory neurons. Neuroscience *269*, 43–58.

Clancy, A., Coquelin, A., Macrides, F., Gorski, R., and Noble, E. (1984). Sexual behavior and aggression in male mice: involvement of the vomeronasal system. J. Neurosci. *4*, 2222–2229.

Dang, S., Feng, S., Tien, J., Peters, C.J., Bulkley, D., Lolicato, M., Zhao, J., Zuberbühler, K., Ye, W., Qi, L., et al. (2017). Cryo-EM structures of the TMEM16A calcium-activated chloride channel. Nat. 2017 5527685 *552*, 426–429.

Dauner, K., Lißmann, J., Jeridi, S., Frings, S., and Möhrlen, F. (2012). Expression patterns of anoctamin 1 and anoctamin 2 chloride channels in the mammalian nose. Cell Tissue Res. *347*, 327–341.

Dawson, Arriza, Jaworsky, Borisy, Attramadal, Lefkowitz, and Ronnett (1993). Beta-adrenergic

receptor kinase-2 and beta-arrestin-2 as mediators of odorant-induced desensitization. Science *259*, 825–829.

Dean, D.M., Mazzatenta, A., and Menini, A. (2004). Voltage-activated current properties of male and female mouse vomeronasal sensory neurons: sexually dichotomous? J. Comp. Physiol. A *190*, 491–499.

Demir, E., Li, K., Bobrowski-Khoury, N., Sanders, J.I., Beynon, R.J., Hurst, J.L., Kepecs, A., and Axel, R. (2020). The pheromone darcin drives a circuit for innate and reinforced behaviours. Nature *578*, 137–141.

Dey, S., Chamero, P., Pru, J.K., Chien, M.S., Ibarra-Soria, X., Spencer, K.R., Logan, D.W., Matsunami, H., Peluso, J.J., and Stowers, L. (2015). Cyclic regulation of sensory perception by a female hormone alters behavior. Cell *161*, 1334–1344.

Dibattista, M., Mazzatenta, A., Grassi, F., Tirindelli, R., and Menini, A. (2008). Hyperpolarization-activated cyclic nucleotide-gated channels in mouse vomeronasal sensory neurons. J. Neurophysiol. *100*, 576–586.

Dibattista, M., Amjad, A., Maurya, D.K., Sagheddu, C., Montani, G., Tirindelli, R., and Menini, A. (2012). Calcium-activated chloride channels in the apical region of mouse vomeronasal sensory neurons. J. Gen. Physiol. *140*, 3–15.

Dibattista, M., Pifferi, S., Boccaccio, A., Menini, A., and Reisert, J. (2017). The long tale of the calcium activated Cl− channels in olfactory transduction. Channels *11*, 399–414.

Dorward, D.A., Lucas, C.D., Chapman, G.B., Haslett, C., Dhaliwal, K., and Rossi, A.G. (2015). The Role of Formylated Peptides and Formyl Peptide Receptor 1 in Governing Neutrophil Function during Acute Inflammation. Am. J. Pathol. *185*, 1172.

Døving, K.B., and Trotier, D. (1998). Structure and function of the vomeronasal organ. J. Exp. Biol. *201*, 2913–2925.

Doyle, W.I., Dinser, J.A., Cansler, H.L., Zhang, X., Dinh, D.D., Browder, N.S., Riddington, I.M., and Meeks, J.P. (2016). Faecal bile acids are natural ligands of the mouse accessory olfactory system. Nat. Commun. 2016 71 *7*, 1–12.

Dulac, C., and Axel, R. (1995). A novel family of genes encoding putative pheromone receptors in mammals. Cell *83*, 195–206.

Dulac, C., and Axel, R. (1998). Expression of candidate pheromone receptor genes in vomeronasal neurons. In Chemical Senses, (Oxford University Press), pp. 467–475.

Dulac, C., and Torello, A.T. (2003). Molecular detection of pheromone signals in mammals: From genes to behaviour. Nat. Rev. Neurosci. *4*, 551–562.

Falzone, M.E., Malvezzi, M., Lee, B.-C., and Accardi, A. (2018). Known structures and unknown mechanisms of TMEM16 scramblases and channels. J. Gen. Physiol. *150*, 933–947.

Ferrera, L., Caputo, A., Ubby, I., Bussani, E., Zegarra-Moran, O., Ravazzolo, R., Pagani, F., and Galietta, L. (2009). Regulation of TMEM16A chloride channel properties by alternative splicing. J. Biol. Chem. *284*, 33360–33368.

Fieni, F., Ghiaroni, V., Tirindelli, R., Pietra, P., and Bigiani, A. (2003). Apical and basal neurones isolated from the mouse vomeronasal organ differ for voltage-dependent currents. J. Physiol. *552*, 425–436.

Francia, S., Pifferi, S., Menini, A., and Tirindelli, R. (2014). Vomeronasal receptors and signal transduction in the vomeronasal organ of mammals. In Neurobiology of Chemical Communication, (CRC Press), pp. 297–323.

Geyer, J., Bakhaus, K., Bernhardt, R., Blaschka, C., Dezhkam, Y., Fietz, D., Grosser, G., Hartmann, K., Hartmann, M.F., Neunzig, J., et al. (2017). The role of sulfated steroid hormones in reproductive processes. J. Steroid Biochem. Mol. Biol. *172*, 207–221.

Griffiths, P.R., and Brennan, P.A. (2015). Roles for learning in mammalian chemosensory responses. Horm. Behav. *68*, 91–102.

Haga-Yamanaka, S., Ma, L., He, J., Qiu, Q., Lavis, L.D., Looger, L.L., and Yu, C.R. (2014). Integrated action of pheromone signals in promoting courtship behavior in male mice. Elife *2014*, 3025.

Haga, S., Hattori, T., Sato, T., Sato, K., Matsuda, S., Kobayakawa, R., Sakano, H., Yoshihara, Y., Kikusui, T., and Touhara, K. (2010). The male mouse pheromone ESP1 enhances female sexual receptive behaviour through a specific vomeronasal receptor. Nature *466*, 118–122.

Hartzell, C., Putzier, I., and Arreola, J. (2004). CALCIUM-ACTIVATED CHLORIDE CHANNELS. Http://Dx.Doi.Org/10.1146/Annurev.Physiol.67.032003.154341 *67*, 719–758.

Hartzell, H.C., Yu, K., Xiao, Q., Chien, L.-T., and Qu, Z. (2009). Anoctamin/TMEM16 family

members are Ca2+-activated Cl− channels. J. Physiol. *587*, 2127–2139.

Hasen, N.S., and Gammie, S.C. (2009). Trpc2 gene impacts on maternal aggression, accessory olfactory bulb anatomy and brain activity. Genes, Brain Behav. *8*, 639–649.

Hattori, T., Osakada, T., Masaoka, T., Ooyama, R., Horio, N., Mogi, K., Nagasawa, M., Haga-Yamanaka, S., Touhara, K., and Kikusui, T. (2017). Exocrine Gland-Secreting Peptide 1 Is a Key Chemosensory Signal Responsible for the Bruce Effect in Mice. Curr. Biol. *27*, 3197-3201.e3.

Holy, T.E., Dulac, C., and Meister, M. (2000). Responses of vomeronasal neurons to natural stimuli. Science (80-.). *289*, 1569–1572.

Huang, F., Zhang, H., Wu, M., Yang, H., Kudo, M., Peters, C.J., Woodruff, P.G., Solberg, O.D., Donne, M.L., Huang, X., et al. (2012a). Calcium-activated chloride channel TMEM16A modulates mucin secretion and airway smooth muscle contraction. Proc. Natl. Acad. Sci. U. S. A. *109*, 16354–16359.

Huang, F., Wong, X., and Jan, L.Y. (2012b). International Union of Basic and Clinical Pharmacology. LXXXV: Calcium-Activated Chloride Channels. Pharmacol. Rev. *64*, 1–15.

Inamura, K., Kashiwayanagi, M., and Kurihara, K. (1997a). Blockage of urinary responses by inhibitors for IP3-mediated pathway in rat vomeronasal sensory neurons. Neurosci. Lett. *233*, 129–132.

Inamura, K., Kashiwayanagi, M., and Kurihara, K. (1997b). Inositol-1,4,5-trisphosphate Induces Responses in Receptor Neurons in Rat Vomeronasal Sensory Slices. Chem. Senses *22*, 93–103.

Ishii, T., and Mombaerts, P. (2008). Expression of nonclassical class I major histocompatibility genes defines a tripartite organization of the mouse vomeronasal system. J. Neurosci. *28*, 2332–2341.

Ishii, T., Hirota, J., and Mombaerts, P. (2003). Combinatorial coexpression of neural and immune multigene families in mouse vomeronasal sensory neurons. Curr. Biol. *13*, 394–400.

Isogai, Y., Si, S., Pont-Lezica, L., Tan, T., Kapoor, V., Murthy, V.N., and Dulac, C. (2011). Molecular organization of vomeronasal chemoreception. Nature *478*, 241–245.

Jemiolo, B., Harvey, S., and Novotny, M. (1986). Promotion of the Whitten effect in female mice by synthetic analogs of male urinary constituents. Proc. Natl. Acad. Sci. U. S. A. *83*, 4576–4579.

Jeng, G., Aggarwal, M., Yu, W.-P., and Chen, T.-Y. (2016). Independent activation of distinct pores in dimeric TMEM16A channels. J. Gen. Physiol. *148*, 393–404.

Karlson, P., and Lusher, M. (1959). 'Pheromones': a New Term for a Class of Biologically Active Substances. Nature *183*, 55–56.

Kato, A., and Touhara, K. (2009). Mammalian olfactory receptors: pharmacology, G protein coupling and desensitization. Cell. Mol. Life Sci. 2009 6623 *66*, 3743–3753.

Kaur, A.W., Ackels, T., Kuo, T.H., Cichy, A., Dey, S., Hays, C., Kateri, M., Logan, D.W., Marton, T.F., Spehr, M., et al. (2014). Murine pheromone proteins constitute a context-dependent combinatorial code governing multiple social behaviors. Cell *157*, 676–688.

Keller, M., Pierman, S., Douhard, Q., Baum, M.J., and Bakker, J. (2006). The vomeronasal organ is required for the expression of lordosis behaviour, but not sex discrimination in female mice. Eur. J. Neurosci. *23*, 521–530.

Keverne, E.B. (1999). The vomeronasal organ. Science (80-.). *286*, 716–720.

Kim, S., Ma, L., and Yu, C.R. (2011). Requirement of calcium-activated chloride channels in the activation of mouse vomeronasal neurons. Nat. Commun. *2*, 365–367.

Kim, S., Ma, L., Jensen, K.L., Kim, M.M., Bond, C.T., Adelman, J.P., and Yu, C.R. (2012). Paradoxical contribution of SK3 and GIRK channels to the activation of mouse vomeronasal organ. Nat. Neurosci. *15*, 1236–1244.

Kim, S.S., Ma, L., Unruh, J., McKinney, S., and Yu, C.R. (2015). Intracellular chloride concentration of the mouse vomeronasal neuron. BMC Neurosci. *16*, 90.

Kimchi, T., Xu, J., and Dulac, C. (2007). A functional circuit underlying male sexual behaviour in the female mouse brain. Nature *448*, 1009–1014.

Kimoto, H., Haga, S., Sato, K., and Touhara, K. (2005). Sex-specific peptides from exocrine glands stimulate mouse vomeronasal sensory neurons. Nature *437*, 898–901.

Kimoto, H., Sato, K., Nodari, F., Haga, S., Holy, T.E., and Touhara, K. (2007). Sex- and Strain-Specific Expression and Vomeronasal Activity of Mouse ESP Family Peptides. Curr. Biol. *17*, 1879–1884.

Kleene, S. (2008). The electrochemical basis of odor transduction in vertebrate olfactory cilia. Chem. Senses *33*, 839–859.

Kroner, Boekhoff, Lohmann, Genieser, and Breer (1996a). Regulation of olfactory signalling via cGMP-dependent protein kinase. Eur. J. Biochem. *236*, 632–637.

Kroner, C., Breer, H., Singer, A.G., and O'Connell, R.J. (1996b). Pheromone-induced second messenger signaling in the hamster vomeronasal organ. Neuroreport *7*, 2989–2992.

Kurahashi, T., and Menini, A. (1997). Mechanism of odorant adaptation in the olfactory receptor cell. Nature *385*, 725–729.

Kurahashi, T., and Shibuya, T. (1990). Ca2(+)-dependent adaptive properties in the solitary olfactory receptor cell of the newt. Brain Res. *515*, 261–268.

Le, S.C., Jia, Z., Chen, J., and Yang, H. (2019). Molecular basis of PIP2-dependent regulation of the Ca2+-activated chloride channel TMEM16A. Nat. Commun. *10*, 1–12.

Van Der Lee, S., and Boot, L. (1955). Spontaneous pseudopregnancy in mice. Acta Physiol Pharmacol Neerl. *4*, 442–444.

Leinders-Zufall, T., Brennan, P., Widmayer, P., Chandramani S., P., Maul-Pavicic, A., Jäger, M., Li, X.H., Breer, H., Zufall, F., and Boehm, T. (2004). MHC class I peptides as chemosensory signals in the vomeronasal organ. Science (80-.). *306*, 1033–1037.

Leinders-Zufall, T., Ishii, T., Chamero, P., Hendrix, P., Oboti, L., Schmid, A., Kircher, S., Pyrski, M., Akiyoshi, S., Khan, M., et al. (2014). A family of nonclassical class I MHC genes contributes to ultrasensitive chemodetection by mouse vomeronasal sensory neurons. J. Neurosci. *34*, 5121–5133.

Leinders-Zufall, T., Storch, U., Bleymehl, K., Mederos y Schnitzler, M., Frank, J.A., Konrad, D.B., Trauner, D., Gudermann, T., and Zufall, F. (2018). PhoDAGs Enable Optical Control of Diacylglycerol-Sensitive Transient Receptor Potential Channels. Cell Chem. Biol. *25*, 215-223.e3.

Leypold, B.G., Yu, C.R., Leinders-Zufall, T., Kim, M.M., Zufall, F., and Axel, R. (2002). Altered sexual and social behaviors in trp2 mutant mice. Proc. Natl. Acad. Sci. U. S. A. *99*, 6376–6381.

Liberles, S.D. (2014). Mammalian pheromones. Annu. Rev. Physiol. *76*, 151–175.

Liberles, S.D., Horowitz, L.F., Kuang, D., Contos, J.J., Wilson, K.L., Siltberg-Liberles, J., Liberles, D.A., and Buck, L.B. (2009). Formyl peptide receptors are candidate chemosensory receptors in the vomeronasal organ. Proc. Natl. Acad. Sci. U. S. A. *106*, 9842–9847.

Lim, N.K., Lam, A.K.M., and Dutzler, R. (2016). Independent activation of ion conduction pores in the double-barreled calcium-activated chloride channel TMEM16A. J. Gen. Physiol. *148*, 375–392.

Liman, E.R., and Corey, D.P. (1996). Electrophysiological characterization of chemosensory neurons from the mouse vomeronasal organ. J. Neurosci. *16*, 4625–4637.

Liman, E.R., Corey, D.P., and Dulac, C. (1999). TRP2: A candidate transduction channel for mammalian pheromone sensory signaling. Proc. Natl. Acad. Sci. U. S. A. *96*, 5791–5796.

Liu, Chen, Ahamed, Li, and Yau (1994). Calcium-calmodulin modulation of the olfactory cyclic nucleotide-gated cation channel. Science *266*, 1348–1354.

Loconto, J., Papes, F., Chang, E., Stowers, L., Jones, E.P., Takada, T., Kumánovics, A., Lindahl, K.F., and Dulac, C. (2003). Functional expression of murine V2R pheromone receptors involves selective association with the M10 and M1 families of MHC class Ib molecules. Cell *112*, 607–618.

Lucas, P., Ukhanov, K., Leinders-Zufall, T., and Zufall, F. (2003). A Diacylglycerol-Gated Cation Channel in Vomeronasal Neuron Dendrites Is Impaired in TRPC2 Mutant Mice: Mechanism of Pheromone Transduction. Neuron *40*, 551–561.

Luo, M., Fee, M.S., and Katz, L.C. (2003). Encoding Pheromonal Signals in the Accessory Olfactory Bulb of Behaving Mice. Science (80-.). *299*, 1196–1201.

Martini, S., Silvotti, L., Shirazi, A., Ryba, N.J.P., and Tirindelli, R. (2001). Co-Expression of Putative Pheromone Receptors in the Sensory Neurons of the Vomeronasal Organ. J. Neurosci. *21*, 843–848.

Maruniak, J., Wysocki, C.J., and Taylor, J. (1986). Mediation of male mouse urine marking and aggression by the vomeronasal organ. Physiol. Behav. *37*, 655–657.

Matsunami, H., and Buck, L.B. (1997). A multigene family encoding a diverse array of putative pheromone receptors in mammals. Cell *90*, 775–784.

Mendoza, A.S. (1993). Morphological studies on the rodent main and accessory olfactory systems: The regio olfactoria and vomeronasal organ. Ann. Anat. *175*, 425–446.

Milenkovic, V.M., Brockmann, M., Stöhr, H., Weber, B.H., and Strauss, O. (2010). Evolution and functional divergence of the anoctamin family of membrane proteins. BMC Evol. Biol. 2010 101 *10*, 1–9.

Mohrhardt, J., Nagel, M., Fleck, D., Ben-Shaul, Y., and Spehr, M. (2018). Signal detection and coding in the accessory olfactory system. Chem. Senses *43*, 667–695.

Mombaerts, P. (2004). Genes and ligands for odorant, vomeronasal and taste receptors. Nat. Rev. Neurosci. *5*, 263–278.

Moore, P.A. (1994). A model of the role of adaptation and disadaptation in olfactory receptor neurons: Implications for the coding of temporal and intensity patterns in odor signals. Chem. Senses *19*, 71–

86.

Mucignat-Caretta, C. (2014a). Neurobiology of chemical communication (CRC Press).

Mucignat-Caretta, C. (2014b). Frontiers in NeuroscienceCentral Processing of Intraspecific Chemical Signals in Mice. In Neurobiology of Chemical Communication, C. Mucignat-Caretta, ed. (CRC Press/Taylor & Francis(c) 2014 by Taylor & Francis Group, LLC.), p.

Münch, J., Billig, G., Hübner, C.A., Leinders-Zufall, T., Zufall, F., and Jentsch, T.J. (2018). Ca2+-activated Cl- currents in the murine vomeronasal organ enhance neuronal spiking but are dispensable for male-male aggression. J. Biol. Chem. *293*, 10392–10403.

Munger, Lane, Zhong, Leinders-Zufall, Yau, Zufall, and Reed (2001). Central role of the CNGA4 channel subunit in Ca2+-calmodulin-dependent odor adaptation. Science *294*, 2172–2175.

Nagai, M., Armelin-Correa, L.M., and and Malnic, B. (2016). Monogenic and Monoallelic Expression of Odorant Receptors. Mol. Pharmacol. *90*, 633–639.

Nodari, F., Hsu, F.F., Fu, X., Holekamp, T.F., Kao, L.F., Turk, J., and Holy, T.E. (2008). Sulfated steroids as natural ligands of mouse pheromone-sensing neurons. J. Neurosci. *28*, 6407–6418.

Novotny, M. V., Ma, W., Wiesler, D., and Žídek, L. (1999). Positive identification of the puberty-accelerating pheromone of the house mouse: The volatile ligands associating with the major urinary protein. Proc. R. Soc. B Biol. Sci. *266*, 2017–2022.

Omura, M., and Mombaerts, P. (2014). Trpc2-Expressing Sensory Neurons in the Main Olfactory Epithelium of the Mouse. Cell Rep. *8*, 583–595.

Ouyang, G., Vuckovic, D., and Pawliszyn, J. (2011). Nondestructive sampling of living systems using in vivo solid-phase microextraction. Chem. Rev. *111*, 2784–2814.

Overath, Sturm, and Rammensee (2014). Of volatiles and peptides: in search for MHC-dependent olfactory signals in social communication. Cell. Mol. Life Sci. *71*, 2429–2442.

Parker, I., and Yao, Y. (1991). Regenerative release of calcium from functionally discrete subcellular stores by inositol trisphosphate. Proc. R. Soc. London. Ser. B Biol. Sci. *246*, 269–274.

Paulino, C., Kalienkova, V., Lam, A.K.M., Neldner, Y., and Dutzler, R. (2017a). Activation mechanism of the calcium-activated chloride channel TMEM16A revealed by cryo-EM. Nature *552*, 421–425.

Paulino, C., Neldner, Y., Lam, A.K.M., Kalienkova, V., Brunner, J.D., Schenck, S., and Dutzler, R. (2017b). Structural basis for anion conduction in the calcium-activated chloride channel TMEM16A. Elife *6*.

Pedemonte, N., and Galietta, L.J.V. (2014). Structure and function of tmem16 proteins (anoctamins). Physiol. Rev. *94*, 419–459.

Peele, R., Salazar, I., Mimmack, M., Keverne, E.B., and Brennan, P.A. (2003). Low molecular weight constituents of male mouse urine mediate the pregnancy block effect and convey information about the identity of the mating male. Eur. J. Neurosci. *18*, 622–628.

Peters, C.J., Gilchrist, J.M., Tien, J., Bethel, N.P., Qi, L., Chen, T., Wang, L., Jan, Y.N., Grabe, M., and Jan, L.Y. (2018). The Sixth Transmembrane Segment Is a Major Gating Component of the TMEM16A Calcium-Activated Chloride Channel. Neuron *97*, 1063-1077.e4.

Pietra, G., Dibattista, M., Menini, A., Reisert, J., and Boccaccio, A. (2016). The Ca2+-activated Cl− channel TMEM16B regulates action potential firing and axonal targeting in olfactory sensory neurons. J. Gen. Physiol. *148*, 293–311.

Pietrobon, M., Zamparo, I., Maritan, M., Franchi, S.A., Pozzan, T., and Lodovichi, C. (2011). Interplay among cGMP, cAMP, and Ca2+ in Living Olfactory Sensory Neurons In Vitro and In Vivo. J. Neurosci. *31*, 8395–8405.

Pifferi, S., Boccaccio, A., and Menini, A. (2006). Cyclic nucleotide-gated ion channels in sensory transduction. FEBS Lett. *580*, 2853–2859.

Pifferi, S., Dibattista, M., and Menini, A. (2009). TMEM16B induces chloride currents activated by calcium in mammalian cells. Pflugers Arch. *458*, 1023–1038.

Del Punta, K., Leinders-Zufall, T., Rodriguez, I., Jukam, D., Wysocki, C.J., Ogawa, S., Zufall, F., and Mombaerts, P. (2002). Deficient pheromone responses in mice lacking a cluster of vomeronasal receptor genes. Nature *419*, 70–74.

Reuter, D., Zierold, K., Schröder, W., and Frings, S. (1998). A depolarizing chloride current contributes to chemoelectrical transduction in olfactory sensory neurons in situ. J. Neurosci. *18*, 6623–6630.

Rivière, S., Challet, L., Fluegge, D., Spehr, M., and Rodriguez, I. (2009). Formyl peptide receptor-like proteins are a novel family of vomeronasal chemosensors. Nature *459*, 574–577.

Roberts, S.A., Simpson, D.M., Armstrong, S.D., Davidson, A.J., Robertson, D.H., McLean, L., Beynon, R.J., and Hurst, J.L. (2010). Darcin: A male pheromone that stimulates female memory and sexual attraction to an individual male's odour. BMC Biol. *8*, 75.

Rock, J.R., O'Neal, W.K., Gabriel, S.E., Randell, S.H., Harfe, B.D., Boucher, R.C., and Grubb, B.R. (2009). Transmembrane protein 16A (TMEM16A) is a Ca2+ -regulated Cl- secretory channel in mouse airways. J. Biol. Chem. *284*, 14875–14880.

Röck, F., Hadeler, K.-P., Rammensee, H.-G., and Overath, P. (2007). Quantitative Analysis of Mouse Urine Volatiles: In Search of MHC-Dependent Differences. PLoS One *2*, e429.

Rodriguez, I. (2016). Vomeronasal Receptors: V1Rs, V2Rs, and FPRs. In Chemosensory Transduction: The Detection of Odors, Tastes, and Other Chemostimuli, (Elsevier Inc.), pp. 175–190.

Rodriguez, I., Feinstein, P., and Mombaerts, P. (1999). Variable patterns of axonal projections of sensory neurons in the mouse vomeronasal system. Cell *97*, 199–208.

Rodriguez, I., Del Punta, K., Rothman, A., Ishii, T., and Mombaerts, P. (2002). Multiple new and isolated families within the mouse superfamily of V1r vomeronasal receptors. Nat. Neurosci. *5*, 134–140.

Ron Yu, C. (2015). TRICK or TRP? What Trpc2-/- mice tell us about vomeronasal organ mediated innate behaviors. Front. Neurosci. *9*, 221.

Roper, S.D., and Chaudhari, N. (2017). Taste buds: cells, signals and synapses. Nat. Rev. Neurosci. *18*, 485–497.

Ruysh, F. (1703). Thesaurus Anatomicus tertium.

Ryba, N.J.P., and Tirindelli, R. (1997). A new multigene family of putative pheromone receptors. Neuron *19*, 371–379.

Schroeder, B.C., Cheng, T., Jan, Y.N., and Jan, L.Y. (2008). Expression Cloning of TMEM16A as a Calcium-Activated Chloride Channel Subunit. Cell *134*, 1019–1029.

Shimazaki, Boccaccio, Mazzatenta, Pinato, Migliore, and Menini (2006). Electrophysiological properties and modeling of murine vomeronasal sensory neurons in acute slice preparations. Chem. Senses *31*, 425–435.

Silva, L., and Antunes, A. (2017). Vomeronasal Receptors in Vertebrates and the Evolution of Pheromone Detection. Annu. Rev. Anim. Biosci. *5*, 353–370.

Silvotti, L., Moiani, A., Gatti, R., and Tirindelli, R. (2007). Combinatorial co-expression of pheromone receptors, V2Rs. J. Neurochem. *103*, 1753–1763.

Silvotti, L., Cavaliere, R.M., Belletti, S., and Tirindelli, R. (2018). In-vivo activation of vomeronasal neurons shows adaptive responses to pheromonal stimuli. Sci. Rep. *8*, 1–10.

Singer, A.G., Beauchamp, G.K., and Yamazaki, K. (1997). Volatile signals of the major histocompatibility complex in male mouse urine. Proc. Natl. Acad. Sci. U. S. A. *94*, 2210–2214.

Singer, D.S., Hare, J., Golding, H., Flaherty, L., and Rudikoff, S. (1988). Characterization of a new subfamily of class I genes in the H-2 complex of the mouse. Immunogenetics *28*, 13–21.

Singh, Brownt, and Roser (1987). MHC antigens in urine as olfactory recognition cues. Nature *327*.

Spehr, J., Hagendorf, S., Weiss, J., Spehr, M., Leinders-Zufall, T., and Zufall, F. (2009). Ca2+-calmodulin feedback mediates sensory adaptation and inhibits pheromone-sensitive ion channels in the vomeronasal organ. J. Neurosci. *29*, 2125–2135.

Spehr, M., Hatt, H., and Wetzel, C.H. (2002). Arachidonic acid plays a role in rat vomeronasal signal transduction. J. Neurosci. *22*, 8429–8437.

Stephan, A.B., Shum, E.Y., Hirsh, S., Cygnar, K.D., Reisert, J., and Zhao, H. (2009). ANO2 is the cilial calcium-activated chloride channel that may mediate olfactory amplification. Proc. Natl. Acad. Sci. *106*, 11776–11781.

Stowers, L., and Liberles, S.D. (2016). State-dependent responses to sex pheromones in mouse. Curr. Opin. Neurobiol. *38*, 74–79.

Stowers, L., Holy, T.E., Meister, M., Dulac, C., and Koentges, G. (2002). Loss of sex discrimination and male-male aggression in mice deficient for TRP2. Science (80-.). *295*, 1493–1500.

Sturm, T., Leinders-Zufall, T., MačEk, B., Walzer, M., Jung, S., Pömmerl, B., Stevanović, S., Zufall, F., Overath, P., and Rammensee, H.G. (2013). Mouse urinary peptides provide a molecular basis for genotype discrimination by nasal sensory neurons. Nat. Commun. *4*.

Ta, Acheson, Rorsman, Jongkind, and Tammaro (2017). Contrasting effects of phosphatidylinositol 4,5-bisphosphate on cloned TMEM16A and TMEM16B channels. Br. J. Pharmacol. *174*, 2984–2999.

Takami, S. (2002). Recent progress in the neurobiology of the vomeronasal organ. Microsc. Res. Tech. *58*, 228–250.

Taniguchi, M., Wang, D., and Halpern, M. (2000). Chemosensitive conductance and inositol 1,4,5-trisphosphate-induced conductance in snake vomeronasal receptor neurons. Chem. Senses *25*, 67–76.

Taruno, A., Nomura, K., Kusakizako, T., Ma, Z., Nureki, O., and Foskett, J.K. (2021). Taste transduction and channel synapses in taste buds. Pflugers Arch. *473*, 3–13.

Tembo, Wozniak, Bainbridge, and Carlson (2019). Phosphatidylinositol 4,5-bisphosphate (PIP 2) and Ca 2+ are both required to open the Cl - channel TMEM16A. J. Biol. Chem. *294*, 12556–12564.

Tirindelli, R., Mucignat-Caretta, C., and Ryba, N.J.P. (1998). Molecular aspects of pheromonal communication via the vomeronasal organ of mammals. Trends Neurosci. *21*, 482–486.

Tirindelli, R., Dibattista, M., Pifferi, S., and Menini, A. (2009). From pheromones to behavior. Physiol. Rev. *89*, 921–956.

Torre, V., Ashmore, J.F., Lamb, T.D., and Menini, A. (1995). Transduction and adaptation in sensory receptor cells. J. Neurosci. *15*, 7757–7768.

Touhara, K. (2007). Molecular Biology of Peptide Pheromone Production and Reception in Mice. Adv. Genet. *59*, 147–171.

Trotier, D., and Døving, K.B. (1998). "Anatomical Description of a New Organ in the Nose of Domesticated Animals" by Ludvig Jacobson (1813). Chem. Senses *23*, 743–754.

Trotier, D., Døving, K.B., and Rosin, J. -F (1993). Voltage-dependent Currents in Microvillar Receptor Cells of the Frog Vomeronasal Organ. Eur. J. Neurosci. *5*, 995–1002.

Trotier, D., Døving, K.B., Ore, K., and Shalchian-Tabrizi, C. (1998). Scanning electron microscopy and gramicidin patch clamp recordings of microvillous receptor neurons dissociated from the rat vomeronasal organ. Chem. Senses *23*, 49–57.

Ukhanov, K., Leinders-Zufall, T., and Zufall, F. (2007). Patch-clamp analysis of gene-targeted vomeronasal neurons expressing a defined V1r or V2r receptor: Ionic mechanisms underlying persistent firing. J. Neurophysiol. *98*, 2357–2369.

Untiet, V., Moeller, L.M., Ibarra-Soria, X., Sánchez-Andrade, G., Stricker, M., Neuhaus, E.M., Logan, D.W., Gensch, T., and Spehr, M. (2016). Elevated cytosolic Cl- concentrations in dendritic knobs of mouse vomeronasal sensory neurons. Chem. Senses *41*, 669–676.

Weis, W., and Kobilka, B. (2018). The Molecular Basis of G Protein-Coupled Receptor Activation. Annu. Rev. Biochem. *87*, 897–919.

Whitten, W.K. (1959). Occurrence of anoestrus in mice caged in groups. J. Endocrinol. *18*, 102–107.

Wong, W.M., Nagel, M., Hernandez-Clavijo, A., Pifferi, S., Menini, A., Spehr, M., and Meeks, J.P. (2018). Sensory adaptation to chemical cues by vomeronasal sensory neurons. ENeuro *5*, 223–241.

Wong, W.M., Cao, J., Zhang, X., Doyle, W.I., Mercado, L.L., Gautron, L., and Meeks, J.P. (2020). Physiology-forward identification of bile acid-sensitive vomeronasal receptors. Sci. Adv. *6*.

Wyatt, T.D. (2014). Pheromones and Animal Behavior: Chemical Signals and Signature Mixes.

Wyatt, T.D. (2017). Pheromones. Curr. Biol. *27*, R739–R743.

Wynn, E.H., Sánchez-Andrade, G., Carss, K.J., and Logan, D.W. (2012). Genomic variation in the vomeronasal receptor gene repertoires of inbred mice. BMC Genomics 2012 131 *13*, 1–13.

Xiao, Q., Yu, K., Perez-Cornejo, P., Cui, Y., Arreola, J., and Hartzell, H.C. (2011). Voltage- and calcium-dependent gating of TMEM16A/Ano1 chloride channels are physically coupled by the first intracellular loop. Proc. Natl. Acad. Sci. *108*, 8891–8896.

Yamaguchi, M., Yamazaki, K., Beauchamp, G.K., Bard, J., Thomas, L., and Boyse, E.A. (1981). Distinctive urinary odors governed by the major histocompatibility locus of the mouse. Proc. Natl. Acad. Sci. U. S. A. *78*, 5817–5820.

Yang, C., and Delay, R.J. (2010). Calcium-activated chloride current amplifies the response to urine in mouse vomeronasal sensory neurons. J. Gen. Physiol. *135*, 3–13.

Yang, H., Shi, P., Zhang, Y.P., and Zhang, J. (2005). Composition and evolution of the V2r vomeronasal receptor gene repertoire in mice and rats. Genomics *86*, 306–315.

Yang, Y.D., Cho, H., Koo, J.Y., Tak, M.H., Cho, Y., Shim, W.-S., Park, S.P., Lee, J., Lee, B., Kim, B.-M., et al. (2008). TMEM16A confers receptor-activated calcium-dependent chloride conductance. Nat. 2008 4557217 *455*, 1210–1215.

Yoles-Frenkel, M., Kahan, A., and Ben-Shaul, Y. (2018). Temporal response properties of accessory olfactory bulb neurons: Limitations and opportunities for decoding. J. Neurosci. *38*, 4957–4976.

Young, J.M., Massa, H.F., Hsu, L., and Trask, B.J. (2010). Extreme variability among mammalian V1R gene families. Genome Res. *20*, 10–18.

Yu, K., Duran, C., Qu, Z., Cui, Y.-Y., and Hartzell, H.C. (2012). Explaining Calcium-Dependent Gating of Anoctamin-1 Chloride Channels Requires a Revised Topology. Circ. Res. *110*, 990–999.

Zancanaro, C. (2014). Vomeronasal Organ: A Short History of Discovery and an Account of Development and Morphology in the Mouse (CRC Press/Taylor & Francis).

Zhang, P., Yang, C., and Delay, R.J. (2008). Urine stimulation activates BK channels in mouse vomeronasal neurons. J. Neurophysiol. *100*, 1824–1834.

Zhang, P., Yang, C., and Delay, R.J. (2010). Odors activate dual pathways, a TRPC2 and a AA-dependent pathway, in mouse vomeronasal neurons. Am. J. Physiol. - Cell Physiol. *298*, C1253.

Zhou, Y., and Rui, L. (2010). Major urinary protein regulation of chemical communication and nutrient metabolism (NIH Public Access).

Zufall, F. (2005). The TRPC2 ion channel and pheromone sensing in the accessory olfactory system. Naunyn. Schmiedebergs. Arch. Pharmacol. *371*, 245–250.

Zufall, F., and Leinders-Zufall, T. (1997). Identification of a long-lasting form of odor adaptation that depends on the carbon Monoxide/cGMP second-messenger system. J. Neurosci. *17*, 2703–2712.

Zufall, F., and Leinders-Zufall, T. (1998). Role of cyclic GMP in olfactory transduction and adaptation. Ann. N. Y. Acad. Sci. *855*, 199–204.

Zufall, F., and Munger, S.D. (2016). Chemosensory Transduction - 1st Edition (Elsevier).

Zufall, and Leinders-Zufall, T. (2000). The cellular and molecular basis of odor adaptation. Chem. Senses *25*, 473–481.